

JIMMA UNIVERSITY

SCHOOL OF GRADUATE STUDIES

JIMMA INSTITUTE OF TECHNOLOGY

FACULTY OF CIVIL AND ENVIROMENTAL ENGINEERING

STRUCTURAL ENGINEERING STREAM

Investigation on the Effect of Geometric Parameter on Reinforced Concrete Exterior Shear Wall-Slab Connection using Finite Element Analysis

A Research Thesis Submitted to School of Graduate Studies of Jimma University in Partial Fulfillment of the Requirements for the Degree of Masters of Science in Structural Engineering

By: - AMAN HAMICHA ROBA

May 2020

JIMMA, ETHIOPIA

JIMMA UNIVERSITY
SCHOOL OF GRADUATE STUDIES
JIMMA INSTITUTE OF TECHNOLOGY
FACULTY OF CIVIL AND ENVIROMENTAL ENGINEERING
STRUCTURAL ENGINEERING STREAM

Investigation on the Effect of Geometric Parameter on Reinforced Concrete Exterior Shear Wall-Slab Connection using Finite Element Analysis

A Research Thesis Submitted to School of Graduate Studies of Jimma University in Partial Fulfillment of the Requirements for the Degree of Masters of Science in Structural Engineering

By: AMAN HAMICHA ROBA

Main Advisor: - Dr.Tamasgen Wondimu(Phd)

Co advisor: -Eng. Goshu Kenea (Msc)

May 2020

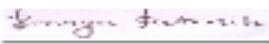
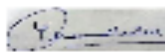
JIMMA, ETHIOPIA

JIMMA UNIVERSITY
SCHOOL OF GRADUATE STUDIES
JIMMA INSTITUTE OF TECHNOLOGY
FACULTY OF CIVIL AND ENVIRONMENTAL ENGINEERING
STRUCTURAL ENGINEERING CHAIR

**INVESTIGATION ON THE EFFECT OF GEOMETRIC PARAMETER ON
REINFORCED CONCRETE EXTERIOR SHEAR WALL SLAB CONNECTION USING
FINITE ELEMENT ANALYSIS**

AMAN HAMICHA ROBA

APPROVED BY BOARD OF EXAMINERS

1. Dr. TemesgenWondimu		02/08/2020
Main advisor	Signature	Date
2. Engr. GoshuKenea		23 / 06 / 2020
Co-advisor	Signature	Date
3. Dr. Binaya Patnaik		20 / 06 / 2020
External Examiner	Signature	Date
4. Engr. Y. AnandBabu		20/ 06/ 2020
Internal Examiner	Signature	Date
5. Engr. Habtamu G/medhin		20/06/2020
Chairperson	Signature	Date

DECLARATION

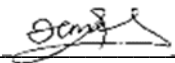
I Aman Hamicha declare that this thesis entitled “Investigation on the Effect of Geometric Parameter on Reinforced Concrete Exterior Shear Wall-Slab Connection using Finite Element Analysis” is my original work and has not been presented by any other person for an award of degree in this or other university.

Aman Hamicha (Candidate)

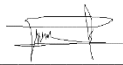
Signature_____Date_____

This thesis has been submitted for examination with my approval as a university advisor.

Advisor: Dr. Tamasgen Wondimu (Phd)

Signature: __________Date_07/03/2020_____

Co-Advisor: Goshu Kenea (Msc)

Signature: __________Date_12/06/2020_____

ABSTRACT

Finite element models are currently used for the assessment of structural behavior, which becomes more accurate and reliable. Since conducting the full experimental test is very expensive and time consuming, it is better to use numerical method to investigate the behaviors of structure because the efficiency of the model can be evaluated by the experimental result and it shows good agreement with the experimental tests.

In this study a non-linear finite element analysis with ABAQUS software package has been taken to investigate the response of reinforced concrete exterior shear wall –slab connection subjected to cyclic loading. The structural responses such as load carrying capacity, energy dissipation, ductility and stiffness degradation has been studied.

Using developed models parametric study have been done to investigate the effect of connection type, aspect ratio of thickness of slab to thickness of shear wall (T_s/T_w), aspect ratio of height of shear wall to effective width of the slab (H/W_e) and concrete grade on the load carrying capacity, energy dissipation, ductility and stiffness degradation of exterior reinforced concrete shear wall-slab connection. A total of 22 models have been used to investigate the parametric study.

The results show that the exterior shear wall-slab connection with U-type connection have high load carrying capacity than the other connection type, as the aspect ratio of T_s/T_w increases the load carrying capacity and energy dissipation capacity increase, as the aspect ratio of H/W_e decrease or as effective width of the slab from shear wall increase the load carrying capacity and energy dissipation capacity decreases and as concrete grade increase the load carrying and energy dissipation increases.

Key Words: *Energy dissipation, Ductility, Stiffness degradation, Cyclic loading, Finite element analysis, Reinforced Concrete*

ACKNOWLEDGEMENT

First and foremost, praise and thanks to the Allah, the Almighty, for His showers of blessings throughout my research work to complete the research successfully.

I would like to express my deep and sincere gratitude to my research advisor Dr. Tamasgen Wondimu (Phd), for providing invaluable guidance throughout this research. His dynamism, vision, sincerity and motivation have deeply inspired me. It was a great privilege and honor to work and study under his guidance. I am extremely grateful for what he has offered me. Also I would like to acknowledge co-advisor Eng. Goshu Kenea for his important support and assistance.

I am extremely grateful to my parents for their love, prayers, caring and sacrifices for educating and preparing me for future. I am very much thankful to my wife Misra Feko for her love, understanding, prayers and continuing support to complete this thesis. I would like to express my gratitude to my friends for their guidance and rigorous moral support not only on my educational success but throughout my life.

Finally, my special thanks goes to Jimma institute of Technology for facilitating this program which helps me for upgrading my profession.

TABLE OF CONTENTS

DECLARATION	i.
ABSTRACT.....	ii
ACKNOWLEDGEMENT	iii
TABLE OF CONTENTS.....	iv
LIST OF TABLE	viii
LIST OF FIGURES	ix
ACRONYMS.....	xii
CHAPTER ONE INTRODUCTION.....	1
1.1 Background of the Study.....	1
1.2 Statement of the Problem	2
1.3 Research Questions	2
1.4 Objective of the Study.....	2
1.4.1 General Objective	2
1.4.2 Specific Objective.....	3
1.5 Significance of the Study	3
1.6 Scope and Limitation of the Study.....	3
CHAPTET TWO	4
REVIEW OF RELATED LITERATURE	4
2.1 General	4
2.2 Studies on Reinforced Concrete Shear Wall-Slab Connection.....	4
2.3 Concrete	10
2.4 Concrete Damage-Plasticity Model for Finite Element Method of Analysis	10
2.4.1 Concrete –Damage Plasticity Model (CDP).....	11
2.4.2 Yield Condition	12

2.4.3 Flow Rule	14
2.4.4 Available Yield Criteria.....	15
2.4.5 Viscoplastic Regularization	16
2.5 Steel Reinforcement	17
2.6 Constitutive Models of Concrete in ABAQUS	17
2.7 Concrete Damage Plasticity Model.....	18
2.7.1 Behavior of Concrete in Compression Model	19
2.7.2 Behavior of Concrete in Tension Model	20
2.7.3 Damage Modeling	22
2.7.4 Behavior of Concrete Under Cyclic Loading	24
2.8 Nonlinear Finite Element Analysis	24
2.8.1 Numerical Integration.....	26
2.8.2 Techniques for Solving Nonlinear Analysis.....	26
2.8.3 Converging Criteria	29
CHAPTER 3	32
RESEARCH METHODOLOGY.....	32
3.1 General	32
3.2 Finite Element Modeling.....	33
3.2.1 Element Type.....	35
3.2.2 Mesh Size	37
3.2.3 Interaction Between Concrete and Reinforcement.....	38
3.3 Material Properties	38
3.3.1 Concrete.....	38
3.3.1.1 Stress- Strain Relationship of Concrete in Compression for Non-Linear Structural Analysis	38

3.3.1.2 Tensile Stress Behavior of Concrete.....	40
3.3.1.3 Concrete Damage Plasticity Parameter.....	41
3.4 Steel Reinforcement	45
3.5 Geometric Modeling and Finite Element Mesh	45
3.6 Interaction.....	49
3.7 Loading and Boundary Conditions	50
3.8 Method for Solving Non-Linear Solution	51
3.9 Load Stepping and Failure Definition for Finite Element Method	54
3.10 Flow Chart of Finite Element Analysis.....	55
3.11 Validation of FE Model of RC Shear Wall-Slab Connection Under Cyclic Loading	56
3.11.1 General Description on the Genesis of Data Used in Experiment	56
CHAPTER FOUR.....	59
RESULTS AND DISCUSSION	59
4.1 General	59
4.2 Validation of Finite Element Analysis by Experimental Result	59
4.3 Parametric Study of Exterior Reinforced Concrete Shear Wall-Slab Connection.....	60
4.3.1 Ultimate Load Carrying Capacity.....	61
4.3.1.1 Ultimate Load Carrying Capacity for U-Type Connection	61
4.3.1.2 Ultimate Load Carrying Capacity for 90 ⁰ --Type Connection.....	61
4.3.1.3 Ultimate Load Carrying Capacity for 135 ⁰ --Type Connection.....	62
4.3.1.4 Ultimate Load Carrying Capacity for 150 ⁰ --Type Connection.....	63
4.3.1. 5 Effect of Aspect Ratio of H/We on Load Carrying Capacity	64
4.3.1.6 Effects of Connection Type on Load Carrying Capacity.....	65
4.3.1.7 Effects of Concrete Grade on Load Carrying Capacity	66
4.3.2 Energy Dissipation and Damping Ratio	67

4.3.2.1 Energy Dissipation for U-Type Connection	68
4.3.2.2 Energy Dissipation for 90 ⁰ -Type Connection.....	69
4.3.2.3 Energy Dissipation for 135 ⁰ -Type Connection.....	70
4.3.2.4 Energy Dissipation for 150 ⁰ -Type Connection.....	71
4.3.2.5 Effect of Aspect Ratio of H/We on Energy Dissipation	72
4.3.2.6 Effects of Connection Type on Energy Dissipation	73
4.3.2.7 Effects of Concrete Grade on Energy Dissipation	73
4.3.3 Displacement Ductility Factor	74
4.3.4 Stiffness Degradation	76
CHAPTER 5	80
CONCLUSION AND RECOMMENDATIONS	80
5.1 Conclusion.....	80
5.2 Recommendation for Future Studies.....	81
References.....	82
Appendix A.....	85
Appendix B	92
Appendix C	100

LIST OF TABLE

Table 3.1 Concrete damaged plasticity parameters used in the proposed ABAQUS model.....	42
Table 3.2 Compressive behavior of concrete damage plasticity.....	42
Table 3.3 Tensile behavior of concrete damage plasticity.....	43
Table 3.4 Sample of slab dimension under study	46
Table 3.5 Sample of slab dimension under study scaled by 1/3.....	46
Table 3.6 The case under study and dimension of the slab reinforcement model.	48
Table 3.7 The case under study and dimension of the slab reinforcement model for 1/3 scaled down.....	48
Table 3.8 The case under study and dimension of the shear wall model.....	49
Table 3.9 The case under study and dimension of the shear wall model for 1/3 scaled down.	49
Table 3.10 Concrete properties of validity parameters (Source :[27])	56
Table 3.11 Steel properties of validity parameters (Source :[27]).....	56
Table 4.1 Comparison of FEA and experimental result.	59
Table 4.2 Cumulative energy dissipation and EVD of U-type Connection.....	68
Table 4.3 Cumulative energy dissipation and EVD of 90 ⁰ -type Connection.	69
Table 4.4 Cumulative energy dissipation and EVD of 135 ⁰ -type Connection.....	70
Table 4.5 Cumulative energy dissipation and EVD of 150 ⁰ -type Connection.	71
Table 4.6 Cumulative energy dissipation and EVD for aspect ratio of H/We.....	73
Table 4.7 Cumulative energy dissipation and EVD of Connection type.....	73
Table 4.8 Cumulative energy dissipation and EVD for grade of concrete.	74
Table 4.9 Summary of displacement at yield and ultimate load for different specimen.	76
Table A.1: Summary of concrete damage parameters	85
Table A.2 Compressive behavior of concrete damage plasticity for C-30.....	85
Table A.3 Tensile behavior of concrete damage plasticity for C-30	86
Table A.4 Compressive behavior of concrete damage plasticity for C-25	88
Table A.5 Tensile behavior of concrete damage plasticity for C-25	88
Table A.6 Compressive behavior of concrete damage plasticity for C-40.....	89
Table A.7 Tensile behavior of concrete damage plasticity for C-40	90
Table A.8 Steel properties.....	91
Table B.1 Samples of the Output from Software.....	92

LIST OF FIGURES

Figure 2. 1 Connection on Detailing of both Specimens (Source: [5])	6
Figure 2.2 Typical Dimensions of Wall-Slab Sub-Assemblage (Source: [5]).....	6
Figure2.3 Experimental setups at laboratory -support conditions (Source: [1]).....	7
Figure 2.4 Experimental setups at laboratory loading conditions (Source: [1]).....	7
Figure 2.5 Yield surfaces in the deviatric plane, corresponding to different values of K.	14
Figure 2.6 Yield surface in plane stress.	14
Figure 2.7 Yield criteria in the meridional plane.	15
Figure 2.8 Compressive stress-strain response of concrete (Source: [18]).....	19
Figure 2.9 Tensile stress-strain response of concrete (Source: [18]).....	20
Figure 2.10 Tensile stress-strain response of concrete (Source :[18]).....	21
Figure 2.11 Tensile stress-strain response of concrete (Source :[18]).....	22
Figure 2.12 Uniaxial behavior of concrete under cyclic loading (Source :[18])	24
Figure 2.13 Basic Technique for Solving the Nonlinear Equation (a) Incremental (b) Iterative (c) Incremental-iterative method (Source:[20])	27
FFigure 2.14 Midpoint Runge-Kutta incremental procedures (Source : [20])	28
Figure 2.15 Incremental-Iterative Procedures Full Newton-Raphson procedure (Source : [21]).	29
Figure 3.1 The stages used in ABAQUS	33
Figure 3.2 Various elements types (Source :[22])	35
Figure 3.3 Shear locking of first-order elements (Source :[22]).....	36
Figure 3.4 The reduction of integration points (Source :[22]).....	36
Figure 3.5 Hour glassing in reduced integration point (Source : [22]).....	37
Figure 3.6 Stress-strain model for concrete in compression (Source :[23])	39
Figure 3.7 Idealized uniaxial stress-strain curve of concrete under tension (Source :[17]).	41
Figure 3.8 Compressive stress versus inelastic strain.....	43
Figure 3.9 Tensile stress versus cracking strain.....	45
Figure 3.10 Meshing of shear wall-slab connection.	47
Figure 3.11 Boundary and loading condition.	51
Figure 3.12 Applied displacement Vs time (Source : [27])	51
Figure 3.13 Full Newton Raphson Method.....	53
Figure 3.14: Modified Newton-Raphson Method.....	53

Figure 3.15 Procedure followed for the finite element in ABAQUS 6.14	55
Figure 3.16 (a) Geometry of test units; (b) Reinforcement details of the test units under experiment set up (Source :[27]).....	57
Figure 3.17 Loading condition of test setup (Source [27]).....	58
Figure 4.1 Comparison of experimental (Source :[27]) and finite element result.	60
Figure 4.2 Comparisons of load carrying capacity of U-type connection with different aspect ratio.	61
Figure 4.3 Comparisons of load carrying capacity of 90 ⁰ -type connection with different aspect ratio.	62
Figure 4.4 Comparisons of load carrying capacity of 135 ⁰ -type connection with different aspect ratio.	63
Figure 4.5 Comparisons of load carrying capacity of 150 ⁰ -type connection with different aspect ratio.	64
Figure 4.6 Comparisons of load carrying capacity with aspect ratio.....	65
Figure 4.7 Comparisons of load carrying capacity of different connection type with the same aspect ratio of Ts/Tw=1.	66
Figure 4.8 Concrete Strength versus Load carrying Capacity	67
Figure 4.9 Definition of energy dissipation and Equivalent Viscous Damping ratio.....	68
Figure 4.10 Comparison of Energy Dissipation Capacity of U-type connection with different aspect ratio of Ts/Tw.	69
Figure 4.11 Comparison of Energy Dissipation Capacity of 90 ⁰ -type connection with different aspect ratio of Ts/Tw.	70
Figure 4.12 Comparison of Energy Dissipation Capacity of 135 ⁰ -type connection with different aspect ratio of Ts/Tw.	71
Figure 4.13 Comparison of Energy Dissipation Capacity of 150 ⁰ -type connection with different aspect ratio of Ts/Tw.	72
Figure 4.14 Method used to define the yield and ultimate displacements (Source:[28]).	75
Figure 4.15 Comparison of load – displacement envelope curves of the specimen.	75
Figure 4.16 The procedure adopted for determining secant stiffness (Source:[29]).	77
Figure 4.17 Relationship between stiffness and number of cycles for aspect ratio of Ts/Tw=0.6.	78

Figure 4.18 Relationship between stiffness and number of cycles for aspect ratio of $T_s/T_w=0.8$.
..... 78

Figure 4.19 Relationship between stiffness and number of cycles for aspect ratio of $T_s/T_w=1$.. 79

Figure A.1 Compressive stress versus inelastic strain 86

Figure A.2 Tensile stress versus cracking strain..... 87

ACRONYMS

CDP	Concrete damage-plasticity model
EVD	Equivalent Viscous Damping
FE	Finite element
H	Height of wall
We	Effective width of the slab
Ts	Thickness of slab
Tw	Thickness of shear wall
ε_c^{in}	Inelastic strain
ε_c	Total compressive strain
ε_{oc}^{el}	Elastic compressive strain corresponding to the undamaged material
σ_c	Compressive stress
E_{co}	Initial undamaged modulus of elasticity
ε_t^{cr}	Cracking strain
ε_t	Total tensile strain,
ε_{ot}^{el}	Elastic tensile strain corresponding to the undamaged material
σ_t	Tensile stress
f_{ck}	Characteristic cylindrical compressive strength of concrete at 28 days
ε_{c1}	Strain at peak stress
ε_{cu}	Ultimate strain
$\bar{\sigma}_c$	Effective compressive cohesion stresses
$\bar{\sigma}_t$	Effective tensile cohesion stresses
ψ	Dilation angle measured in the p - q plane at high confining pressure;
$\sigma_{t\theta}$	Uniaxial tensile stress at failure

CHAPTER ONE

INTRODUCTION

1.1 Background of the Study

Framed structures with RC structural walls constitute a large stock of midrise buildings, especially in regions of moderate to high seismicity. The induced oscillation during earthquakes causes stress reversal under repetitive loading, and the structural joints are the worst affected areas that usually lead to catastrophic structural failures. The lessons learned from the past earthquakes and the research works being carried out in laboratories give better understanding about the performance of the structure and their components[1].

Reinforced concrete shear walls have been used as lateral-load resisting systems in multistory buildings. The floor slabs and shear walls together act as a rigid jointed frame in resisting gravity loads and lateral loads due to wind and earthquake. The junction between the wall and the slab is subjected to severe stress concentration.

As one of the most favorable architectural systems, shear walls play great role in resisting lateral force, which normally located at lift shaft or external wall. The lateral load may come from wind loading, earthquake loading, hydrodynamic pressure from tsunami and landslide. However, the connections between floor slabs and shear walls constitute a potential weak link in structures to resist the combination of lateral and vertical loading. Wall-slab connection can develop a critical stress contour line under the worst combination of loading in this region during sway mode. To avoid redistribution of forces from wall panel to floor slab, the connection should be designed with sufficient percentage of reinforcement, and by considering stress concentration at the jointing system. The study of the behavior of connection between slab and shear wall is of paramount importance in understanding the seismic resistance of slab – wall systems. Therefore, this research was concerned on the effect of geometric parameter, connection type and concrete grade on exterior shear wall –slab connection, under cyclic load using finite element analysis.

1.2 Statement of the Problem

Very high concentration of flexural, shear and torsional stresses occurs at the wall-slab junctions in a laterally loaded tall building consisting of planar walls and coupling slabs. Due to this concentration of stresses and their interaction, there are great chances of failure to occur at the junction. Also the flexural stresses are not uniformly distributed and have the highest intensity near the periphery of exterior walls but are reduced drastically as we move away from the wall-slab junction.

Connection between floor slab and shear wall constitute an essential link in the lateral-load resisting mechanism of slab-wall and frame-wall system, and their performance can influence the pattern and distribution of lateral forces among the vertical elements of structure.

Most of the researcher are concerned on the factors that affect shear wall-slab connection such as types of connection used namely cross and anchorage bracings, types of reinforcement and detailing conditions. There is gap especially on the effect of geometric parameter on exterior shear wall-slab connection under cyclic loading.

1.3 Research Questions

In this study, the effect of geometric parameter and connection type on exterior shear wall-slab connection were investigated to answer the following questions.

1. How the ratio of height of shear wall to effective width (H/W_e) affect the exterior shear wall-slab connection?
2. How the Ratio of Thickness of Slab to Shear Wall (T_s/T_w) affect the exterior shear wall slab-connection?
3. How the behavior of exterior shear wall-slab connection affected under cyclic loading?
4. How the joint type affects the exterior shear wall-slab connection under cyclic loading?

To answer all above-mentioned questions this research presents an analytical investigation on exterior shear wall-slab connection under cyclic loading using finite element (FE).

1.4 Objective of the Study

1.4.1 General Objective

- To investigate the load carrying capacity, energy dissipation, ductility and stiffness degradation on reinforced concrete exterior shear wall-slab connection under cyclic loading.

1.4.2 Specific Objective

- To investigate the effect of height of shear wall to effective width of slab ratio (H/W_e) on exterior shear wall-slab connection under cyclic load.
- To investigate the effects of ratio of Thickness of Slab to Shear Wall (T_s/T_w) on exterior shear wall-slab connection under cyclic load.
- To investigate the behavior of exterior shear wall-slab connection under cyclic loading.
- To investigate the effect of connection type and which have a better resistance under cyclic loading.

1.4 Significance of the Study

Slab-wall connections in structure resisting lateral forces constitute a potential weak link in the preferred load path from slabs to walls, thereby influencing the pattern of lateral load distribution to the vertical members of system. One of the most critical areas in the design and construction of seismic resistant structures is the shear wall-slab joint. Since it is very expensive and time, taking to conduct large-scale experimental tests this research will help to examine the behavior of exterior shear wall-slab connection using numerical analysis. This analysis will be used to understand the behavior of exterior RC shear wall-slab connection under cyclic loading. In addition, it will provide better awareness about the effect of geometric parameter and type of connection on exterior shear-wall slab connection to select the economic section.

1.5 Scope and Limitation of the Study

The research mainly focused on the study of load carrying capacity, energy dissipation, ductility and stiffness degradation of RC exterior shear wall-slab connection based on aspect ratio of thickness of slab to thickness of shear wall (T_s/T_w) of 0.6, 0.8, 1, aspect ratio height of shear wall to effective width of the slab (H/W_e) of 1.67, 1.46, 1.30, connection type of U-type connection, 90° -type connection, 135° -type connection, 150° -type into core region, concrete grade of 25Mpa, 30Mpa, 40Mpa and steel with yield strength of 432Mpa under cyclic loading. Twelve (12) samples were considered for T_s/T_w , three (3) samples were considered for H/W_e , four (4) samples were considered for type of connection and three (3) samples were considered for connection type.

CHAPTET TWO

REVIEW OF RELATED LITERATURE

2.1 General

As already explained, a study of the behavior of joints is a paramount importance in understanding the seismic resistance of structures. To analyze such behavior, it requires modeling of materials, modeling of the structure and modeling of the loading. Finite element analysis will probably be the best choice to incorporate the variances in the above parameters. Despite several structural analysis packages being available, developing a finite element model is indeed a difficult task. There have been several attempts at modeling and analyzing reinforced concrete structural elements and joints. A review of this literature is presented in the next sections. Experimental based testing has been widely used as a means to study the behavior of structural components. While this may lead to near real life response, it is extremely time consuming, quite costly. Therefore, a comprehensive literature survey was carried out to study the research on experimental behavior of shear wall – slab connection and the influence of detailing of reinforcements at various joints. Of these the more significant literatures are briefly summarized in this chapter

2.2 Studies on Reinforced Concrete Shear Wall-Slab Connection

According to [2] study on inelastic static pushover analyses were preformed to investigate the design and capacity evaluation of shear walls. The results illustrate that the shear capacity of walls may be close to twice that calculated by codes of practice. The largest over strengths were observed in shear walls with low height-to-length ratios in which a significant portion of the lateral load was taken by direct strut action to the foundation and without placing demands on the longitudinal tension reinforcement in the shear walls. They conclude that methods in codes of practice for calculating shear wall demands and capacities need to be improved if good seismic performance of parking structures is to be achieved.

The experimental investigation were carried out on the behaviors of the RC frames (equipped with the design and implementation defects commonly encountered in the buildings in Turkey and having weak poor earthquake behavior) after they were strengthened with external shear walls with and without coupling beams. The tests give an overview of the structural behavior of bare frames and strengthened frames with external RC-SW. The study also presents the results obtained

at the end of the tests. Mixed system, established by applying external shear wall as one-side strengthening on the RC frame-type structures, significantly increases lateral load strength, rigidity and energy dissipation capacity of the bare frame. Test results showed that maximum lateral load capacity, initial rigidity and energy dissipation behaviors of the samples strengthened with external shear wall were much better than those of the bare frames [3].

Investigation carried out to study the so-called structural system "transfer-slabs", used in mid-rise buildings, in the research they performed linear and non-linear analysis for slab-wall models, using the finite element method with ANSYS program. The models were subjected to vertical and horizontal loads. The thickness of the slab, the material of walls (masonry or reinforced concrete), and the length of the wall were the studied parameters. The models used non-linear properties, so that capacity curves were obtained. They performed stress analysis at specific points for each model. They also carried out a comparative analysis of the initial stiffness of each system, and hence, they proposed Limit States from the observed behavior. When they compared the results of the models for transfer-slab (flexible base) against models with rigid base, they could observe significant differences in the behavior of both systems. The capacity of deformation and shear resistance are significantly reduced in the structural shear walls [4].

Experiment on structural performance of two types of wall-slab connection was performed. Namely cross and anchorage bracings under reversible quasi-static cyclic loading. Two identical sub-assembly of wall-slab connections are designed, constructed and tested in heavy structural laboratory. A load actuator together with load cell was positioned horizontally at the upper part of the wall for applying the lateral cyclic load. The experimental result shows that the anchorage bracing connection has higher strength, higher ductility, better energy absorption and less structural damage as compared to cross-bracing connections. They consider only the sub-assembly of reinforced concrete wall slab Connection with lateral cyclic loading applied at the upper end of the wall. The proposed dimension of the wall panel is $2000 \times 1000 \times 150$ mm and the slab dimension is $2000 \times 1000 \times 150$ mm. The sub-assembly of the specimen was attached to a foundation beam with dimension of $1800 \times 900 \times 375$ mm. Figure 2 shows the isometric view of wall, slab and foundation which was prepared in heavy structural laboratory before testing take place [5].

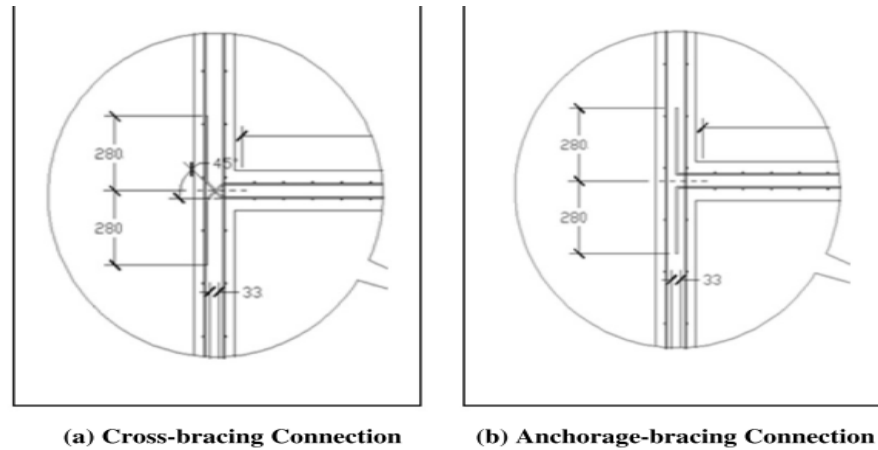


Figure 2. 1 Connection on Detailing of both Specimens (Source:[5])

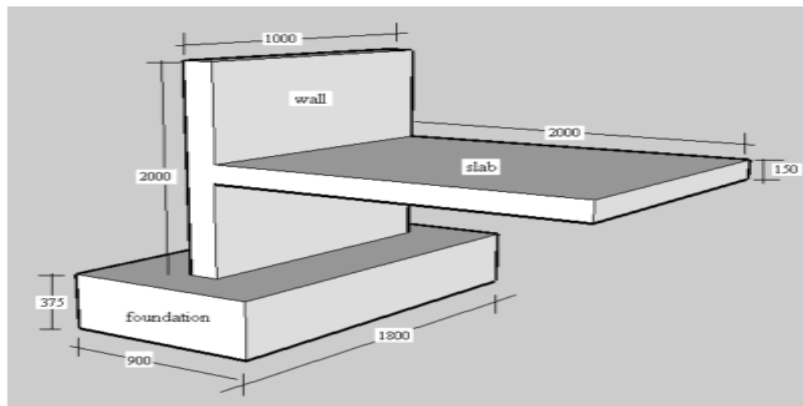


Figure 2.2 Typical Dimensions of Wall-Slab Sub-Assemblage (Source: [5])

Based on the study of [6] the seismic behavior of reinforce concrete exterior wide beam-column connections is investigated through computational simulations using ABAQUS. This study mainly focuses on the load transfer paths and different performances of the joints with conventional and wide beams. Wide beam-column connections with different beam widths and conventional beam-column joint specimen are simulated through three-dimensional analyses subjected to quasi-static cyclic loads. The numerical results show that wide beam-column joints have lower strengths and stiffness as compared to the conventional beam-column connection. It is found that lesser crack opening occurs in wide beam-column connections; hence less pinched hysteresis loops are observed. The beam width has significant effect on the load transfer paths in wide beam and joint core. The results also indicate that joint shear stress in wide beam-column connections is higher than that of conventional beam-column ones.

As per the study of [1] on experimental investigation on the effect of geometric parameters on the performance of exterior shear wall –floor slab joints subjected to cyclic loading. A prototype building situated at Chennai, India was analyzed and estimated the force components in the exterior shear wall –slab joint. The force components and the dimensions were scaled down for 1/4th model following Cauchy’s law of similitude. Experimental investigations were carried out on eight numbers of 1/4th scaled models. The loading was applied at the end of the slab. The parameters considered are (1) ratio of height of shear wall and the effective width to the slab (H/W_e), (2) ratio of thickness of slab to shear wall (t_s/t_w), and (3) developmental length of reinforcing bars.



Figure 2.3 Experimental setups at laboratory -support conditions (Source:[1])



Figure 2.4 Experimental setups^(b) at laboratory loading conditions (Source: [1])

From experimental investigation they conclude that with respect to the load-carrying capacity, the specimen has exhibited higher ultimate strength when the confining U hooks are extended for an effective width of $H/2.25$ (PT2) when compared with $H/2.8$ (PT1)

The seismic behavior of buildings is strongly affected by the arrangement of shear walls, the rigidity of floors and the connections of floors to the walls [7].

Based on the study of [8] on effect of special form of reinforcement consisting of ½ inch wide “I” sections placed at various locations within the slab around the wall periphery. This type of

reinforcement seems to have a very favorable effect and therefore the performance of wall – slab junction could be improved to the desired level. A method has been proposed which can be employed for the design of wall – slab junction using this reinforcement. Wall – Slab junction of tall building consisting of shear walls and floor slabs is one of the most highly stressed area. Possibility of junction failure increases with the increase in the height of a building. Particularly this is due to the effect of lateral forces caused by wind and earthquake. The failure is sudden, brittle and without impending warning. Therefore, attempt was made previously to increase the strength and ductility of wall – slab junction by the addition of steel wire couplets twisted together along the periphery of wall- slab junction

According to [9] carried out an experimental investigation on assembled shear wall built with precast two-way hollow slab is a new-typed shear wall built with precast concrete. In order to study its mechanical property, a quasi-static experiment is conducted with 1 reinforced concrete shear wall and 2 new type shear walls as the study objects. It was found that the internal and vertical joints of the wall body were vulnerable parts so that the new-typed shear wall experienced the loading process from the whole wall to the portioned wall. So, brittle shear failure can be avoided, deformability and anti-collapse performance are greatly improved, and shear capacity of wall body is reduced. The new-typed shear wall is reasonably structured, with convenient and reliable horizontal and vertical reinforcement, which leads to satisfactory vertical joint force-bearing capacity. Thus, it can be applied in practical construction. [10] justified that very high concentration of flexural, shear and torsional stresses occurs at the wall-slab junctions in a laterally loaded tall building consisting of planar walls and coupling slabs. Due to this concentration of stresses and their interaction, there are great chances of failure to occur at the junction. Also the flexural stresses are not uniformly distributed and have the highest intensity near the periphery of inner walls but are reduced drastically as we move away from the wall-slab junction. Numerous attempts have been made to strengthen the wall-slab junction by using various types of shear reinforcement to ensure that shear failure should not occur. Various methods including fiber reinforcement consisting of twins of twisted steel couplets have already been used. This paper describes a new method of placing 2-inch-wide flange I-sections at appropriate locations to improve the shear strength of the wall-slab junctions. Based on systematic research, a new procedure has also been developed to assess the strength of wall-slab junction using the new reinforcement method. Test results showed that a substantial increase, up to 57%, in the shear

strength of specimens was obtained by using the new method of shear reinforcement in a laterally loaded tall building. The seismic behavior of shear wall–flat slab connections with various reinforcement detailing at the joint region were studied. The modelling and assessment of scaled down exterior wall– slab connection sub-assemblages subjected to static reverse cyclic loading is presented. Three-dimensional nonlinear finite element models with different reinforcement detailing at the joint region were developed using ABAQUS/CAE software [11].

Nonlinear time history analyses were carried out, under different levels of recorded earthquake ground motion, using the computer program ABAQUS to study the seismic damage in shear wall – slab junction of an RC wall-frame building. The beams, columns, shear walls and slabs are discretized with eight-noded solid elements. The incurred cumulative damage is determined at various locations for all the three models. It is observed that the damage gets primarily concentrated at the wall – slab junction region with increasing levels of ground motion [12].

Analytical investigation carried out to understand the interaction between laterally loaded shear wall and floor slabs in building with fiber reinforced concrete at the junction of shear wall and slab. He used a ten floor building with cross wall system is analyzed. using ETABS and the shear wall slab junction was modelled using ANSYS 14.5. The models are sorted into 5 groups including control model with normal concrete and four other models with different steel fiber ratios from 0.5 to 2 percent. Non-linear analysis of models subjected to in plane and out of plane bending. The performance of the junction in terms of load-deflection, ultimate load, post cracking behavior are compared. Fiber reinforced concrete performed well for in plane bending, increasing the ultimate load and also resistance to crack, and better post cracking behavior [13].

The mechanical performance of the new-typed walls with different horizontal bars strength, quasi-static tests were carried-out for two hollow slab shear walls. The results show that strength of horizontal bars has a little influence on the hysteretic behavior and the deformation ability. While the decrease of the strength of horizontal bars can increase, the yield displacement and the peak displacement of the hollow slab shear walls. The hollow slab shear wall structure has good deformation capacity, and the brittle shear failure can be avoided [14].

2.3 Concrete

Reinforced concrete is a composite material consisting of steel reinforcement and concrete. These two materials had vastly different properties. The required mechanical properties of reinforcing steel are generally known. However, those for concrete are more difficult to define depending upon the particular condition of mixing, placing, curing, nature, rate of loading and environmental influences. Concrete contains a large number of micro-cracks, especially at interfaces between coarse aggregate and mortar, even before any load has been applied. This property is decisive for the mechanical behavior of concrete. The propagation of these micro cracks during loading contributes to the nonlinear behavior of concrete at low stress level and cause volume expansion at failure. The response of a reinforced concrete structure is determined in part by the material response of the plain concrete of which it is composed. Thus, analysis and prediction of structural response to static or dynamic loading requires prediction of concrete response to variable load histories. The fundamental characteristics of concrete behavior are established through experimental testing of plain concrete specimens subjected to specific, relatively simple load histories. Continuum mechanics provides a framework for developing an analytical model that describe these fundamental characteristics. Experimental data provide additional information for refinement and calibration of the analytical model. However, those for concrete are more difficult to define depending upon the particular condition of mixing, placing, curing, nature, rate of loading and environmental influences. Concrete contains a large number of micro-cracks, especially at interfaces between coarse aggregate and mortar, even before any load has been applied. This property is decisive for the mechanical behavior of concrete. The propagation of these micro cracks during loading contributes to the nonlinear behavior of concrete at low stress level and cause volume expansion at failure.

2.4 Concrete Damage-Plasticity Model for Finite Element Method of Analysis

Current design practice for reinforced concrete structures is an interested blend of elastic analysis to compute forces and moments, plasticity theory to proportion cross-sections for moment, axial load, and for shear. The analysis gives elastic stresses and strains, the design methods are based on forces and moments. On the other hand, finite element analysis, by breaking the structure down into small elements, it is possible to get an estimate of internal stresses and strains. The finite element approach is incompatible with modern limit state methods of proportioning concrete

structures. It is essential that proper guidance be developed to aid engineers in making the transition from finite element analyses to the selection of reinforcement.

2.4.1 Concrete –Damage Plasticity Model (CDP)

The concrete damaged plasticity model is primarily intended to provide a general capability for the analysis of concrete material and/or structures under cyclic and/or dynamic loading. The model is also suitable for the analysis of other quasi-brittle materials, such as rock, mortar, cement paste and ceramics; but it is the behavior of concrete that is used in the remainder of this section to motivate different aspects of the constitutive theory.

The CDP is currently one of the most popular concrete models used for simulation of concrete behavior in Abaqus. The main assumptions of this model are: tensile cracking and compressive crushing of concrete of concrete failure, and material stiffness is reduced by two damage parameters; the yield function is specified according to [15] and the flow potential is a hyperbolic function (Abaqus User Manual); the plastic flow is non-associated. The plastic-damage model is a form of classical plasticity theory in which the usual hardening variable is replaced by a plastic-damage variable k , similar to the former in that it never decreases, and only if plastic deformation takes place. However, the plastic damage variable cannot increase beyond the limiting value. The variable k can be non-dimensioned so that its maximum value is unity. The essential elements of the plasticity model are the yield criterion, the flow rule and the hardening rule. The plastic-damage model in Abaqus is based on the models proposed by [15] and by [16].

Features and advantages of Concrete Damaged Plasticity Model

Intended as a general capability for the analysis of concretes under monotonic cyclic and dynamic loading.

Scalar (isotropic) damage model, with tensile cracking and compressive crushing modes.

Degradation of elastic stiffness in both tension and compression.

Takes into account stiffness recovery effects in cyclic loading provides a general capability for modeling concrete and other quasi-brittle materials in all types of structures (beams, trusses, shells and solids).

Uses concepts of isotropic damage elasticity in combination with isotropic tensile and plasticity to represent the inelastic behavior of concrete even though it is intended primarily for the analysis of reinforced concrete structure.

Can be used with rebar to model concrete reinforcement.

Is designed for applications in which concrete is subjected to monotonic, cyclic and dynamic loading under low confining pressures.

Consists of the combination of no associated multi-hardening plasticity and scalar (isotropic) damaged elasticity to describe the irreversible damage elasticity to describe the irreversible damage that occurs during the fracturing process.

Allows user control of stiffness recovery effects during cyclic load reversals.

Can be used in conjunction with viscoelastic regularization of the constitutive equations in ABAQUS /Standard to improve the convergences rate in the softening regime.

2.4.2 Yield Condition

The plastic-damage concrete model uses a yield condition based on the yield function proposed by Lubliner *et al.*(1989) and incorporates the modifications proposed by [16] to account for different evolution of strength under tension and compression. In terms of effective stresses, the yield function takes the form

$$F(\bar{\sigma}, \tilde{\varepsilon}^{pl}) = \frac{1}{1-\alpha} \{\bar{q} - 3\alpha\bar{p} + \beta(\tilde{\varepsilon}^{pl})\langle \tilde{\sigma}_{max} \rangle\} - \tilde{\sigma}_c(\tilde{\varepsilon}_c^{pl}) \leq 0 \quad 2.1$$

Where α and γ are dimensionless material constants;

The effective hydrostatic pressure is;

$$\bar{p} = -\frac{1}{3}\bar{\sigma}:I \quad 2.2$$

The Misses equivalent effective stress is;

$$\bar{q} = \sqrt{\left(\frac{3}{2}\bar{S}:\bar{S}\right)} \quad 2.3$$

The deviatric part of the effective stress tensor is $\bar{\sigma}$

$$\bar{S} = P\bar{I} + \bar{\sigma} \quad 2.4$$

$\tilde{\sigma}_{max}$: is the algebraically maximum eigenvalue of $\bar{\sigma}$. The function $\beta(\tilde{\varepsilon}^{pl})$ is given as

$$\beta(\tilde{\varepsilon}^{pl}) = \frac{(\bar{\sigma}_c(\tilde{\varepsilon}_c^{pl}))}{(\bar{\sigma}_t(\tilde{\varepsilon}_t^{pl}))} (1 - \alpha) - (1 + \alpha) \quad 2.5$$

Where $\bar{\sigma}_c$ and $\bar{\sigma}_t$ are the effective compressive and tensile cohesion stresses, respectively.

In biaxial compression, with $\tilde{\sigma}_{max} < 0$ equation 2.1 reduces to well-known Drucker-Prager yield condition. The coefficient α can be determined from the initial equibiaxial and uniaxial compressive yield stress, σ_{bo} and σ_{co} as

$$\alpha = \frac{\sigma_{bo} - \sigma_{co}}{2\sigma_{bo} - \sigma_{co}} \quad 2.6$$

Typical experimental values of the ratio σ_{bo}/σ_{co} for concrete are in the range from 1.10 to 1.16, yielding values of α between 0.08 and 0.12 [15].

The coefficient γ enters the yield function only for stress states of triaxial compression, when $\tilde{\sigma}_{max} < 0$ along the tensile and compressive meridians. By definition, the *tensile meridian* (TM) is the locus of stress states satisfying the condition $\tilde{\sigma}_{max} = \tilde{\sigma}_1 > \tilde{\sigma}_2 = \tilde{\sigma}_3$ and the *compressive meridian* (CM) is the locus of the stress such that $\tilde{\sigma}_{max} = \tilde{\sigma}_1 = \tilde{\sigma}_2 > \tilde{\sigma}_3$, where $\tilde{\sigma}_1, \tilde{\sigma}_2$ and $\tilde{\sigma}_3$ are the eigenvalues of the effective stress tensor. It can be easily shown $(\tilde{\sigma}_{max})_{TM} = \frac{2}{3}\bar{q} - \bar{p}$ and $(\tilde{\sigma}_{max})_{CM} = \frac{1}{3}\bar{q} - \bar{p}$ along the tensile and compressive meridians, respectively. With $\tilde{\sigma}_{max} < 0$ corresponding yield conditions are

$$\left(\frac{2}{3}\gamma + 1\right)\bar{q} - (\gamma + 3\alpha)\bar{p} = (1 - \alpha)\bar{\sigma} \quad , (TM) \quad 2.7$$

$$\left(\frac{1}{3}\gamma + 1\right)\bar{q} - (\gamma + 3\alpha)\bar{p} = (1 - \alpha)\bar{\sigma} \quad , (CM) \quad 2.8$$

Let $K_C = \bar{q}(TM)/\bar{q}(CM)$ for any given value of the hydrostatic pressure \bar{p} with $\tilde{\sigma}_{max} < 0$; then

$$K_C = \frac{\gamma+3}{2\gamma+3} \quad 2.9$$

The fact that K_C is constant does not seem to be contradicted by experimental evidence[15]. The coefficient γ is, therefore evaluated as

$$\gamma = \frac{3(1-K_C)}{2K_C-1} \quad 2.10$$

A value of $K_C = \frac{2}{3}$, which is typical for concrete, gives $\gamma = 3$.

If $\tilde{\sigma}_{max} > 0$ the yield conditions along the tensile and compressive meridians reduce to

$$\left(\frac{2}{3}\beta + 1\right)\bar{q} - (\gamma + 3\alpha)\bar{p} = (1 - \alpha)\bar{\sigma} \quad , (TM) \quad 2.11$$

$$\left(\frac{1}{3}\beta + 1\right)\bar{q} - (\gamma + 3\alpha)\bar{p} = (1 - \alpha)\bar{\sigma} \quad , (CM) \quad 2.12$$

Let $K_t = \bar{q}(TM)/\bar{q}(CM)$ for any given value of the hydrostatic pressure \bar{p} with $\tilde{\sigma}_{max} > 0$; then

$$K_t = \frac{\beta+3}{2\beta+3}$$

2.13

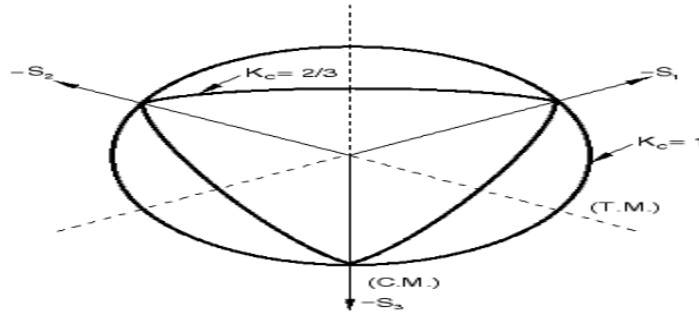


Figure 2.5 Yield surfaces in the deviatoric plane, corresponding to different values of K .

Typical yield surfaces are shown in Figure 2–5 in the deviatoric plane and in Figure 2–6 for plane-stress conditions.

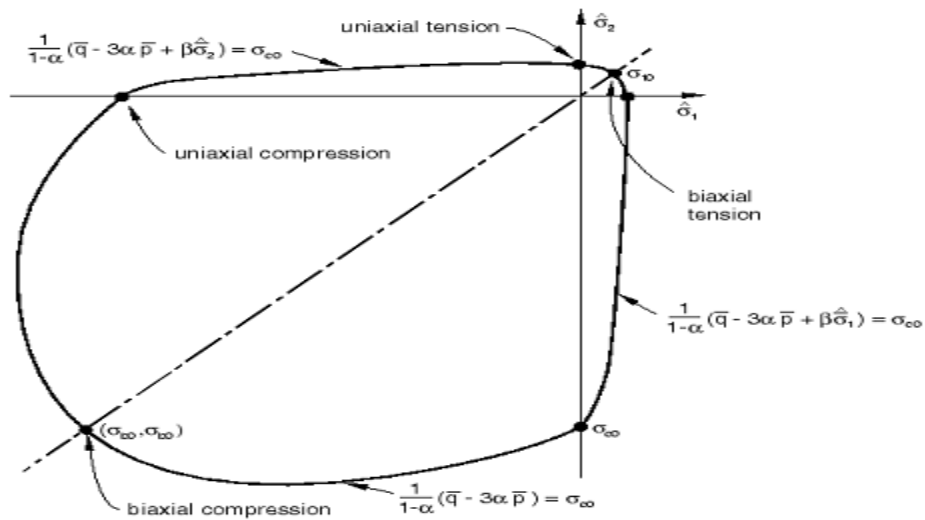


Figure 2.6 Yield surface in plane stress.

2.4.3 Flow Rule

The plastic-damage model assumes no associated potential flow,

$$\dot{\epsilon}^{pl} = \lambda \frac{\partial G(\bar{\sigma})}{\partial \bar{\sigma}} \quad 2.14$$

The flow potential G chosen for this model is the Drucker-Prager hyperbolic function:

$$\sqrt{(\epsilon \sigma_{t\theta} \tan \phi)^2 + \bar{q}^2} - \bar{p} \tan \phi \quad 2.15$$

Where ψ is the dilation angle measured in the p - q plane at high confining pressure; $\sigma_{t\theta}$ is the uniaxial tensile stress at failure; and ε is a parameter, referred to as the eccentricity that defines the rate at which the function approaches the asymptote (the flow potential tends to a straight line as the eccentricity tends to zero). This flow potential, which is continuous and smooth, ensures that the flow direction is defined uniquely. The function asymptotically approaches the linear Drucker-Prager flow potential at high confining pressure stress and intersects the hydrostatic pressure axis at 90° .

Because plastic flow is no associated, the use of the plastic-damage concrete model requires the solution of non-symmetric equations. The models described here are extensions of the original Drucker-Prager model (Drucker and Prager 1952). In the context of geotechnical materials, the extensions of interest include the use of curved yield surfaces in the meridional plane, the use of noncircular yield surfaces in the deviatoric stress plane, and the use of no associated flow laws. In the context of polymeric and composite materials, the extensions of interest are mainly the use of no associated flow laws and the inclusion of rate-dependent effects. In both contexts, the models have been extended to include creep.

2.4.4 Available Yield Criteria

Three yield criteria are provided in this set of models. They offer differently shaped yield surfaces in the meridional plane (p - q plane): a linear form, a hyperbolic form, and a general exponent form (See Figure 2:7)

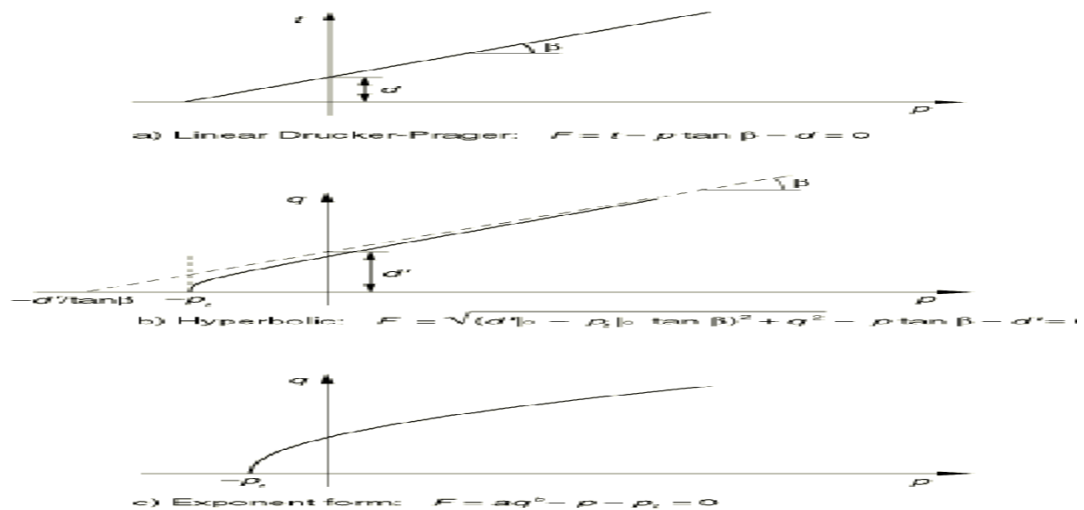


Figure 2.7 Yield criteria in the meridional plane.

The choice of model depends largely on the material, the experimental data available for calibration of the model parameters, and on the range of pressure stress values likely to be encountered. The linear model (available in Abaqus/Standard) provides a noncircular section in the deviatoric (II) plane, associated inelastic flow in the deviatoric plane, and separate dilation and friction angles. The smoothed surface used in the deviatoric plane differs from a true Mohr-Coulomb surface that exhibits vertices. This has restrictive implications, especially with respect to flow localization studies for granular materials, but this may not be of major significance in many routine design applications. Input data parameters define the shape of the yield and flow surfaces in the deviatoric plane as well as the friction and dilation angles, so that a range of simple theories is provided; for example, the original Drucker-Prager model (Drucker and Prager, 1952) is available within this model. The hyperbolic and general exponent models (available in Abaqus/Standard only) use a von Mises (circular) section in the deviatoric stress plane with associated plastic flow. A hyperbolic flow potential is used in the meridional plane, which, in general means non-associated flow.

2.4.5 Viscoplastic Regularization

Material models exhibiting softening behavior and stiffness degradation often lead to severe convergence difficulties in implicit analysis programs. Some of these convergence difficulties can be overcome by using a viscoplastic regularization of the constitutive equations. The concrete damaged plasticity model can be regularized using viscoplasticity, therefore permitting stresses to be outside of the yield surface. We use a generalization of the Duvaut-Lions regularization, according to which the viscoplastic strain rate tensor

$$\dot{\varepsilon}_v^{\sim pl} = \frac{1}{\mu} (\varepsilon^{pl} - \varepsilon_v^{pl}) \quad 2.16$$

Here μ is the viscosity parameter representing the relaxation time of the viscoplastic system and ε^{pl} is the plastic strain evaluated in the inviscid backbone model. Similarly, a viscous stiffness degradation variable, \dot{d}_v for the viscoplastic system is

$$\dot{d}_v = \frac{1}{\mu} (d - d_v) \quad 2.17$$

Where d is the degradation variable evaluated in the inviscid backbone model. The stress-strain relation of the viscoplastic model is given as

$$\sigma = (1 - d_v) D_0^{el} : (\varepsilon - \varepsilon_v^{pl}) \quad 2.18$$

The solution of the viscoplastic system relaxes to that of the inviscid case as $t/\mu \rightarrow \infty$ where t represents time. Using the viscoplastic regularization with a small value for the viscosity parameter (small compared to the characteristic time increment) usually, helps improve the rate of convergence of the model in the softening regime, without compromising results.

2.5 Steel Reinforcement

Since the reinforcing bars are normally long and relatively slender, they can generally be assumed to be capable of transmitting axial forces only. The useful strength of ordinary reinforcing steels in tension as well as compression (yield strength) is about 15 times the compressive strength of common structural concrete and well over 100 times its tensile strength. Steel reinforcement is a high cost material compared with concrete. It also used to resist compressive force in addition to tension force. The most common types of reinforcement are hot rolled round deformed bars. The closely spaced rib shaped surface deformations of the reinforcing bars provide a high degree of interlocking of the two materials.

The uniaxial tensile stress–strain behavior of reinforcement was assumed to be elastic with conventional Young’s modulus and Poisson’s ratio. The plastic behavior is also modeled including yield stress and corresponding plastic strain. Properties of plastic phase is defined to the model using bilinear behavior.

2.6 Constitutive Models of Concrete in ABAQUS

There are three concrete constitutive models supported by ABAQUS, and their application depends on the type of structural loading and cracking analysis. These models include: Smeared Crack Model (SCM), Brittle Cracking Model (BCM), and Concrete Damaged Plasticity Model (CDPM). The three models are fully capable of modeling a variety of concrete structures such as beams, trusses, shells, and solids. Although, these models can be used for plain concrete or other quasi-brittle materials, they are mainly utilized to model reinforced concrete structures [17].

The Smeared Crack Model (SCM) can be employed in ABAQUS/Standard and is primarily used for concrete structures subjected to monotonic loadings at low confining pressure. Cracking of concrete is one of the most crucial aspects in any structural analysis, and thus it is imperative to implement the cracking and post-cracking behavior of concrete in the modelling. A smeared crack approach is usually used to reflect the discontinuous brittle response of cracked concrete.

However, this technique does not track the formation of macro cracks; instead, it updates the stress and stiffness material properties to account for the crack effect.

The Brittle Cracking Model (BCM) is usually implemented in ABAQUS/Explicit and is intended for applications in which tensile cracking of materials is dominant. This approach is suitable for ceramics, brittle rocks, and plain concrete. In this model, the concrete compressive behavior is assumed to be linear-elastic which is an enormous simplification of the actual response. Thus, the BCM is only practical in applications where tensile behavior overshadows the assumption of linear-elastic compression model. The BCM only represents the brittle aspects of concrete behavior (i.e. when micro-cracks merge to form discrete macro-cracks resulting in a highly localized deformation).

On the other hand, the Concrete Damaged Plasticity Model (CDPM) can be utilized in both ABAQUS/Standard and ABAQUS/Explicit. It is usually used to analyze plain concrete and other quasi-brittle materials. The CDPM can be implemented for the analysis of concrete structures under monotonic, cyclic, and dynamic loading under low confining pressure. It is proven that Concrete Damaged Plasticity Model is highly flexible in modelling concrete under different loading conditions. Therefore, the CDPM model was selected for the analysis of concrete materials in this study, and will be reviewed in broader details in the following section.

2.7 Concrete Damage Plasticity Model

In most recent numerical studies of concrete materials, including this research work, plasticity and damage evolution of concrete parts are considered in the basic finite element modelling. The typical damaged plasticity model uses the concepts of isotropic tensile and compressive plasticity to represent the inelastic behavior of concrete. These concepts are reflected by the assumption of two failure mechanisms: tensile cracking and compressive crushing of concrete composites. Hardening variables correspond to the extent of damage in concrete, and stiffness degradation parameter is used to characterize the uniaxial tensile and compressive stress-strain relationships under applied loads. The hardening variables are then used in cooperation with the yield surface to identify the failure mechanisms under tensile and compressive loading. In concrete modelling, a non-associated plastic flow potential is implemented using the Drucker Pager hyperbolic function to represent flow potential. Furthermore, a Viscoplastic regularization of the constitutive models is sometimes used to improve the convergence rate in the concrete softening and stiffness

regimes. The following sections give more details on the available constitutive models which are used for the concrete plasticity concepts.

2.7.1 Behavior of Concrete in Compression Model

Fig. 2.8 shows the concrete behavior in uniaxial loading in compression. Under uniaxial compression the response is linear until the value of initial yield, σ_{co} is reached. In the plastic regime the response is typically characterized by stress hardening followed by strain softening beyond the ultimate stress, σ_{cu} . When the concrete specimen is unloaded from any point on the strain softening branch of the stress-strain curves, the unloading response is weakened and the elastic stiffness of the material is degraded or damaged. The degradation of the elastic stiffness is characterized by damage variable, d_c , which can take values from zero, representing the undamaged material, to one, representing the total loss of strength.

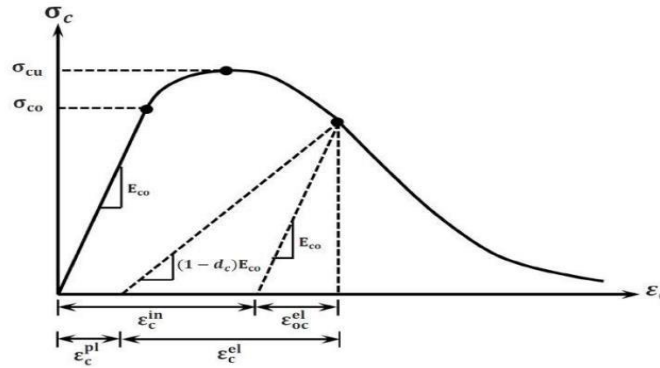


Figure 2.8 Compressive stress-strain response of concrete (Source: [18])

The elastic compression behavior of concrete can be modeled by calculating the initial undamaged modulus of elasticity, E_{co} . For the inelastic response, compressive stresses are provided in a tabular form as a function of the inelastic strain, ε_c^{in} which can be calculated by the following equation:

$$\varepsilon_c^{in} = \varepsilon_c - \varepsilon_{oc}^{el} = \varepsilon_c - \frac{\sigma_c}{E_{co}} \quad 2.19$$

Where ε_c^{in} the inelastic strain, ε_c is the total compressive strain, ε_{oc}^{el} is the elastic compressive strain corresponding to the undamaged material, σ_c is the compressive stress, and E_{co} is the initial undamaged modulus of elasticity. The inelastic strain data are inputted in the material definition section of ABAQUS model as positive values, starting at zero value corresponding to the initial yield point.

2.7.2 Behavior of Concrete in Tension Model

Fig.2.9 illustrates the concrete behavior in uniaxial loading in tension. The stress-strain response follows a linear elastic relationship until the failure stress (σ_{to}). Beyond the failure stress, there will be a softening stress-strain response. When the concrete specimen is unloaded from any point on the strain softening branch of the stress-strain curve, the unloading response is weakened and the elastic stiffness of the material is degraded or damaged. The degradation of the elastic stiffness is characterized by damage variable in tension d_t , which can take value from zero, representing the undamaged material, to one, representing the total loss of strength.

In a typical reinforced concrete beam, the concrete (a quasi-brittle material) is bonded to the reinforcement. When cracking initiates in the member, concrete continues to resist some tensile stresses between the cracks. This characteristic is referred to as “tension stiffening”, and it helps improve the control of the deformation of an RC member and the growth of crack widths.

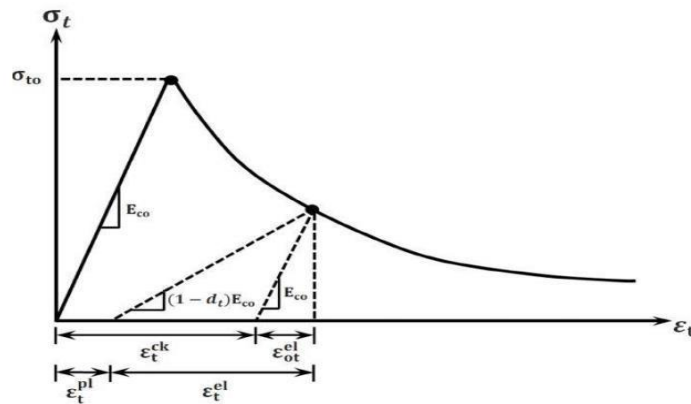


Figure 2.9 Tensile stress-strain response of concrete (Source: [18])

In ABAQUS, the user is required to define the post-peak tensile response of concrete in order to account for the interaction between the concrete and the reinforcing bars. The Concrete Damaged Plasticity Model in ABAQUS provides three different methods that can be used to characterize the post-peak response of concrete in tension:

1. The tensile stress in concrete can be entered in a tabular form as a function of the corresponding cracking strain, ϵ_t^{CT} .
2. The tensile stress can be entered in a tabular form as a function of the crack opening displacement, w .
3. The value of concrete fracture energy, G_f can be simply inputted into the model.

In the first method, the user can plot a stress-strain curve similar to that illustrated in Figure 3.3. The post-peak response can be determined in a procedure similar to the one described in the concrete compression model. The cracking “inelastic” strain ε_t^{cr} can be calculated using the following expression:

$$\varepsilon_t^{cr} = \varepsilon_t - \varepsilon_{ot}^{el} = \varepsilon_t - \frac{\sigma_t}{E_{co}} \quad 2.20$$

Where ε_t^{cr} is the cracking strain, ε_t is the total tensile strain, ε_{ot}^{el} is the elastic tensile strain corresponding to the undamaged material, σ_t is the tensile stress, and E_{co} is the initial undamaged modulus of elasticity. Similarly, the cracking strain data are entered in the Concrete Damaged Plasticity Model of ABAQUS model in a positively increasing manner. The first value is set as zero corresponding to the initial yield stress.

In the second method, the post-peak tensile behavior of concrete is defined in a way that the user has to input the tensile stress as a function of the crack-opening-displacement, w .

Hillerborg, Mod er and Petersson, (1976) has proposed the concept of using fracture energy, G_f , in this method. This fracture energy of a brittle material corresponds to the energy required to open a crack of unit area. Therefore, the post-peak behavior of concrete is idealized by a stress-displacement response rather than a stress-strain response as in the first method. The user has the liberty to modify the tension stiffening response of the concrete member by selecting one of the proposed examples of stress-displacement curves as shown in Figure 2.10.

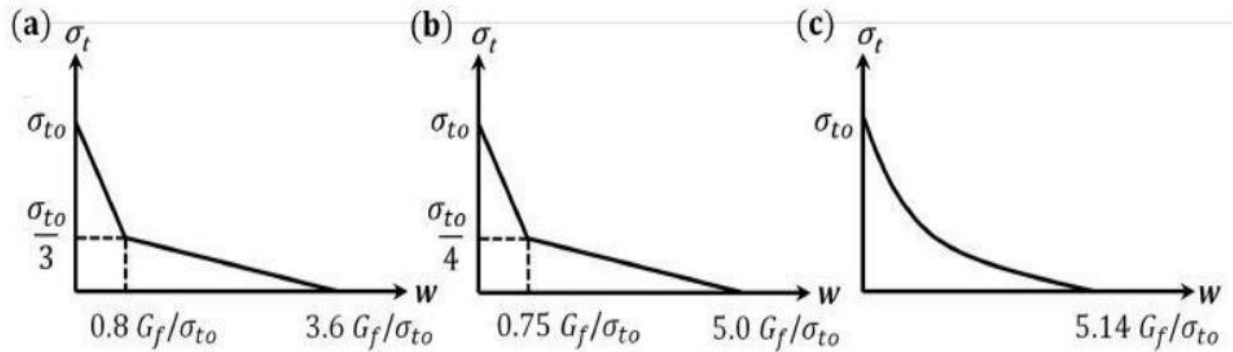


Figure 2.10 Tensile stress-strain response of concrete (Source: [18])

It is worth mentioning that the area under these curves represents the fracture energy of the material. Therefore, this method has the advantage of allowing the user to define the rate of strength loss after cracking and also the material’s fracture energy [17].

Finally, the third method allows the user to simply define the tensile peak stress, σ_{to} and the value of the fracture energy, G_f . As it can be seen in Figure 2.11, this method assumes a linear stress-displacement post-failure response.

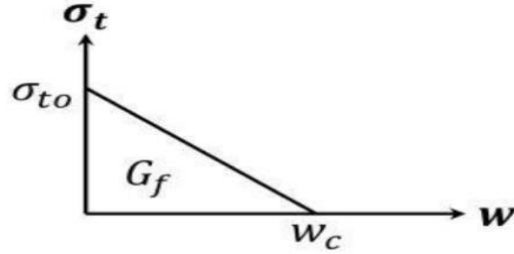


Figure 2.11 Tensile stress-strain response of concrete (Source: [18])

The user is expected to identify the value of the peak stress and the area under the linear curve (i.e. the calculated fracture energy). Then after, the maximum crack displacement corresponding to a complete loss of strength, w_c is computed by the equation:

$$w_c = \frac{2G_f}{\sigma_{to}} \quad 2.21$$

2.7.3 Damage Modeling

Sometimes, unloading of the concrete member can occur within the post-peak region of the compression and tension stress-strain curves. In such case, the unloading response becomes weaker and degraded, and modulus of elasticity is utilized to account for this degradation as expressed in Figure 2.8 and Figure 2.9. This degradation during the unloading phase is identified by two damage variables, d_c and d_t for member subjected to compression and tension, respectively. The damage parameters are functions of the plastic strains ε_c^{pl} and ε_t^{pl} , temperature θ , and other predefined field variables f_i , as can be seen in the next equations.

It is noted that the values of the damage parameters ranges from zero (corresponding to the undamaged material) to one (for the material with complete loss of strength).

$$d_c = d_c(\varepsilon_c^{pl}, \theta, f_i) \quad 0 \leq d_c \leq 1.0 \quad 2.22$$

$$d_t = d_t(\varepsilon_t^{pl}, \theta, f_i) \quad 0 \leq d_t \leq 1.0 \quad 2.23$$

As it has been mentioned previously, the damage parameters are functions of plastic strains, and hence, ABAQUS will automatically generate the plastic strains from the user-defined inelastic or

cracking strain. The plastic strain in compression is obtained by converting the inelastic strain ε_c^{in} , and damage parameters, d_c as expressed below:

$$\varepsilon_c^{pl} = \varepsilon_c^{in} - \frac{d_c}{1-d_c} \frac{\sigma_c}{E_{co}} \quad 2.24$$

Where: E_{co} : is the initial undamaged modulus of elasticity However, the calculation of plastic strain in tension depends on the method used to define the tensile post-peak response of concrete. If the first method was used, damage parameters are provided as functions of the cracking strains, ε_t^{cr} which are converted to plastic strains as shown below:

$$\varepsilon_t^{pl} = \varepsilon_t^{cr} - \frac{d_t}{1-d_t} \frac{\sigma_t}{E_{co}} \quad 2.25$$

However, if method two or three was used to define the tensile post-peak curve of the concrete member, damage parameter values are considered as functions of the crack-opening displacement, u_t^{cr} (also referred to as w). The plastic displacements are then obtained by the equation:

$$u_t^{pl} = u_t^{cr} - \frac{d_t}{1-d_t} \frac{\sigma_t l_o}{E_{co}} \quad 2.26$$

and the term l_o corresponds to the specimen length which is assumed to be equal to 1.0. Furthermore, the value of the damage parameter ought to be controlled within the range of 0.99 to avoid severe damage, and thus possible convergence issues [17]. When the initial undamaged modulus of elasticity E_{co} is identified, the stress-strain response of the concrete under tension and compression with consideration of the degradation of the elastic stiffness can be represented by:

$$\sigma_c = (1 - d_c) E_{co} (\varepsilon_c - \varepsilon_c^{pl}) \quad 2.27$$

$$\sigma_t = (1 - d_t) E_{co} (\varepsilon_t - \varepsilon_t^{pl}) \quad 2.28$$

It should, however, be mentioned that a concrete structure subjected to uniaxial load will exhibit crack initiation and propagation. Therefore, a reduction in the expected load carrying area is expected which in turn increases the concrete effective stresses. ABAQUS accounts for that phenomenon by calculating these effective compressive and tensile stresses, σ_c and σ_t , respectively. These terms are expressed in the following equation:

$$\bar{\sigma}_c = \frac{\sigma_c}{1-d_c} E_{co} (\varepsilon_c - \varepsilon_c^{pl}) \quad 2.29$$

$$\bar{\sigma}_t = \frac{\sigma_t}{1-d_t} E_{co} (\varepsilon_t - \varepsilon_t^{pl}) \quad 2.30$$

2.7.4 Behavior of Concrete Under Cyclic Loading

It is known that reinforced concrete recover stiffness even if tensile cracking and stiffness reduction occurs in the tension side. It is result from closing crack again in the process of stress is shifted to the compression side. In order to simulate the crack closing process, the stiffness recovering coefficient of w_t and w_c are set for Abaqus.

Figure 2.12 is a schematic diagram of a process of a stiffness recovery shown in the Abaqus theory guide. Thus, user can set a stiffness recovering behavior by using a coefficient w_c ($0 \sim 1$) how the tension damage involves the stiffness at the transition to compression side. In addition, it is the same for a transition back to the tension side. Figure 2.12 shows default settings of Abaqus that represents stiffness recovering at the transition from tension to compression side and damage cumulating at the transition from compression to tension side.

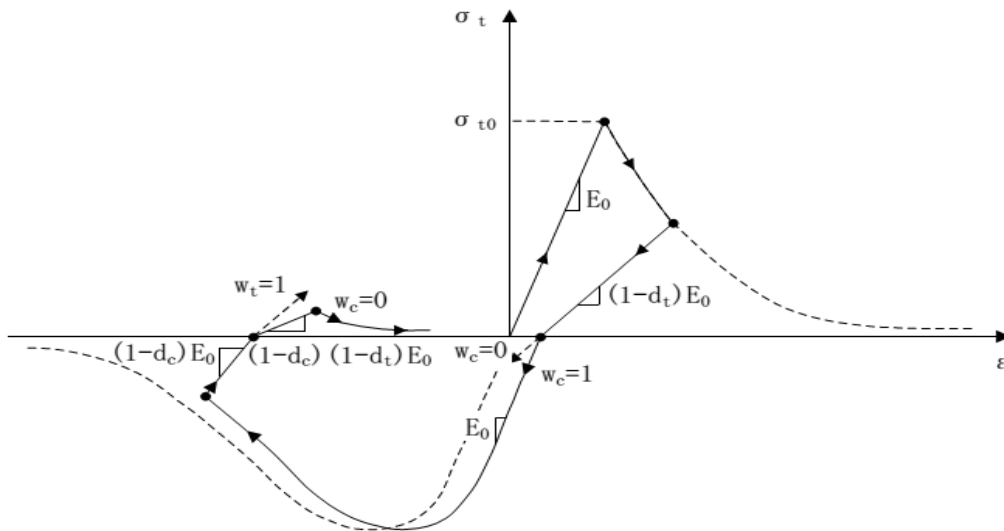


Figure 2.12 Uniaxial behavior of concrete under cyclic loading (Source: [18])

2.8 Nonlinear Finite Element Analysis

In any three-dimensional finite element analysis, the performance of any structural member under load depends on the behavior of the type of material used to construct the member. In concrete members which are made of different materials, concrete and reinforcing bars are brought together to behave as a composite system. The steel can be considered as a homogeneous material that exhibits a similar stress-strain relationship in tension and compression. While, the behavior of

concrete is monitored to have grossly heterogeneous internal structure because it is dependent on the properties of each of its components; namely, cement mortar, aggregates and air voids. One of the main objectives of the finite element analysis of structures is to determine the response of the structure under loading. A nonlinear structural problem must obey the basic laws of continuum mechanics, i. e. equilibrium, compatibility, and the constitutive relations of the material. Displacement compatibility is automatically satisfied in the displacement finite element technique. Common nodes between elements ensure continuity and compatibility of displacements along internal element boundaries (including the nodes) and polynomial shape functions ensure continuity and single valued displacements internally. Therefore, it becomes only necessary to enforce that the nonlinear constitutive relations are correctly satisfied whilst at the same time preserving the equilibrium of the structure.

In general, for a particular load level, a number of successive linear solutions are required to remove the residual forces to a desired degree of accuracy. The method is obviously iterative in nature and the final results will depend on the factors associated with the iterative process, for example the increment size, accuracy required, the exact type of solution process employed etc. Clearly it is impossible to obtain a unique solution to a particular problem because of these many factors.

There can be several causes of nonlinear behavior in a structure, which can be divided into two classes:

- a. Nonlinear material behavior,
- b. Geometric changes (i.e. large deformations) in the structure, including changing boundary conditions.

Stress-strain relations are a major source of nonlinearity. These can vary from short-term nonlinear relationships between stress and strain such as plasticity, cracking, nonlinear elasticity, etc., to time-dependent effects such as creep, viscoelastic behavior, shrinkage, etc.

Changes in the external boundary conditions are, in a sense, another source of geometric nonlinearity. For example, beams on elastic foundations in which the size and location of contact zones between beam and foundation depends on the nature of the applied force. In certain circumstances, reinforced concrete structures present another example where boundary conditions change with varying load. Cracking and crushing cause separation of adjacent parts of the

structure, which can be interpreted as a new geometric configuration, and this interpretation can be included in analytical procedures, such as the spring element method.

2.8.1 Numerical Integration

In most finite element analyses, the element stiffness matrix $[K_e]$ cannot be obtained analytically. Thus, to perform the integration required to evaluate the element stiffness matrix, a suitable scheme of numerical integration has to be used. In this study numerical integration is required because analytical integration is impossible. For this purpose, Gauss-Legendre quadrature rules have been used extensively because of their higher efficiency over other forms of quadrature. They can integrate exactly a polynomial $f(\xi)$ of degree $(2n-1)$, where n is the number of sampling points. Also they are suitable for isoparametric elements because the range of these integration rules are ± 1 which coincides with the local coordinate system of limits ± 1 on element boundaries.

The application of the three-dimensional finite element analysis in connection with the nonlinear behavior of structures needs a large amount of computation time due to frequent evaluation of the stiffness matrix. Therefore, it is necessary to choose a suitable integration rule that minimizes the computation time but with sufficient accuracy.

Hence, the equations of the stiffness matrix element in one, two and three dimensions can be expressed as equation (a, b, c) respectively [20]:

$$I = \int_{-1}^1 f(\xi) d\xi \approx \sum_{j=1}^m W_j f(\xi_j) \quad 2.31$$

$$I = \int_{-1}^1 \int_{-1}^1 f(\xi, \eta) d\xi d\eta \approx \sum_{i=1}^n \sum_{j=1}^m W_i W_j f(\xi_i, \eta_j) \quad 2.32$$

$$I = \int_{-1}^1 \int_{-1}^1 \int_{-1}^1 f(\xi, \eta, \zeta) d\xi d\eta d\zeta \approx \sum_{i=1}^n \sum_{j=1}^m \sum_{k=1}^l W_i W_j W_k f(\xi_i, \eta_j, \zeta_k) \quad 2.33$$

Where: n, m, l Total number of integration points.

ξ_i, η_j, ζ_k Coordinate of the $i^{\text{th}}, j^{\text{th}}$ and k^{th} integration point.

W_i, W_j, W_k the $i^{\text{th}}, j^{\text{th}}$ and k^{th} weighting factor

2.8.2 Techniques for Solving Nonlinear Analysis

The finite element discrimination process yields a set of simultaneous equations:

$$[F^a] = [K][U] \quad 2.34$$

Where: $[K]$: is the stiffness matrix

$[U]$: is the vector of nodal displacements

$[F^a]$: is the vector of applied loads.

The solutions of nonlinear problems by the finite element method are usually attempted by one of three basic techniques [20]:

- Incremental (step-wise procedure).
- Iterative (Newton method).
- Incremental-iterative (mixed procedure).

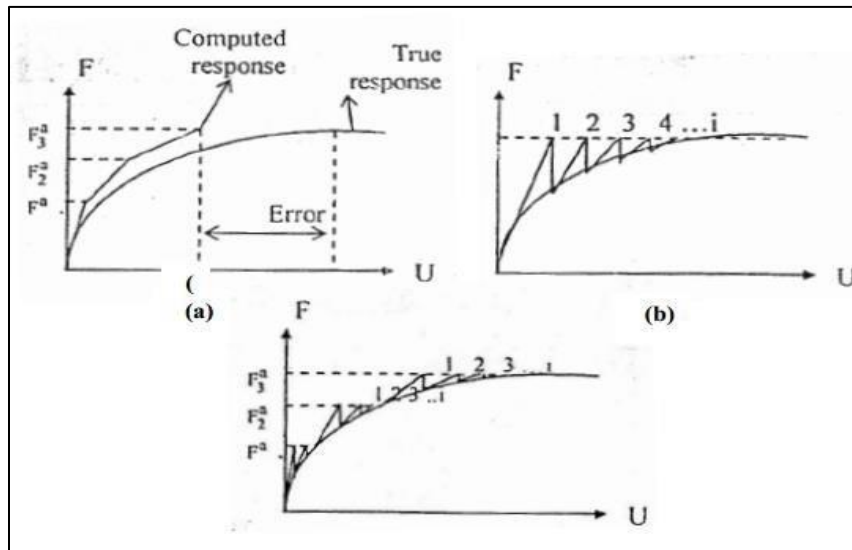


Figure 2.13 Basic Technique for Solving the Nonlinear Equation (a) Incremental (b) Iterative (c) Incremental-iterative method (Source:[20])

A. Incremental method

The basis of the incremental method is the subdivision of the total applied load vector into smaller load increments, which do not necessarily need to be equal. During each load increment, the equation (2.34) is assumed to be linear, i. e. a fixed value of $[K]$ is assumed using material data existing at the end of the previous increment. Nodal displacements can then be obtained for each increment and these are added to the previously accumulated displacements. The process is repeated until the total load is reached.

The accuracy of this procedure depends on the increment size; the smaller the increments the better the accuracy, but at the same time the more computational effort required. A modification of this method is the "midpoint Runge-Kutta" method [20]. In this, the first step is to apply half the load increment and to calculate new stiffness's corresponding to the total stresses at this value. This stiffness's are then utilized to compute an approximation for the full load increment.

The incremental method in its original and modified form do not account for force redistribution during the application of the incremental load (i. e. No iteration process exists to restore equilibrium).

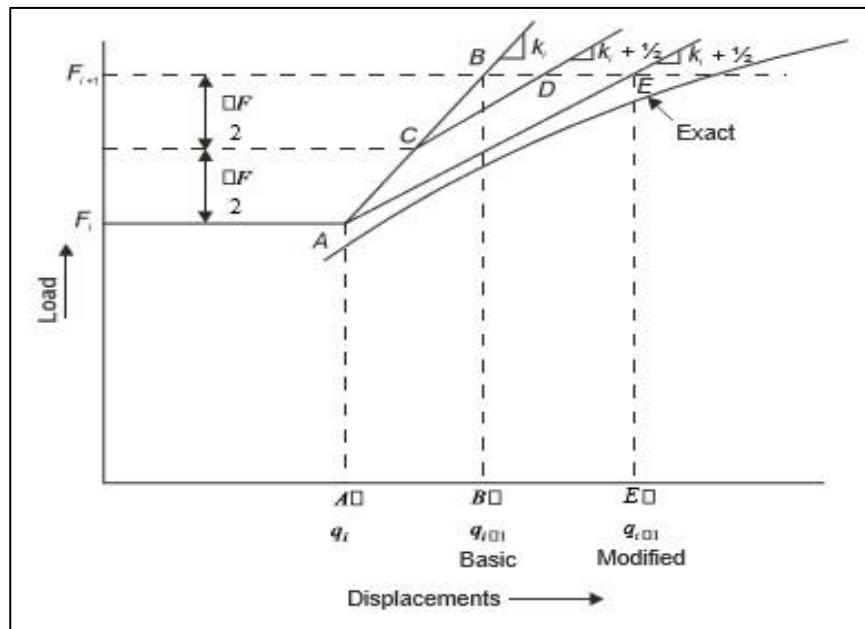


Figure 2.14 Midpoint Runge-Kutta incremental procedures (Source: [20])

B. Iteration method

In the iteration method, the full load is applied in one increment. Stresses are evaluated at that load according to the material law. This gives equivalent forces which may not be equal to the external applied forces, i. e. equilibrium is not necessarily satisfied. Then, the portion of the total loading that is not balanced is calculated as the difference between the total applied load vector and internal nodal forces. These are the unbalanced nodal forces $[F]$ which are then used to compute an additional increment of displacements, and hence new stresses, which give a new set of equivalent nodal forces. This process is repeated until equilibrium is approximated to a certain degree of

accuracy. When this stage is reached the total displacement is calculated by summing the displacements from each iteration.

This process can be written as:

$$[K_i^T][\Delta U_i] = [F^a] - [F^{nr}] \quad 2.35$$

$$[\Delta U_{i+1}] = [U_i] + [\Delta U_i] \quad 2.36$$

Where: $[K]$: is the stiffness matrix

(i): is the subscript representing the current equilibrium iteration and

F^{nr} : is the internal load vector.

This procedure fails to produce information about the intermediate stage of loading. For structural analysis including path-dependent nonlinearities increments are in equilibrium in order to correctly follow the load path. This can be achieved by using the combined incremental iterative method.

C. Incremental-iterative method

In this method a combination of the incremental and iterative process is used. The load is applied in increments and the solution at that load is obtained iteratively until equilibrium is obtained.

When Full Newton-Raphson procedure is applied the stiffness matrix is formed at every iteration. The advantage of this procedure may give more accurate result. The disadvantage of this procedure is that a large amount of computational effort may be required to form and decompose the stiffness matrix, as shown in Figure 2.15.

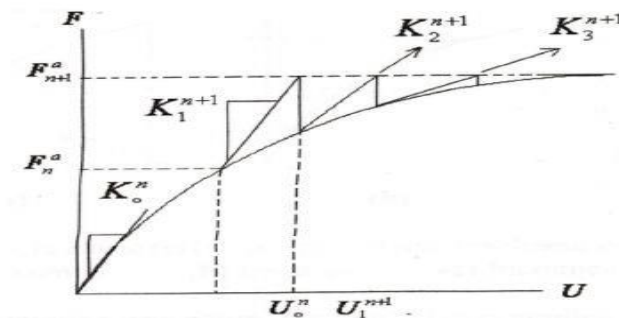


Figure 2.15 Incremental-Iterative Procedures Full Newton-Raphson procedure (Source: [21])

2.8.3 Converging Criteria

If a solution strategy based on iterative methods is to be effective, realistic criteria should be used for the termination of the iteration. At the end of each iteration, the solution obtained should be

checked to see a convergence. If the convergence tolerances are too loose, inaccurate results are obtained, and if the tolerances are too tight, much computational effort is spent to obtain needless accuracy. For every incremental load the iteration continues until convergence is achieved. The convergence criterion for the nonlinear analysis of structural problems can be classified as: force criterion, displacement criterion and stress criterion.

In displacement criterion, the incremental displacements at iteration i^{th} and the total displacements are determined. The solution is considered to be converged when the norm of the incremental displacements is within a given tolerance of the norm of the total displacements; infinite norm is used and takes the form:

$$\|\{\Delta U_i\}\| = (\max|\Delta U_i|) \leq T_n(\max|\Delta U_i|) \quad 2.37$$

Where: U may equal u, v, w or θz .

For force criteria the norm of the residual forces at the end of each iteration are checked against the norm of the current applied forces as:

$$\|\{R\}\| = (\sum R_i^2)^{0.5} \leq T_n(\sum F_i^2)^{0.5} \quad 2.38$$

Where $\{R\}$ is the residual vector:

$$\{R\} = \{F^a\} - \{F^{nr}\} \quad 2.39$$

The main function of convergence criteria is to control the number of iterations in an increment. The control is exercised by the user through the choice of convergence tolerances and the type of norm. In most cases the user will also specify a maximum number of iterations allowed, irrespective of the state of convergence. The number of iterations will influence the predicted shape of the load- deformation curve and ultimate load, e. g. too few might give an over stiff response.

Hence it is of paramount importance that the user understands the factors influencing convergence behavior and redistribution of forces. Very little information on these aspects exist in published literature, but it is clear that more is required if unreliable results are to be avoided. Fine tolerances are theoretically desirable but can be very expensive to obtain because they quite often require a lot of iterations.

They can be particularly difficult to achieve when discontinuous material laws (such as tension cracking) form part of the nonlinear behavior. Steep discontinuities in material laws can cause large residuals and these residuals need to be redistributed. However, this redistribution will cause more discontinuities and hence residuals in other parts in subsequent iterations. In such cases the rate of accumulation of residuals can be higher than the rate of distributing them. Another situation is when residuals are nearly redistributed and another discontinuity occurs which increases the residuals again and requires more iterations. These effects cause a high number of iterations which will continue until a stable crack situation is reached.

CHAPTER 3

RESEARCH METHODOLOGY

3.1 General

To meet the objectives of the study the methodology describes in brief, how to execute the work, what will be done, what tools are proposed, and the methods of analysis. The implementation of nonlinear material laws in finite element analysis codes is generally tackled by the software development industry in one or more ways. A number of powerful finite element software packages have been becoming commercially available. They include ABAQUS, ANSYS, COSMOSM, MARC and LUSAS.

In recent years, using ABAQUS finite element software, many research works have been performed successfully to simulate the behavior of reinforced concrete elements (beams, walls, columns and other structures).

In order to meet the objectives of this research, the reinforced concrete shear wall-slab connection was modeled using ABAQUS version 6.14 software program. The research significantly reveals the effect of geometric parameters and connection types on the effect of shear wall-slab connection under cyclic loading. This chapter explains the process to build the model and the process to run the nonlinear analysis using ABAQUS software programs.

A complete ABAQUS analysis usually consists of three distinct stages: preprocessing, simulation, and post processing. These three stages are discussed as follows:

Preprocessing (ABAQUS/CAE): In this stage, you must define the model of the physical problem and create an ABAQUS input file. The model is usually created graphically using ABAQUS/CAE or another preprocessor, although the ABAQUS input file for a simple analysis can be created directly using a text editor.

Simulation (ABAQUS /Standard or ABAQUS /Explicit): The simulation, which normally is run as a background process, is the stage in which ABAQUS/Standard or ABAQUS/Explicit solves the numerical problem defined in the model. Examples of output from a stress analysis include displacements and stresses that are stored in binary files ready for post processing. Depending on the complexity of the problem being analyzed and the power of the computer being used, it may take anywhere from seconds to days to complete an analysis run.

Post processing (ABAQUS /CAE): You can evaluate the results once the simulation has been completed and the displacements, stresses, or other fundamental variables have been calculated. The evaluation is generally done interactively using the Visualization module of ABAQUS/CAE or another postprocessor. The Visualization module, which reads the neutral binary output database file, has a variety of options for displaying the results, including color contour plots, animations, deformed shape plots, and X–Y plots. The ABAQUS/CAE is the Complete ABAQUS Environment that provides a simple, consistent interface for creating ABAQUS models, interactively submitting and monitoring ABAQUS jobs, and evaluating results from ABAQUS simulations. ABAQUS/CAE is divided into modules, where each module defines a logical aspect of the modeling process; for example, defining the geometry, defining material properties, and generating a mesh. As you move from module to module, you build up the model. When the model is complete, ABAQUS/CAE generates an input file that you submit to the ABAQUS analysis product. The input file may also be created manually.

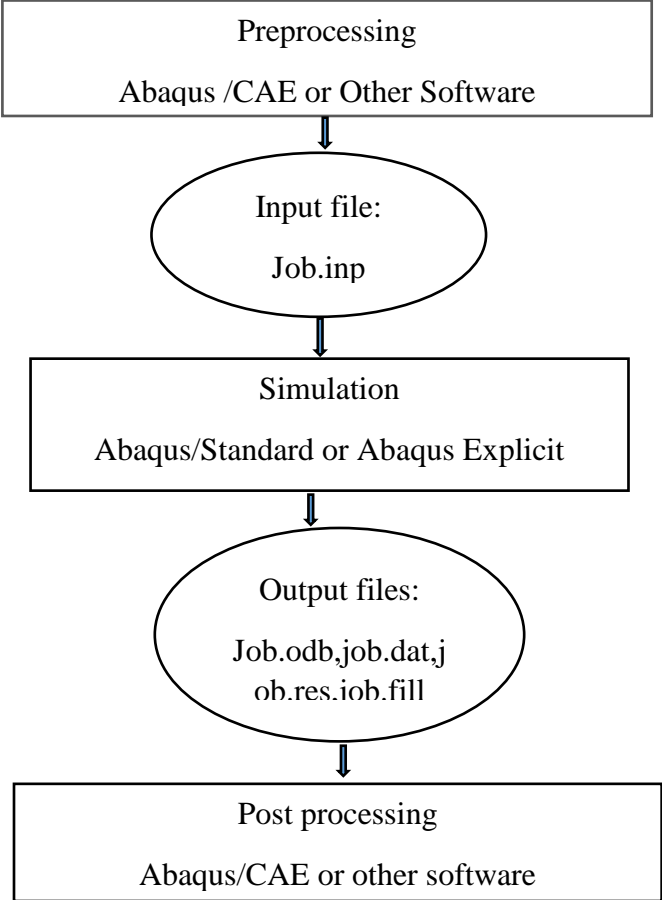


Figure 3.1 The stages used in ABAQUS

3.2 Finite Element Modeling

Reinforced concrete structures are widely employed in engineering practice for a variety of situations and applications. While traditional methods remain adequate for the analysis and design of reinforced concrete members, the development of the finite-element method has provided means for the analysis of much more complex systems in a more realistic way.

The main obstacle to the finite-element analysis of reinforced concrete structures is the difficulty in the characterization of material properties. Much effort has been spent in the search of a realistic model to predict behavior of reinforced concrete structures. Due to complex composite nature of the material, proper modelling of such structures is considered a highly challenging task. Finite Element (FE) Method is commonly used in evaluating and determining nonlinear load-displacement, hysteresis behavior and cracking behavior of reinforced concrete structural members and systems. The plastic behavior of steel and concrete is quite complicated and hard to analytically model. Lumped and distributed plasticity models as well as continuum mechanics-based models were developed for inelastic modeling of concrete. Most realistic simulations can be carried out by the finite element analysis of 3D models. Many finite element packages are available to consider for the analysis of reinforced concrete systems. Each package can have its own strengths and weaknesses, i.e., some can report crack locations and/or widths while others allow easy embedding of reinforcing bars, etc. Steel rebar's can be modeled as smeared within a finite element or can be taken account discretely. Discrete steel rebar's can be embedded inside concrete solid elements quite easily through embedding constraint, which does not consider slip of reinforcement. The reinforcement interaction with concrete can be taken into account by introducing tension stiffening in the definition of material model. Two-node truss and eight-node solid finite elements are usually preferred in modeling steel reinforcement and concrete, respectively. When embedding constraint is used, the truss elements of reinforcement are joined to concrete solid elements. This option constrains the translational degrees of freedom of the embedded truss nodes to the interpolated values of the corresponding degrees of freedom of the concrete solid element. Therefore, the reinforcement was assumed to be fully bonded to the concrete solid elements. For concrete material, there are two modeling options in ABAQUS. One is "Smeared crack concrete model" and the other is "Concrete Damaged Plasticity Model (CDPM)". Smeared crack concrete model is preferred for applications where concrete is subjected to monotonic straining. CDPM can be used with monotonic, cyclic, and/or dynamic loading

conditions. For this particular research, concrete damaged plasticity model was used. The CDPM required concrete compressive and tensile constitutive relationship, cracking and crushing damage parameters and special parameters such as dilation angle, eccentricity, biaxial loading ratio, the coefficient K and viscosity parameter.

ABAQUS/CAE can provide solutions for the linear, nonlinear and explicit problems. Its powerful graphic interface allows an accurate definition of the model, and is particularly useful for the visualization and presentation of analytical results.

3.2.1 Element Type

The general procedure of modeling any structure in ABAQUS is to assemble meshed sets of finite elements into one global assembly, and then evaluate its overall response under loading. ABAQUS provides an extensive library of elements that can be effectively used to model a variety of materials. The geometry and the type of an element is characterized by several parameters including: family, degree of freedom, number of nodes, formulation, and integration. Each element in ABAQUS has a unique name, which is derived from the five aspects mentioned previously. Figure 3.2 illustrates some of the most commonly used elements.

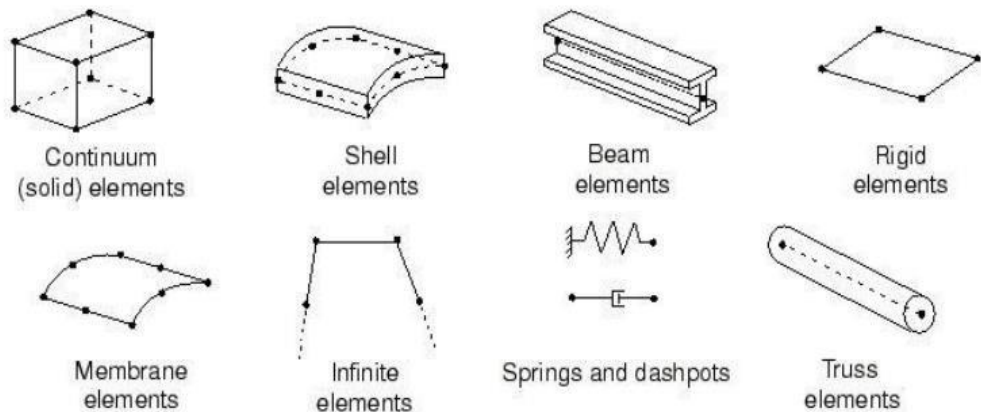


Figure 3.2 Various elements types (Source: [22])

In a standard stress analysis, the degrees of freedom of interest are the translations of the element nodes. In order to evaluate the field variables (usually displacements) at all nodes within the element domain, interpolation of these nodal values is performed. The number of nodes per elements determines the order of the interpolation (e.g. linear, quadratic, cubic, etc.). The 8-node continuum brick element, shown in Figure 3.8, uses linear interpolation and is referred to as a first-order element. On the other hand, a 20-node continuum element utilizes quadratic interpolation

and known as a second-order element. In theory, second-order elements provide more accurate results than first-order elements, if they were used in adequately small applications. However, the use of higher-order elements has some of drawbacks associated with convergence issues, especially when used in highly nonlinear analyses. For that reason, it is imperative to select the appropriate type of elements to achieve a sound numerical analysis. Although first-order elements are a quite practical choice for a large number of applications, they happen to exhibit a phenomenon called “shear locking”. This phenomenon can be seen as a constrained distortion which may lead to drastic convergence issues. For example, when the two-dimensional block illustrated in Figure 3.3(a) is subjected to pure bending, the entire element will deform in the manner shown in Figure 3.3(b). However, if a two-dimensional, 4-noded, quadrilateral, linear element with four integration points is used to model that block, the material is expected to deform as seen in Figure 3.3(c).

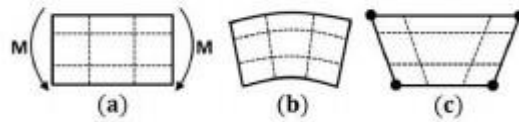


Figure 3.3: Shear locking of first-order elements (Source:[22])

In figure 3.3(c), the dashed lines are no longer perpendicular at each integration point which implies that the shear is not zero at these points. This development contradicts the assumption that materials under pure bending do not exhibit shear stresses. This is attributed to the inability of linear elements to have curved edges. Consequently, strain energy is generating shearing deformation as opposed to the expected bending deformation, which results in a stiffer element. However, one of the effective resolutions to this issue is to reduce the number of integration points per element so the excessive restraint is prevented (check Figure 3.4)

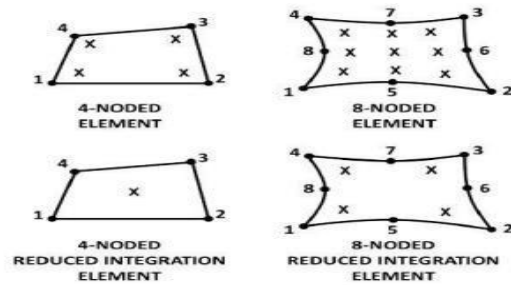


Figure 3.4: The reduction of integration points (Source:[22])

The reduced integration method is considered rather advantageous in modelling three dimensional problem as it decreases the time of analysis. Within the environment of ABAQUS, the user can choose the type of integration to be performed on the elements. A solid element such C3D8 is an 8-node continuum element with 8 integration points refers to full integration option. While a C3D8R is the same element with the exception of having only one reduced integration point (reduced integration option). Although, this practice is effective in eliminating shear locking, it may also result in a phenomenon named “hour glassing”. The quadrilateral element in Figure 3.5 has only one integration point (reduced from a fully integrated element with four (4) integration points). When this element is subjected to pure bending, the length of the two dashed lines and the angle between them remain unchanged. This implies that all the components of stress at the element’s single point of integration are equal to zero. In another word, the strain energy in the element is assumed to be zero, and thus the element will not resist this type of deformation as it has no stiffness under this loading. As a result, the occurrence of hour glassing may cause significant uncontrolled distortions in the mesh [17]. However, ABAQUS offers elements with hourglass control to overcome this issue.

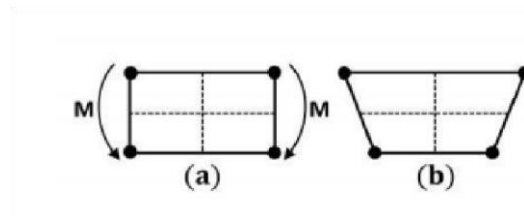


Figure 3.5 Hour glassing in reduced integration point (Source:[22])

For this particular paper, Solid 3D elements 8-node bricks (C3D8R) were used to model ordinary concrete and reinforcing bar was modelled using beam elements (B31, two-node linear beam).

3.2.2 Mesh Size

As an initial step, the finite element analysis requires meshing of the model. Hence, the model is divided into a number of small elements. After the application of the load, the stress and the strain are calculated at integration points of these elements. An important step in finite element modelling is the selection of the mesh density. A convergence of results is obtained when an adequate number of elements are used in a model. This is achieved when an increase in the mesh density has a negligible effect on the result. Therefore, it is very important to study the mesh

convergence to determine an appropriate mesh density. For this particular research, the models are meshed with 50mm size of elements as shown in figure 3.10.

3.2.3 Interaction Between Concrete and Reinforcement

One of the most important factors that affects the accuracy of the results is modelling the interaction between concrete and steel reinforcement. In a statically analysis, choosing suitable contact conditions between different parts of the model must be carefully considered to allow the transfer of the forces between these parts. The ABAQUS library provides a wide range of contact models required to define the interaction between different parts of any model. In the current research investigation, full bond between concrete and reinforcement was assumed using the embedded region constraint interaction between steel and concrete sections. This interaction constrains the translational degree of freedom of the nodes of the embedded elements with respect to the response of the host elements. Therefore, the interaction between concrete and reinforcement was modelled by using the embedded region option available in ABAQUS 6.14.1 which represents perfect bond between concrete and reinforcement. Slab and shear walls are bonded using tie option under interaction module so that slabs directly tied to shear walls.

3.3 Material Properties

3.3.1 Concrete

3.3.1.1 Stress- Strain Relationship of Concrete in Compression for Non-Linear Structural Analysis

The stress strain relation for concrete can be obtained from uni-axial compression test. Inelastic strains ε_c^{in} are used in the CDP model. It is determined using the graph from laboratory test by deducting elastic part (corresponding to the undamaged material) from the total strains registered in the uni-axial compression test. According to researchers' inelastic strain can be calculated from the following equation [21]

$$\tilde{\varepsilon}_c^{in} = \varepsilon_c - \varepsilon_{oc}^{el} \quad 3.1$$

$$\varepsilon_{oc}^{el} = \frac{\sigma_c}{E_o} \quad 3.2$$

The stress-strain data for concrete in compression and tension is crucial for analysis utilizing concrete damaged plasticity model. However, this was not reported as part of the experimental results, only the ultimate compressive strength of the concrete at 28 days was recorded in

experimental test. The curves were created using mathematical models found in literature. The compressive stress strain of concrete data was generated using [23] mathematical model for this research paper as shown in Figure 3.6.

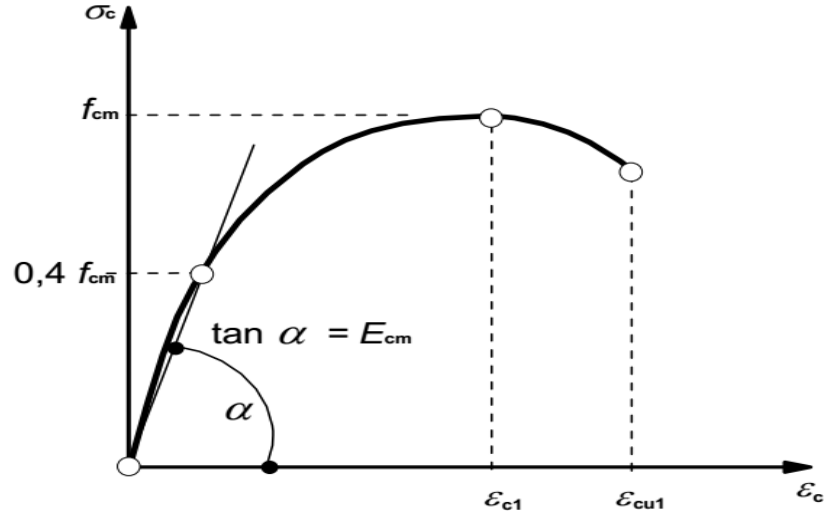


Figure 3.6: Stress-strain model for concrete in compression (Source: [23])

$$\frac{\sigma_c}{f_{cm}} = \frac{k\eta - \eta^2}{1 + (k-2)\eta} \quad 3.3$$

The parameter in equation 3.3 can be expressed as follows

$$f_{cm} = f_{ck} + 8 \left(\frac{N}{mm^2} \right) \quad 3.4$$

$$k = 1.05 E_{cm} \left(\frac{\varepsilon_{c1}}{f_{cm}} \right) \quad 3.5$$

$$\eta = \frac{\varepsilon_i}{\varepsilon_{c1}} \quad 3.6$$

$$\varepsilon_{c1} = 0.7 f_{cm}^{0.32} < 2.8 \quad 3.7$$

$$\varepsilon_{cu} = 0.0035$$

Where:

f_{ck} : is the characteristic cylindrical compressive strength of concrete at 28 days

ε_{c1} : is the strain at peak stress

ε_{cu} : is the ultimate strain

The modulus of elasticity of concrete (Young's modulus) was computed using the simplified relationship provided by [23] :

$$E_{cm} = 22 [f_{cm}/10]^{0.3} \quad 3.8$$

Equations 3.1 up to 3.8 were used to calculate the compressive behavior of concrete damage plasticity data shown in table 3.2.

3.3.1.2 Tensile Stress Behavior of Concrete

The tensile strength of concrete under uniaxial stress is seldom determined through a direct tension test because of the difficulties involved in its execution and the large scatter of the results. Indirect methods, such as sample splitting or beam bending, tend to be used [23]:

$$f_{ctm} = 0.30f_{ck}^{2/3} \quad 3.9$$

The term cracking strain $\tilde{\varepsilon}_t^{ck}$ is used in CDP model numerical analyses. The aim is to take into account the phenomenon called tension stiffening. Concrete under tension is not regarded as a brittle-elastic body and such phenomena as aggregate interlocking in a crack and concrete-to steel adhesion between cracks are taken into account. This assumption is valid when the pattern of cracks is fuzzy. Then stress in the tensioned zone does not decrease sharply but gradually. The strain after cracking is defined as the difference between the total strain and the elastic strain for the undamaged material:

$$\tilde{\varepsilon}_t^{ck} = \varepsilon_t - \varepsilon_{ot}^{el} \quad 3.10$$

$$\varepsilon_{ot}^{el} = \frac{\varepsilon_t}{E_c} \quad 3.11$$

In order to plot curve $\sigma_t - \varepsilon_t$ one should define the form of the weakening function. According to the ABAQUS user's manual, stress can be linearly reduced to zero, starting from the moment of reaching the tensile strength for the total strain ten times higher than at the moment of reaching f_{ctm} . However, to accurately describe this function the model needs to be calibrated with the results predicted for a specific analyzed case.

The proper relation was proposed by, among others,[24]:

$$\sigma_t = E_t \varepsilon_t, \text{ if } \varepsilon_t \leq \varepsilon_{cr} \quad 3.12$$

$$\sigma_t = f_{ctm} (\varepsilon_{cr} / \varepsilon_t)^{0.4} \text{ if } \varepsilon_t \geq \varepsilon_{cr} \quad 3.13$$

The tensile strength of concrete beyond the cracking is often ignored in design standards. Nevertheless, in reality concrete is capable of carrying some tensile stresses between cracks when there is sufficient bond between the concrete and the internal reinforcement. This phenomenon is known as "tension stiffening", and can be modeled using a descending post peak tensile response (see Figure 3.2).

Equations 3.9 up to 3.13 were used to calculate the tensile behavior of concrete damage plasticity data shown in table 3.3.

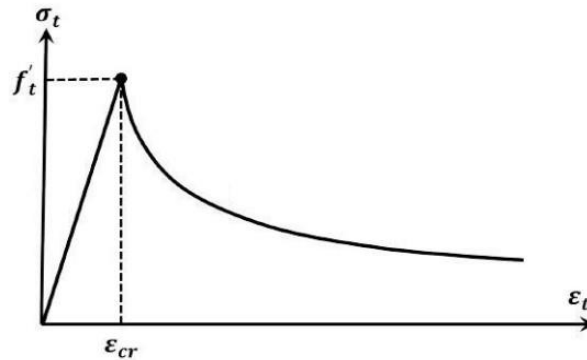


Figure 3.7 Idealized uniaxial stress-strain curve of concrete under tension (Source:[17]).

3.3.1.3 Concrete Damage Plasticity Parameter

For definition, the behavior of concrete by using concrete damage plasticity in ABAQUS software three main sections should be completed such as plasticity, compressive behavior and tensile behavior. The data for compressive and tensile behavior comes from uniaxial compression and uniaxial tension test respectively but the plasticity section needs five parameters. Some of these parameters are given a specific value in ABAQUS whereas the others have a range between two values. Two parameters have a specific value in ABAQUS.

Hyperbolic flow potential eccentricity (ϵ) which is defined in ABAQUS as a small positive number that represents the rate at which the hyperbolic flow potential approaches its asymptote. The default value given in ABAQUS for is 0.1, which is the value, selected for the current model.

Ratio of concrete strength in the biaxial state to that in the uniaxial state ($\frac{\sigma_{bo}}{\sigma_{co}}$) the value chosen for the proposed model is 1.16 which is the Default value in ABAQUS.

Three parameters of five parameters including dilation angle(ψ), Ratio of the second stress invariant in tension to that in compression (K_c) and viscosity parameter have been calibrated in this study but for two other parameters the default value have been used.

Dilation angle(ψ), which is defined as a material parameter that controls the plastic strain of concrete. It is also defined as the internal friction angle of concrete or the angle of inclination of the failure surface, which evaluates the inclination of the plastic potential under high confining

pressure. Higher dilation angle values result in more ductile behavior of concrete whereas low values lead to brittle concrete behavior [25]. The minimum value accepted in ABAQUS is close to zero while the maximum value is 56.3°. In the current model, the value of the dilation angle that gave the closest results to the normal strength concrete results was 38°. This value was selected based on comparison between the load deflection and the load damages results of the current model.

Ratio of the second stress invariant in tension to that in compression (K_c) the value of which must be between 0.5 and 1.0. In the current default, value of 0.667 given in ABAQUS was selected for the proposed model.

Viscosity parameter, which represents the relaxation time of the viscous system and helps to overcome some convergence problems. It was mentioned that a small value should be used for the viscosity parameter to influence the simulation time and improve the convergence of the model [26]. The default value given in ABAQUS for the viscosity parameter is zero. However, the value selected for the proposed model is 0.0001 to reduce the simulation time.

The values of the parameters required to define the concrete damaged plasticity model are shown in Table 3.1.

Table 3.1 Concrete damaged plasticity parameters used in the proposed ABAQUS model

Dilation angle	Eccentricity	$\frac{\sigma_{bo}}{\sigma_{co}}$	K_c	Viscosity parameter
38°	0.1	1.16	0.67	0.001

Table 3.2 Compressive behavior of concrete damage plasticity

Compressive behavior		Compressive damage	
σ_c	e_{in}	d_c	e_{in}
15.2	0	0	0
21.45	9.14196E-05	2.96688E-05	1.9E-06
26.72	0.000180841	0.000507873	3.2E-05
31.01	0.000300453	0.00148381	9.1E-05
34.28	0.000450669	0.003002457	0.00018
36.54	0.000631913	0.005135187	0.0003

37.76	0.000844611	0.007972838	0.00045
38	0.00100463	0.011623379	0.00063
37.94	0.001089203	0.016208805	0.00084
37.06	0.001366134	0.019862497	0.001
35.10	0.001675857	0.021861358	0.00109
32.04	0.002018834	0.028719182	0.00137
27.88	0.002395537	0.036921546	0.00168
22.47	0.002815562	0.046603813	0.00202
		0.021861358	0.0024
		0.071195419	0.00282

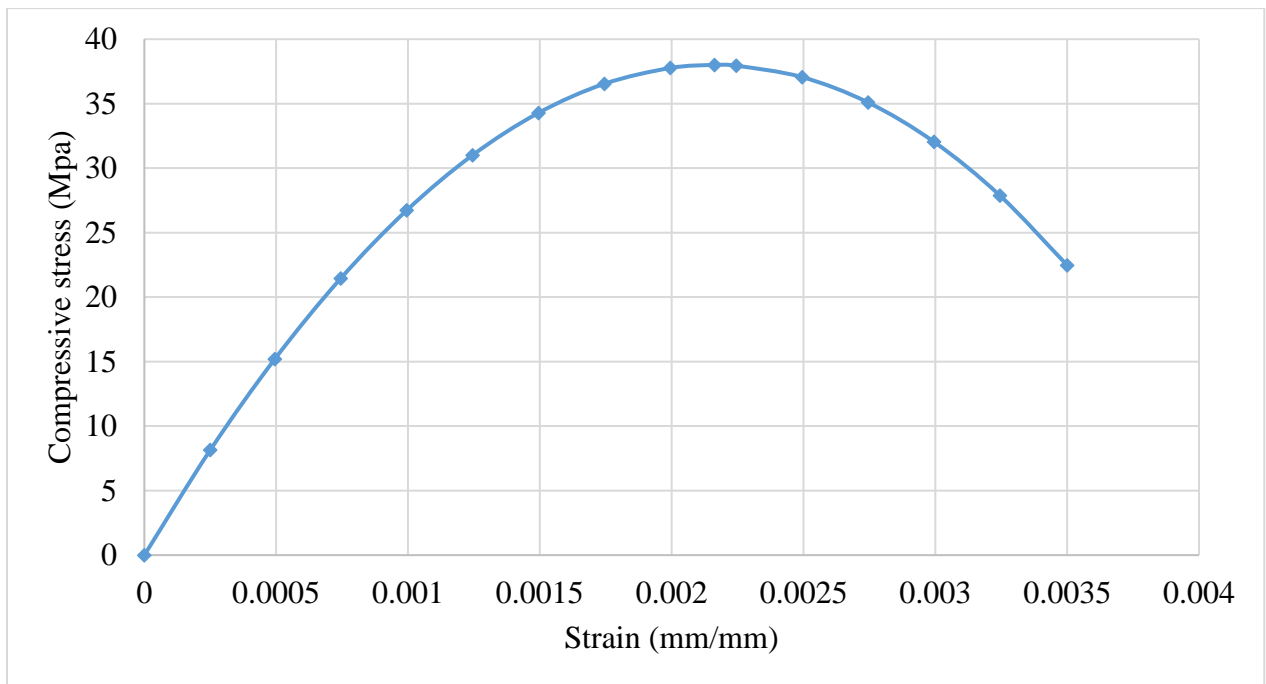


Figure 3.8 Compressive stress versus inelastic strain.

Table 3.3 Tensile behavior of concrete damage plasticity.

Tensile stress		Tension damage	
σ_t (Mpa)	ϵ_{cr} (mm/mm)	d_t	ϵ_{cr}
2.91192	0	0	0

2.20273	0.000432199	0.00576	1.1E-05
1.68238	0.001247676	0.21761	0.00043
1.30981	0.002458758	0.54285	0.00125
1.0473	0.004066566	0.8105	0.00246
0.86339	0.006072037	0.94429	0.00407
0.73349	0.0084759	0.9882	0.00607
0.63933	0.010896062		
0.56793	0.011278701		
0.51044	0.014480825		
0.46116	0.018082535		
0.41659	0.026485326		
0.37476	0.031286571		
0.33471	0.036487762		
0.2961	0.04208891		
0.25892	0.048090016		
0.22333	0.054491075		
0.18955	0.061292079		
0.15778	0.068493024		
0.12818	0.076093905		
0.10082	0.084094719		
0.07574	0.092495465		
0.05289	0.101296144		
0.0322	0.11049676		

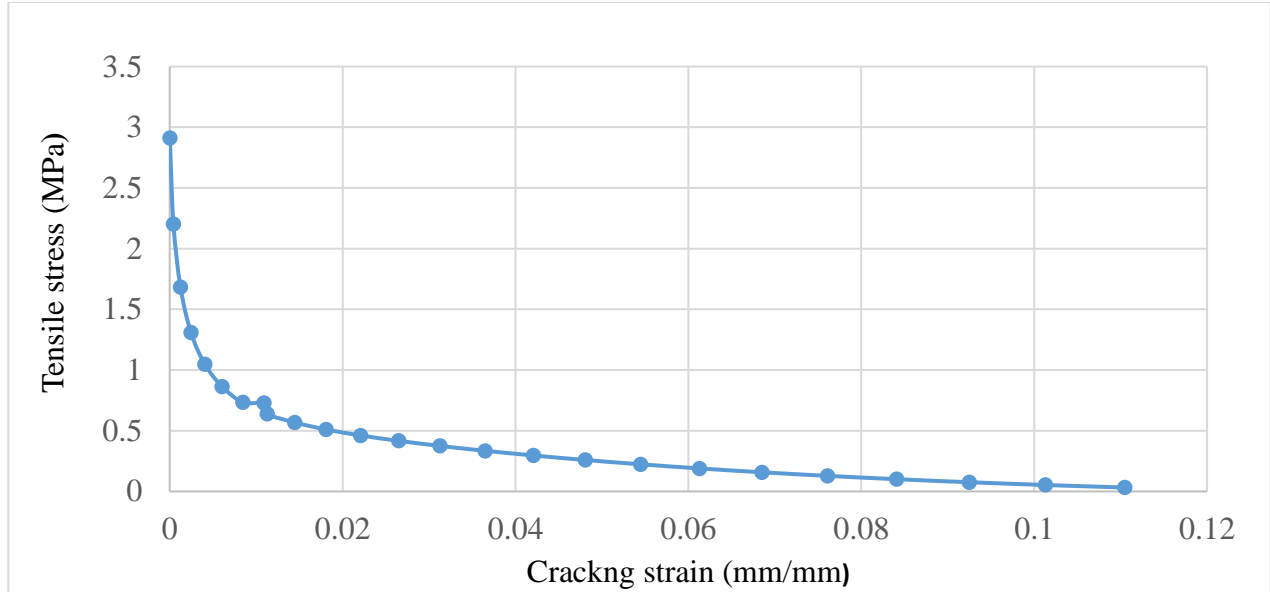


Figure 3.9 Tensile stress versus cracking strain.

3.4 Steel Reinforcement

The steel for the finite element models has been assumed to be an elasto-plastic material and identical in tension and compression. It is based on a linear elastic response up to yielding and a constant stress from the point of yielding to the ultimate strain. For this particular study, the steel reinforcement having Poisson’s ratio of 0.3 and Elastic modulus of 200,000 Mpa has been used.

In a nonlinear analysis, ABAQUS requires the input of the steel stress-strain curves in the form of true stress versus true plastic strain. The true stress (σ_{true}) and true strain (ϵ_{true}) were converted from the engineering stresses (σ) and engineering strains (ϵ) as equation (3.13 and 3.14) (Phama & Hancockb, 2010):

$$\sigma_{true} = \sigma(1 + \epsilon) \quad 3.14$$

$$\epsilon_{true} = \ln(1 + \epsilon) - \frac{\sigma_{true}}{E} \quad 3.15$$

$$\epsilon_{true} = \ln(1 + \epsilon) - \frac{\sigma_{true}}{E}$$

3.5 Geometric Modeling and Finite Element Mesh

Geometry is the important factor that determines the behavior of reinforced concrete shear wall-slab connection. In this research paper twenty two (22) different reinforced concrete shear wall-slab connection were modeled to evaluate the ultimate load carrying capacity and energy

absorption behavior with respect to changing geometric parameter and type of connection. Among those, three shear wall-slab connection are connected using U type connection with different geometric parameters. Three shear wall-slab connection are connected using 90° bent configurations into core joint type with different geometric parameters. Three shear wall –slab connections are connected using 90° top bar bent into configuration and bottom bar of slab bent at 135° into core region Connection type with different geometric parameters. Three shear wall –slab connections are connected using 90° top bar bent into configuration and bottom bar of slab bent at 150° into core region Connection type with different geometric parameters. Four shear wall –slab connections are modeled using four different types of connection type. Three shear wall-slab connection was modeled using different concrete grade and three was also modeled with different aspect ratio of H/We. The designation and dimension of each shear wall-slab sub assemblage have been presented in table 3.6. All are modeled using ABAQUS. The dimension of shear wall is constant throughout the study which is given by (h*L*t) =3500mm*1800mm*300mm and the dimension of slab is given on the table shown below.

Table 3.4 Sample of slab dimension under study

Slab	Length (mm)	Width (mm)	Thickness(mm)
S1	1800	2100	180
S2	1800	2400	240
S3	1800	2700	300

Table 3.5 Sample of slab dimension under study scaled by 1/3

Slab	Scale factor	Length (mm)	Width (mm)	Thickness(mm)
S1		600	700	60
S2		600	800	80
S3		600	900	100

Geometry of the reinforcement bars are greatly influence shear wall-slab sub-assemblage geometry for analysis. The reinforcement bars have a circular cross section and hence, they are modeled with a circular cross-section. Detail reinforces of the models are shown below.

The size of the finite element mesh has a significant effect on the results of the analysis of shear wall-slab connection. The model with an unnecessarily fine mesh requires an extra amount of

computation time while the model with a mesh that is too coarse might not be adequate to represent the behavior of the shear wall-slab connection correctly. The proper size of the finite element mesh for reinforced concrete members depends greatly on the nature of the problem being studied. Because there are no definite rules for selecting the proper mesh size for the analysis of reinforced concrete members, testing of finite element models with different mesh sizes is usually a good way to gain an initial understanding about the proper mesh size and the sensitivity of the results to different mesh sizes. In this study, the optimal mesh size has been found 50mm for concrete and for the reinforcement bars.

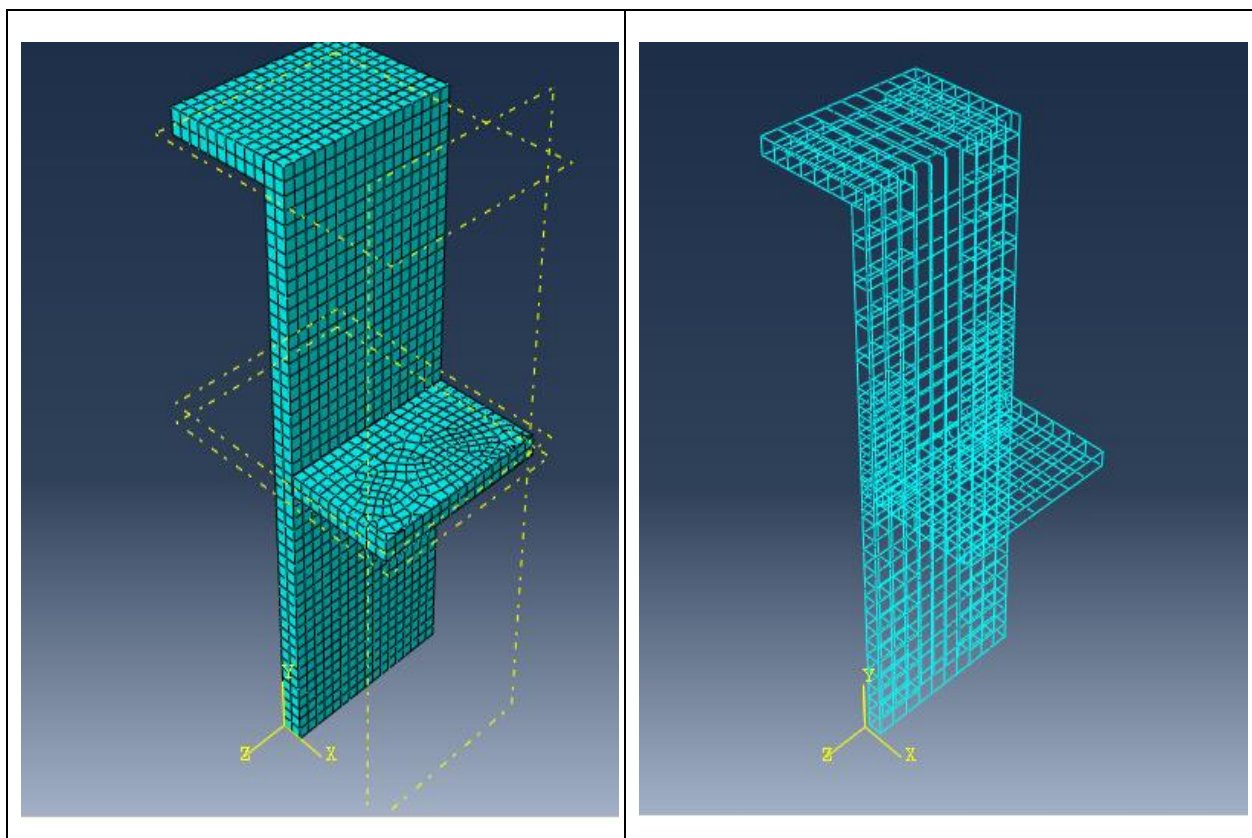


Figure 3.10 Meshing of shear wall-slab connection.

Table 3.6 The case under study and dimension of the slab reinforcement model.

No	Designated By:	Slab	
		Longitudinal reinforcement (mm)	Transverse reinforcement (mm)
1	C1SWS1	Use $\phi 12\text{mm}@290$	Use $\phi 12\text{mm}@280$
2	C1SWS2	Use $\phi 12\text{mm}@210$	Use $\phi 12\text{mm}@200$
3	C1SWS3	Use $\phi 12\text{mm}@160$	Use $\phi 12\text{mm}@160$
4	C2SWS1	Use $\phi 12\text{mm}@290$	Use $\phi 12\text{mm}@280$
5	C2SWS2	Use $\phi 12\text{mm}@210$	Use $\phi 12\text{mm}@200$
6	C2SWS3	Use $\phi 12\text{mm}@160$	Use $\phi 12\text{mm}@160$
7	C3SWS1	Use $\phi 12\text{mm}@290$	Use $\phi 12\text{mm}@280$
8	C3SWS2	Use $\phi 12\text{mm}@210$	Use $\phi 12\text{mm}@200$
9	C3SWS3	Use $\phi 12\text{mm}@160$	Use $\phi 12\text{mm}@160$
10	C4SWS1	Use $\phi 12\text{mm}@290$	Use $\phi 12\text{mm}@280$
11	C4SWS2	Use $\phi 12\text{mm}@210$	Use $\phi 12\text{mm}@200$
12	C4SWS3	Use $\phi 12\text{mm}@160$	Use $\phi 12\text{mm}@160$

Table 3.7 The case under study and dimension of the slab reinforcement model for 1/3 scaled down.

No	Designated By:	Slab	
		Longitudinal reinforcement (mm)	Transverse reinforcement (mm)
1	C1SWS1	Use $\phi 4\text{mm}@96\text{mm}$	Use $\phi 4\text{mm}@93\text{mm}$
2	C1SWS2	Use $\phi 4\text{mm}@70\text{mm}$	Use $\phi 4\text{mm}@66\text{mm}$
3	C1SWS3	Use $\phi 4\text{mm}@53\text{mm}$	Use $\phi 4\text{mm}@53\text{mm}$
4	C2SWS1	Use $\phi 4\text{mm}@96\text{mm}$	Use $\phi 4\text{mm}@93\text{mm}$
5	C2SWS2	Use $\phi 4\text{mm}@70\text{mm}$	Use $\phi 4\text{mm}@66\text{mm}$

6	C2SWS3	Use $\phi 4\text{mm}@53\text{mm}$	Use $\phi 4\text{mm}@53\text{mm}$
7	C3SWS1	Use $\phi 4\text{mm}@96\text{mm}$	Use $\phi 4\text{mm}@93\text{mm}$
8	C3SWS2	Use $\phi 4\text{mm}@70\text{mm}$	Use $\phi 4\text{mm}@66\text{mm}$
9	C3SWS3	Use $\phi 4\text{mm}@50\text{mm}$	Use $\phi 4\text{mm}@50\text{mm}$
10	C4SWS1	Use $\phi 4\text{mm}@96\text{mm}$	Use $\phi 4\text{mm}@93\text{mm}$
11	C4SWS2	Use $\phi 4\text{mm}@70\text{mm}$	Use $\phi 4\text{mm}@66\text{mm}$
12	C4SWS3	Use $\phi 4\text{mm}@50\text{mm}$	Use $\phi 4\text{mm}@50\text{mm}$

Table 3.8 The case under study and dimension of the shear wall model.

Shear wall	Vertical Reinforcement	Horizontal Reinforcement	Stirrups
SW1	Provide $\phi 18\text{c/c } 270\text{mm}$ vertical bar on both faces of shear wall	Provide $\phi 12\text{c/c } 390\text{mm}$ horizontal bar on both faces of shear wall	Provide $2L\phi 6\text{c/c } 390\text{mm}$

Table 3.9 The case under study and dimension of the shear wall model for 1/3 scaled down.

Shear wall	Vertical Reinforcement	Horizontal Reinforcement	Stirrups
SW1	Provide $\phi 6\text{c/c } 90\text{mm}$ vertical bar on both faces of shear wall	Provide $\phi 4\text{c/c } 130\text{mm}$ horizontal bar on both faces of shear wall	Provide $4L\phi 2\text{c/c } 130\text{mm}$

3.6 Interaction

As the rebar and concrete surfaces were directly adjoined in the test setup, so the contact analysis procedure is developed in the FE model to simulate the experimental condition. The contact interaction option in ABAQUS is used in modelling the contact between rebar and concrete in the reinforced shear wall-slab connection by providing the geometric and mechanical properties for

the interaction. First, the mechanical properties are specified and then associated with geometric features of the interaction to complete the contact assignment process. The slab was connected to shear wall as tie connection in the interaction module. The reinforcement bars of the shear wall-slab connection are modelled as embedded regions in the concrete by using „embedded constraint“ option in the interaction module. This interaction constrains the translational degree of freedom of the nodes of the embedded elements with respect to the response of the host elements

3.7 Loading and Boundary Conditions

The numerical model under observation was fixed at the bottom to restrain each component of the shear wall in all degrees of freedom and to reflect the characteristics of the shear wall used for the experimental study. The top of the shear wall was restrained for in plane and out of plane movement. The axial load at the top of the subassembly was distributed as pressure at the top face of the model. The displacement controlled loading was achieved by defining partitions of circular profile (of same dimensions of the load cell as in the case of test conducted) and assigning the prescribed displacement to the partitions. The partitions were assigned to the same displacement cycles as in the loading history of the test conducted. The prescribed displacement was achieved by using amplitude function in the boundary condition module.

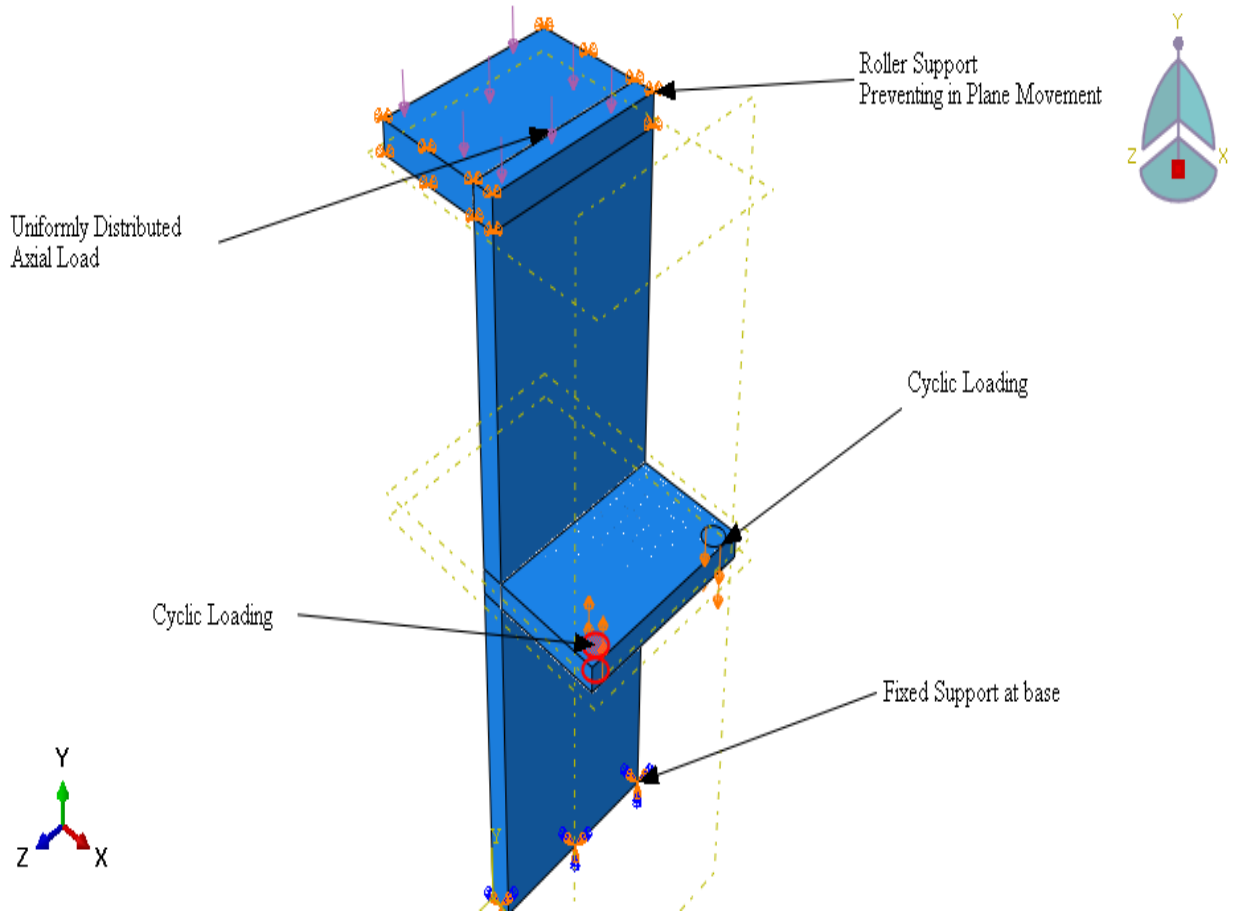


Figure 3.11 Boundary and loading condition.

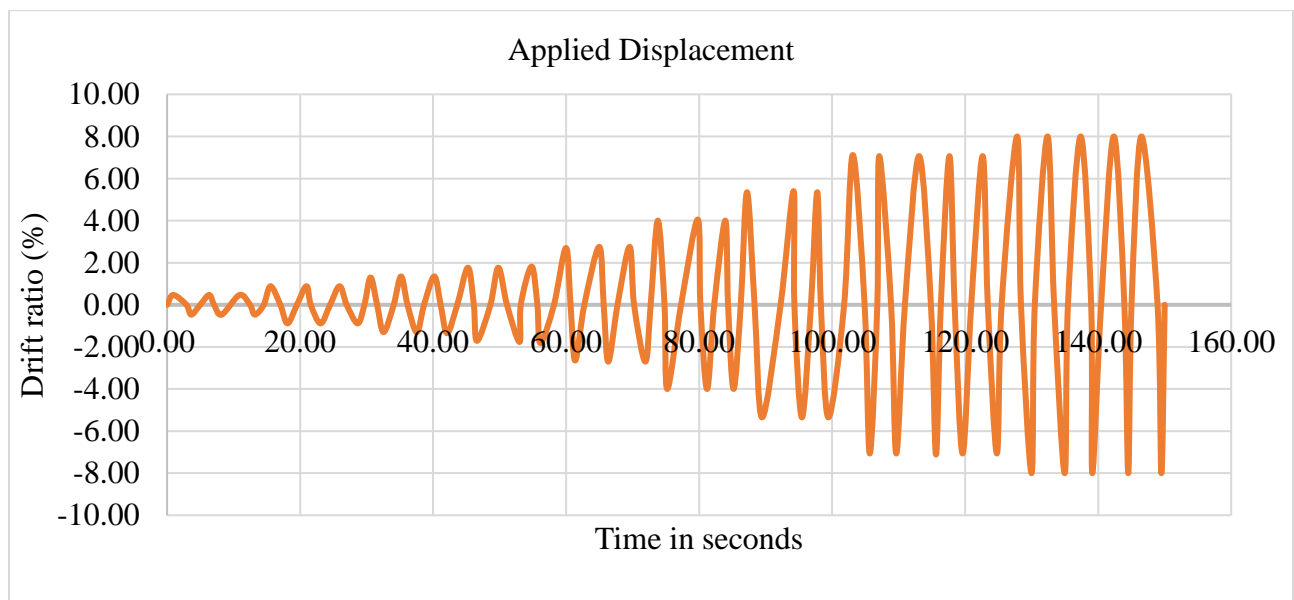


Figure 3.12 Applied displacement Vs time (Source:[27])

3.8 Method for Solving Non-Linear Solution

There are different methods available in Abaqus for finding the solution of non-linear equations such as the linear method, the Newton Raphson method and the modified Newton Raphson method. In this study, the modified Newton Raphson method has been used for solving the simultaneous equations and finding incremental equilibrium. This is an iterative process of solving the non-linear equations.

One approach of non-linear solution is to break the load into a series of load increments. The load increments can be applied either over several loads or over several load steps within a load step. At the completion of each incremental solution, the program adjusts the stiffness matrix to reflect the non-linear changes in structural stiffness before proceeding to the next load increment. The ABAQUS program overcomes this difficulty by using the Full Newton Raphson method, or the modified Newton Raphson method, which drives the solution to equilibrium convergence at the end of each load increment. In the Full Newton Raphson method, it uses the following set of non-linear equations:

$$k(p)\Delta p = q - f(p) \quad 3.16$$

Where q is the vector of total applied joint loads, $f(p)$ is the vector of internal joint force, Δp is the deformation increment due to loading increment, p are the deformations of the structure prior to the load increment and $k(p)$ is the stiffness matrix, relating loading increments to deformation increments. Figure 3.14 illustrates the use of the Newton Raphson equilibrium iterations in non-linear analysis. Before each solution, the Newton Raphson method evaluates the out of balance load vector, which is the difference between restoring forces (the load corresponding to the element stress) and the applied load. The program then performs a linear solution using the out of balance loads and checks for convergence. If convergence criteria are not satisfied the out of balance load vector is re-evaluated and the stiffness matrix is updated, then a new solution is obtained. This iterative procedure continues until the problem converges to within defined criteria.

Sometimes the most time consuming part of the Full Newton Raphson method solution is the recalculation of the stiffness matrix at each iteration. In many cases, this is not necessary and we can use the matrix from the first iteration of the step. This is the basic idea of the so-called Modified Newton Raphson method. It produces very significant time savings. On the other hand, it also

exhibits a slower convergence of the solution procedure. The simplification adopted in the Modified Newton Raphson method can be mathematically expressed by:

$$k(p_i - 1) = K(p_o) \tag{3.17}$$

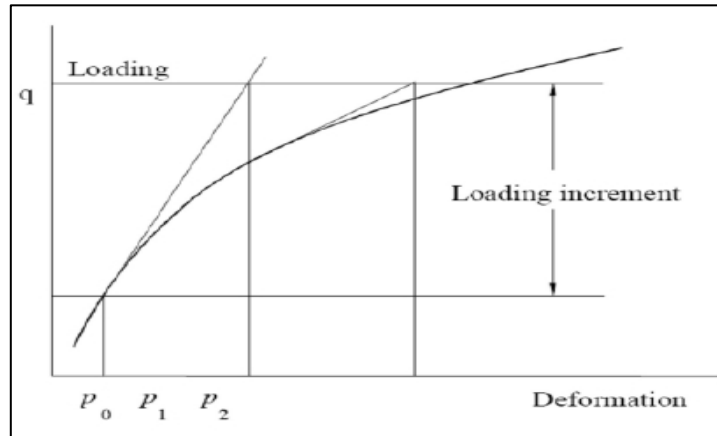


Figure 3.13 Full Newton Raphson Method

The modified Newton Raphson method, which was used in this study, is as shown, which when compared to the Full Newton Raphson method it shows that the Modified Newton Raphson method converges more slowly than the original Full Newton Raphson method.

On the other hand, a single iteration costs less computing time because it is necessary to assemble and invert the stiffness matrix only once. In practice, a careful balance of the two methods is usually adopted in order to produce the best performance for any particular case. Usually it is recommended to start a solution with the original Newton Raphson method and later i.e. near extreme points switch to the modified procedure to avoid divergence.

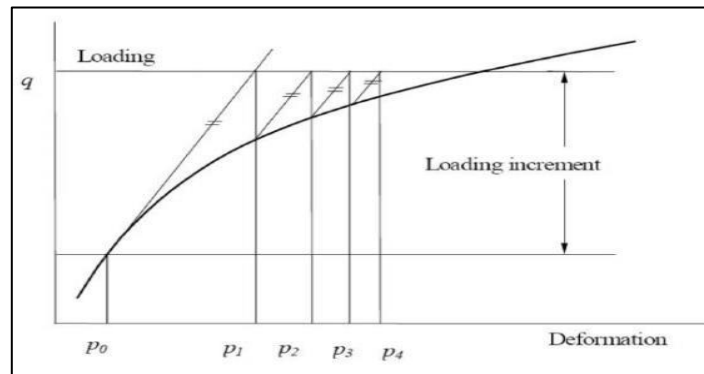


Figure 3.14: Modified Newton-Raphson Method

3.9 Load Stepping and Failure Definition for Finite Element Method

For the nonlinear analysis, automatic time stepping in the Abaqus program predicts and controls load step size. Based on the previous solution history and the physics of the models, if the convergence behavior is smooth, automatic time stepping will increase the load increment up to a selected maximum load step size. If the convergence behavior is abrupt, then the automatic time stepping will bisect the load increment until it is equal to a selected minimum load step size. The maximum and the minimum load step sizes are required for the automatic time stepping.

In this particular study the time period, the maximum number of increments, the initial increment, minimum increment size and maximum increment size were set to 30, 10000, 0.01, 1E-020 and 0.1 respectively.

3.10 Flow Chart of Finite Element Analysis

Figure 3.15 shows the procedure followed to analysis the shear wall-slab connection in ABAQUS 6.14 software package program.

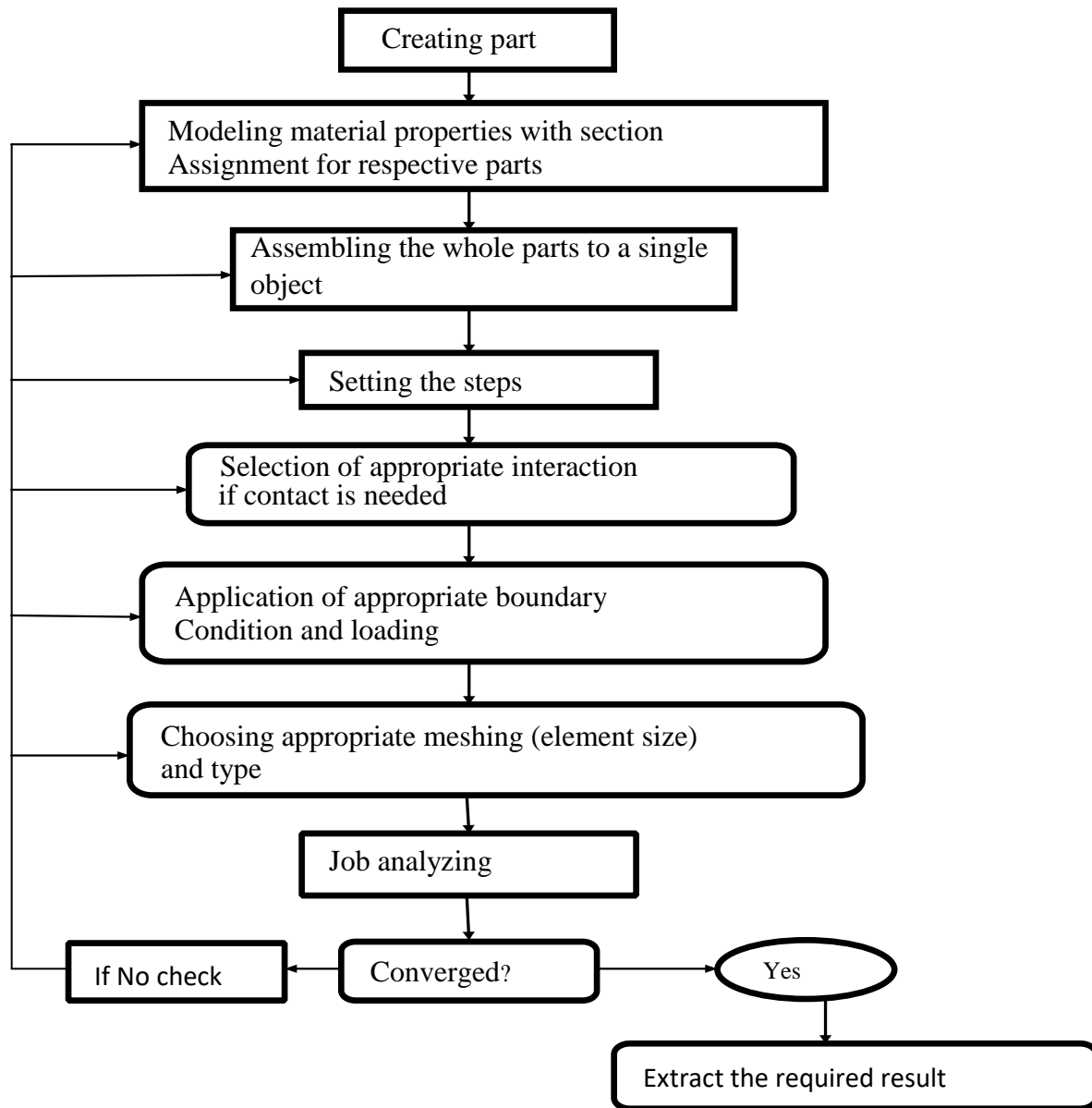


Figure 3.15 Procedure followed for the finite element in ABAQUS 6.14.

3.11 Validation of FE Model of RC Shear Wall-Slab Connection Under Cyclic Loading

The validity of the proposed analytical model is checked through extensive comparisons between analytical and experimental results of RC exterior shear wall-slab connection under cyclic loading. The hysteresis curve has been presented experimentally under lateral cyclic with loading protocol, which was assigned to the circular partitions at the slab end. The theoretical results from finite element analysis showed in general a good agreement with the experimental values.

3.11.1 General Description on the Genesis of Data Used in Experiment

a. Material Properties of Concrete

The concrete is defined as an isotropic material in the modeling, and should be deliberately expressed in verification genesis.

Table 3.10 Concrete properties of validity parameters (Source:[27])

Concrete properties	Magnitude
Elastic Modulus	3283.66 Mpa
Poisson's Ratio	0.2
Compressive strength	30 Mpa
Tensile strength	2.578Mpa

b. Reinforcement steel

Steel reinforcement with the same diameter and yield strength were used in the experimental setup of the reinforced exterior shear wall-slab connection. The yield strength of steel f_y used in the model for 6mm bar diameters was 432 Mpa with modulus of elasticity 200Gpa. The properties of steel reinforcement are summarized in table 3.11.

Table 3.11 Steel properties of validity parameters (Source:[27])

Steel properties	Diameter of bar
	ϕ 6mm
Elastic Modulus	200000 Mpa
Poisson's Ratio	0.3
Yield Strength	432Mpa

b. Geometry

Test specimens having a total length of 1/3 scaled down of overall height of shear wall $h=2417\text{mm}$, overall length $L=835\text{mm}$, thickness of 100mm and the dimension of slab having a total length of 835mm , overall width of 500mm and thickness of 83.5mm . The clear concrete cover thickness was 10mm and 15mm for the slab and shear wall respectively. The dimensions and reinforcement detail of the test specimen was shown below in detail.

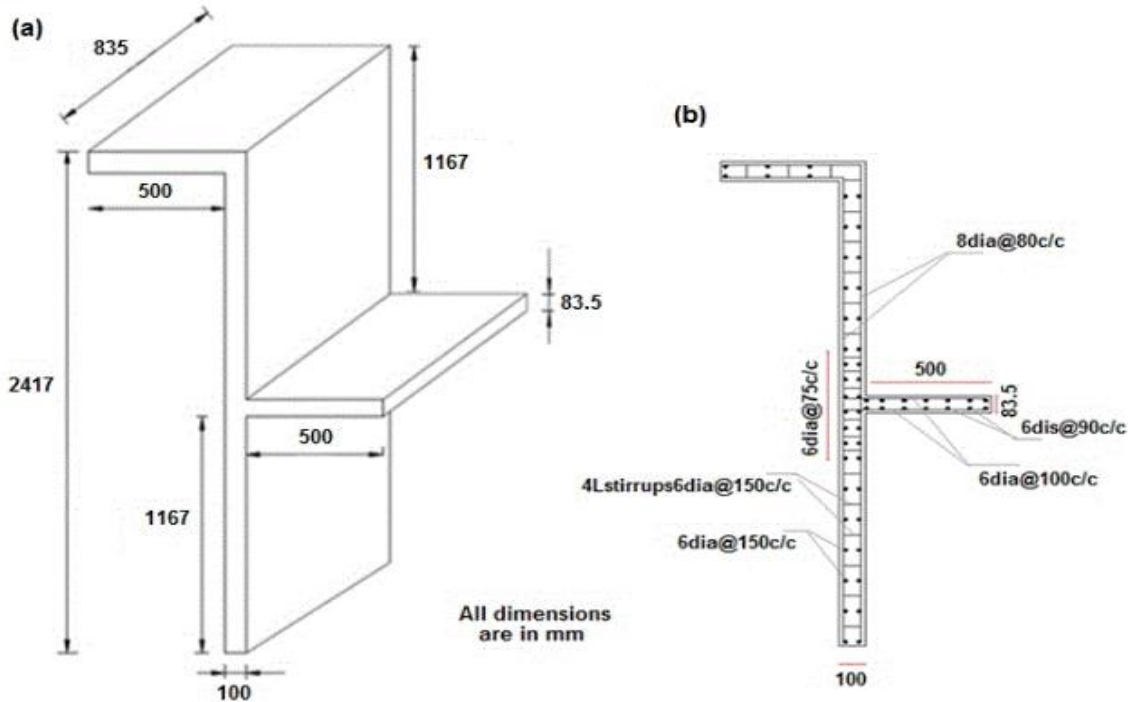


Figure 3.16 (a) Geometry of test units; (b) Reinforcement details of the test units under experiment set up (Source:[27])

C. Test set up and loading

The test units were tested in a well- equipped setup as shown schematically in Fig 3.17. The shear wall was fixed at the bottom by attaching it to two steel channels using four high-strength threaded rods. The steel channels were properly anchored to the strong test floor. The top of the shear wall was restrained for displacements in both directions to ensure complete shear transfer at the joint. A total load of 8 kN was applied by assembling cubes to simulate the axial load at the second storey height. The units were tested under displacement controlled system subjected to reverse cyclic loading up to failure. The pattern of cyclic displacements applied by the hydraulic jack during test is given in Fig 3.17. To apply the simulated reverse cyclic load on the units, 100-kN capacity hand- controlled

hydraulic jacks (four numbers) were connected to a reaction steel frame. Four hydraulic jacks were linked to the top and bottom of the slab ends as shown in Fig 3.17. The units were subjected to an increasing displacement in a cyclic manner up to failure. The displacement amplitude at the end of the slab was increased by steps of 0.5 mm up to a displacement of 2 mm, then by steps of 1 mm up to failure, with 3 cycles for each amplitude levels. The loading sequence was observed using load cells with least count of 10 kg for applying cyclic load. The units were instrumented with load cells, dial gauges, and strain gauges to monitor the behavior of units during testing. Fig 3.17 shows the view of test in progress

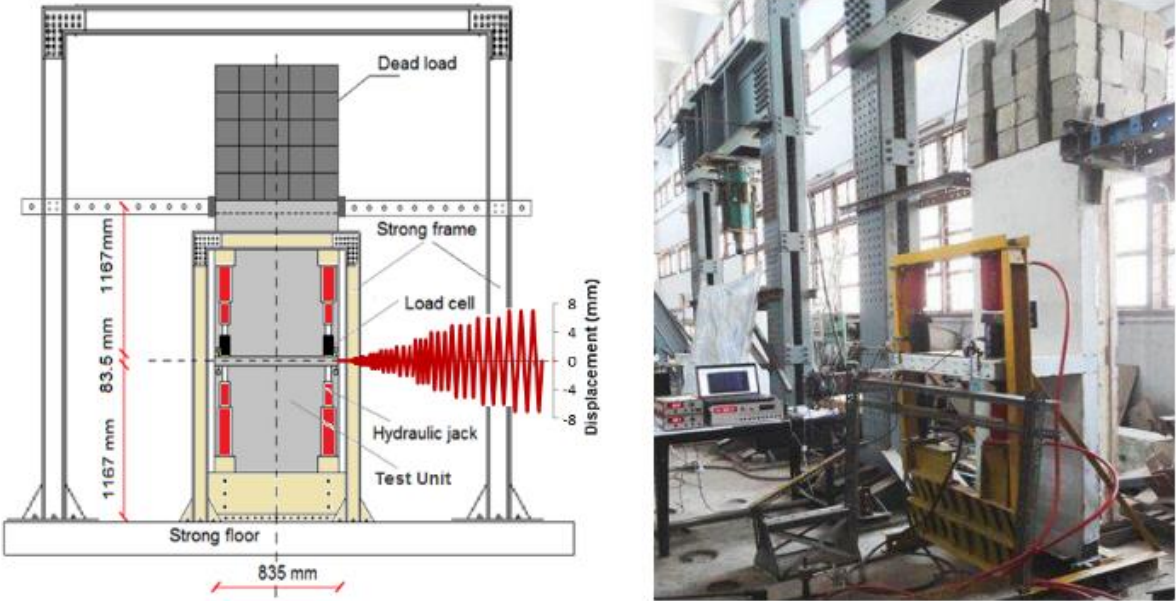


Figure 3.17 Loading condition of test setup (Source :[27])

CHAPTER FOUR

RESULTS AND DISCUSSION

4.1 General

This chapter presents the results of the cyclic behaviors and its effects on the load carrying capacity energy dissipation, ductility and stiffness degradation of reinforced concrete shear wall-slab connection. The study was undertaken by considering the effect of different height of shear wall to effective width of slab ratio (H/W_e), thickness of slab to shear wall (T_S / T_w) ratio, Connection type, and concrete grade on load carrying capacity , energy dissipation ,ductility and stiffness degradation.

4.2 Validation of Finite Element Analysis by Experimental Result

To capture the cyclic behavior of exterior shear wall-slab connection a lot of parameters have been considered in this study. Some of the things are material model for steel and concrete, different loading rate (amplitude), boundary condition, mesh size and element type. The selected model captures the failure mode, the stress distribution and the lateral load capacity of the exterior shear wall-slab connection but cannot capture the hysteresis loops exactly. This seems like the material models integrated in Abaqus modules have some difficulties to capture the cyclic behavior of structural elements.

Table 4.1 Comparison of FEA and experimental result.

Experimental	Dependent variable	Finite element model	Experimental result	Difference	Percentage difference
[27]	Ultimate load	36.40KN	37.8KN	1.40	3.704%

The results obtained from laboratory test were used to compare with the results obtained from the finite element analysis. Hence, the finite element model was implemented based on the parameters and conditions used in the laboratory test. The hysteresis curve for both experimental and finite element analysis (ABAQUS Software package) has been presented in figure 4.1. The comparison showed a good agreement between experimental and finite element result.

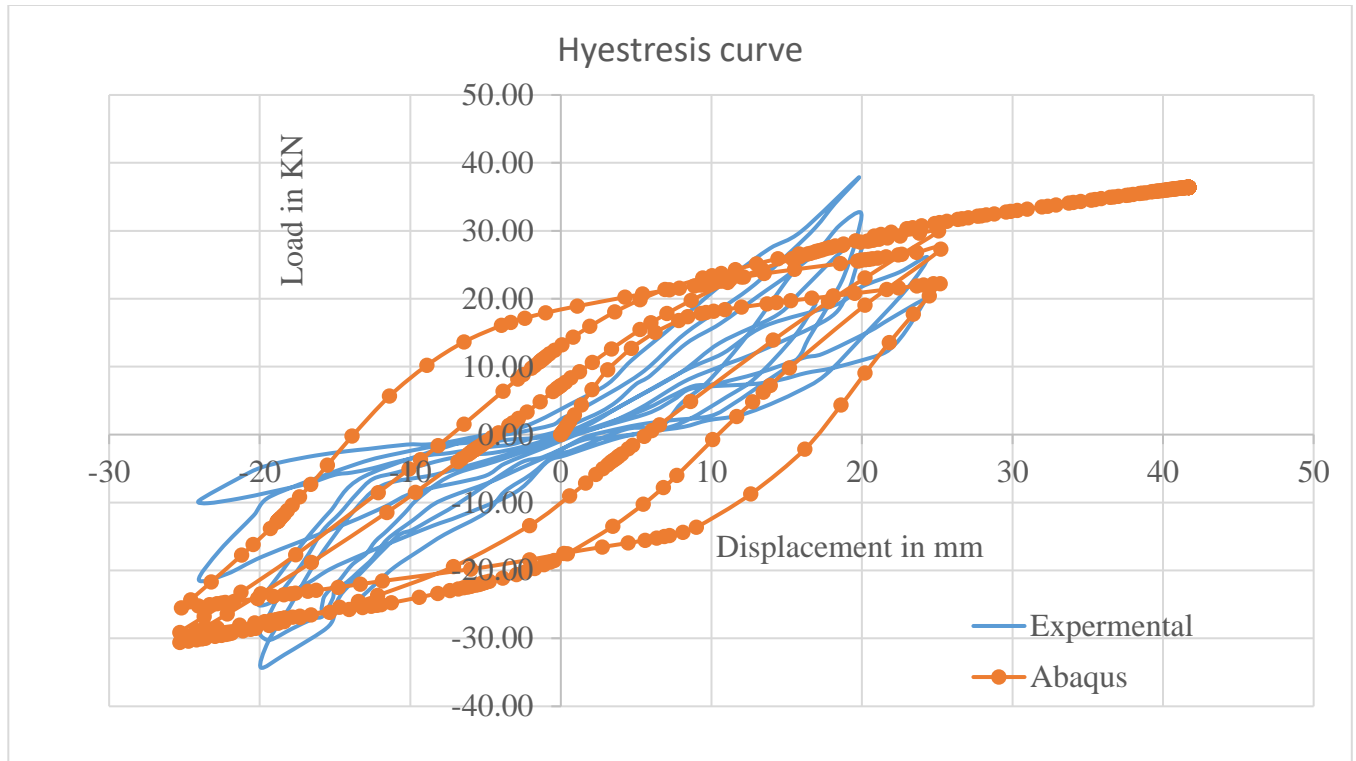


Figure 4.1 Comparison of experimental (Source:[27]) and finite element result.

From figure 4.1 due to Pinching behavior of reinforced concrete hysteresis curve of finite element cannot capture exact behavior of hysteresis curve of experimental around the origin. In reinforced concrete, pinching is typically produced by opening of cracks when displacement is imposed in one direction. Partial stiffness recovery occurs when cracks are closed during displacements imposed in the other direction.

4.3 Parametric Study of Exterior Reinforced Concrete Shear Wall-Slab Connection

The finite element model developed in chapter-3 has been found to predict the behavior of exterior shear wall-slab connections. This chapter presents a detailed parametric study on exterior RC shear wall-slab connection using the developed finite element model. The cases under study are connection type, aspect ratio of thickness of slab to thickness of shear wall (T_s/T_w), aspect ratio of height of shear wall to effective width of the slab (H/W_e) and concrete grade. The result obtained from Abaqus was discussed in terms of load carrying capacity, Energy dissipation, ductility and stiffness degradation as follows.

4.3.1 Ultimate Load Carrying Capacity

4.3.1.1 Ultimate Load Carrying Capacity for U-Type Connection

The comparison of strength of the three exterior shear wall-slab connection with same U-type connection, grade of concrete, reinforcement, but with different aspect ratio is given in Figure 4.2. The specimen with the type C1SWS2 detailing performed better than the C1SWS1 specimen. The C1SWS2 specimen exhibited the load carrying capacity that is by 61.7 % greater than C1SWS1 specimen. The specimen with type C1SWS3 detailing performed better than the C1SWS1 and C1SWS2 specimen. The C1SWS3 specimen exhibited the load carrying capacity that is by 73.34 % greater than C1SWS2 specimen.

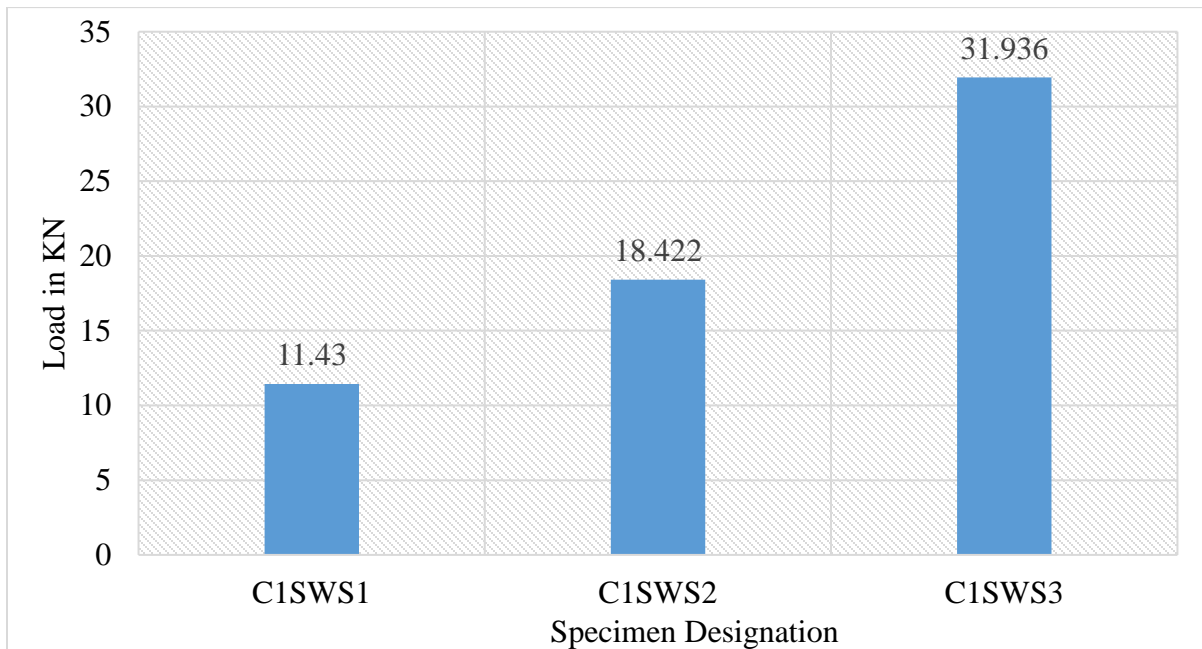


Figure 4.2 Comparisons of load carrying capacity of U-type connection with different aspect ratio.

4.3.1.2 Ultimate Load Carrying Capacity for 90°-Type Connection

The comparison of strength of the three exterior shear wall-slab connection with same 90°-type connection, grade of concrete, reinforcement, but with different aspect ratio is given in Figure 4.3. The specimen with the type C2SWS2 detailing performed better than the C2SWS1 specimen. The C2SWS2 specimen exhibited the load carrying capacity that is by 61.49 % greater than C2SWS1 specimen. The specimen with type C2SWS3 detailing performed better than the C2SWS1 and

C2SWS2 specimen. The C2SWS3 specimen exhibited the load carrying capacity that is by 71.86 % greater than C2SWS2 specimen.

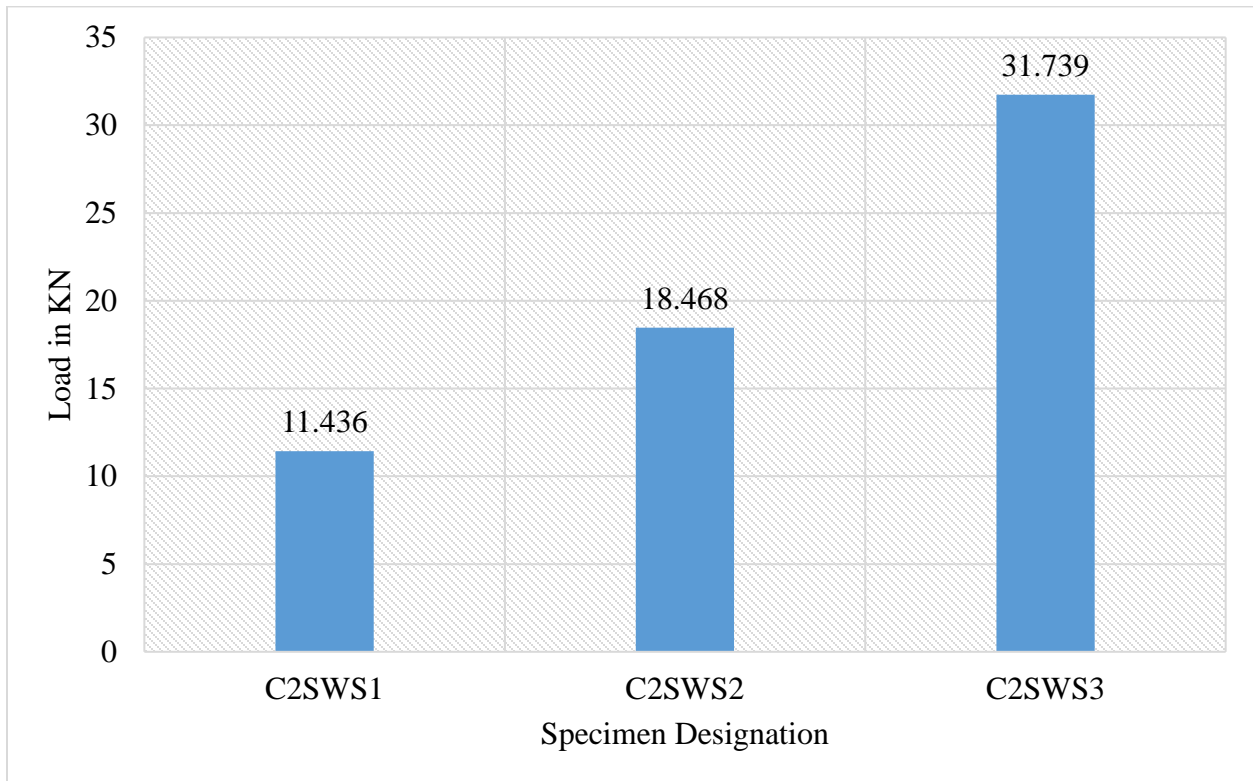


Figure 4.3 Comparisons of load carrying capacity of 90⁰-type connection with different aspect ratio.

4.3.1.3 Ultimate Load Carrying Capacity for 135⁰--Type Connection

The comparison of strength of the three exterior shear wall-slab connection with same 135⁰-type connection, grade of concrete, reinforcement, but with different aspect ratio is given in Figure 4.4. The specimen with the type C3SWS2 detailing performed better than the C3SWS1 specimen. The C3SWS2 specimen exhibited the load carrying capacity that is by 61.64 % greater than C3SWS1 specimen. The specimen with type C3SWS3 detailing performed better than the C3SWS1 and C3SWS2 specimen. The C3SWS3 specimen exhibited the load carrying capacity that is by 72.35 % greater than C3SWS2 specimen.

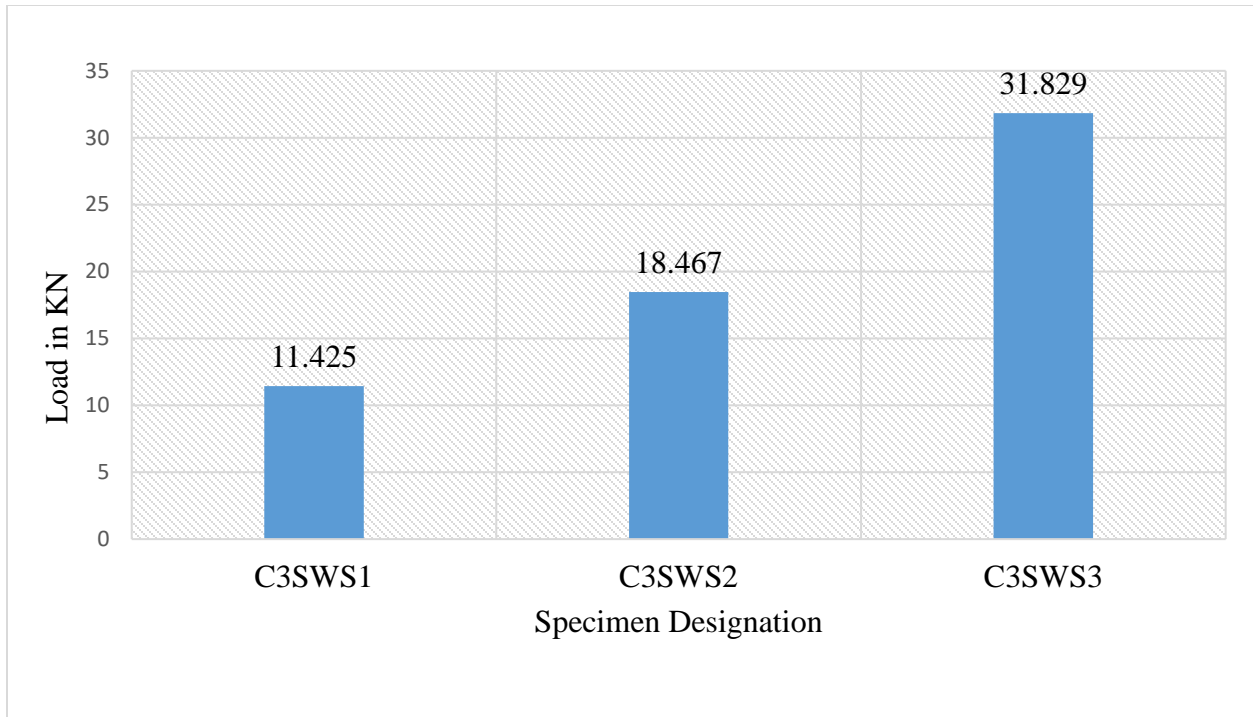


Figure 4.4 Comparisons of load carrying capacity of 135°-type connection with different aspect ratio.

4.3.1.4 Ultimate Load Carrying Capacity for 150°-Type Connection

The comparison of strength of the three exterior shear wall-slab connection with same 150°-type connection, grade of concrete, reinforcement, but with different aspect ratio is given in Figure 4.5. The specimen with the type C4SWS2 detailing performed better than the C4SWS1 specimen. The C4SWS2 specimen exhibited the load carrying capacity that is by 61.43 % greater than C4SWS1 specimen. The specimen with type C4SWS3 detailing performed better than the C4SWS1 and C4SWS2 specimen. The C4SWS3 specimen exhibited the load carrying capacity that is by 72.49 % greater than C4SWS2 specimen.

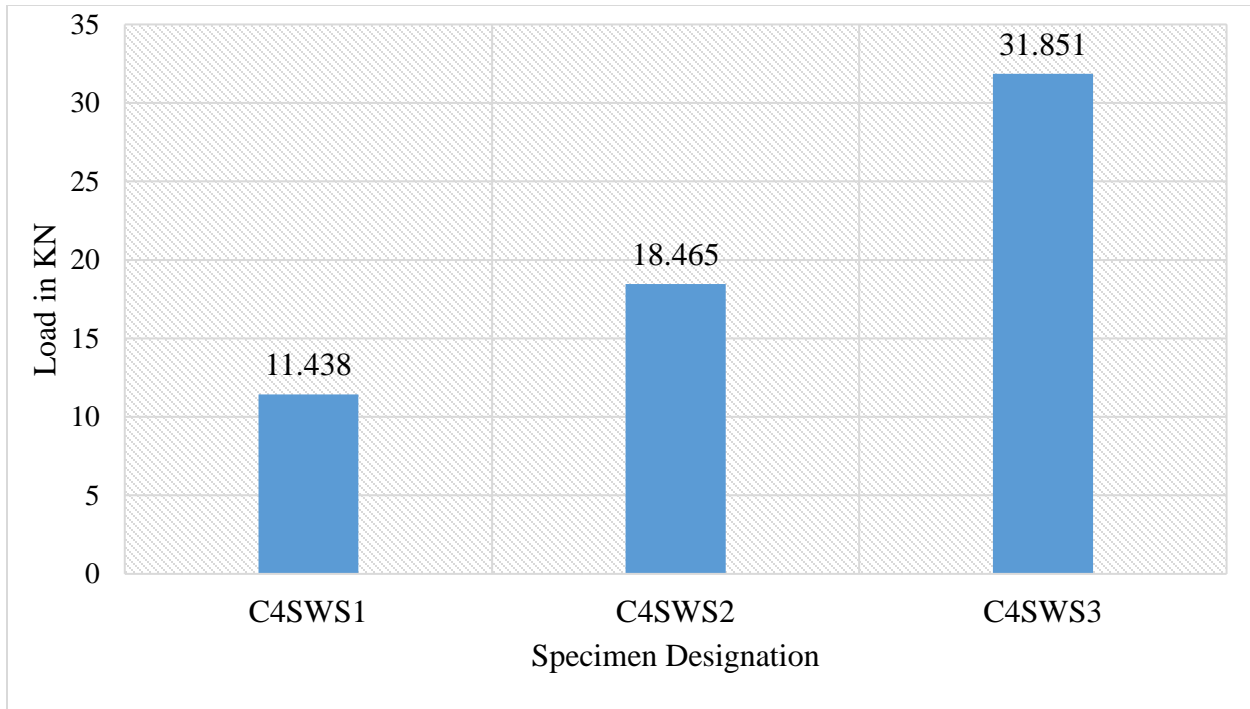


Figure 4.5 Comparisons of load carrying capacity of 150°-type connection with different aspect ratio.

4.3.1. 5 Effect of Aspect Ratio of H/We on Load Carrying Capacity

Figure 4.6 below describes the results of load carrying capacity of reinforced concrete shear wall-slab slab connection. The walls are the same with C1SWS1 and the only difference between these walls is the aspect ratio of H/We of 1.67, 1.46 and 1.30. It indicates that load carrying capacity of shear wall-slab connection decrease as effective width of the slab increase from shear wall. The specimen with aspect ratio of 1.67 performed better resistance than the aspect ratio of 1.46 and 1.30 specimen. The 1.67 aspect ratio exhibited the load carrying capacity that is by 1.15 % greater than 1.46 aspect ratio and 1.6% greater than 1.3 aspect ratio. With the decrease of aspect ratio, the load carrying capacity of shear wall-slab connection decreases.

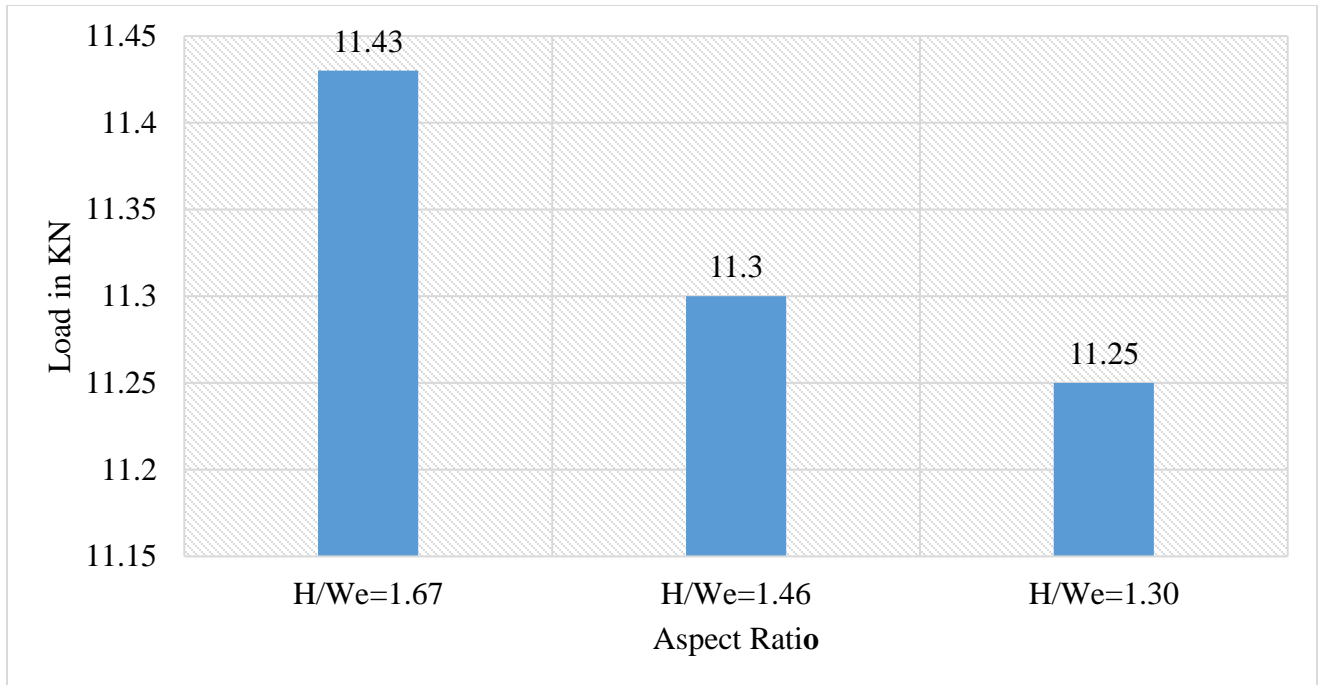


Figure 4.6 Comparisons of load carrying capacity with aspect ratio H/We.

4.3.1.6 Effects of Connection Type on Load Carrying Capacity

Four exterior shear wall –slab connection with different connection type are modelled by ABAQUS 6.14 software. All four shear wall-slab connection have the same aspect ratio, the same reinforcement, the same boundary condition, and the same concrete strength. The result shows that the specimen C1SWS3 shows better performance than the other connection. The C1SWS3 specimen exhibited the load carrying capacity that is by 0.621 % greater than C2SWS3, 0.336 % greater than C3SWS3 and 0.267 % greater than C4SWS3 specimen. The load carrying capacity versus connection type is shown below in the figure 4.7.

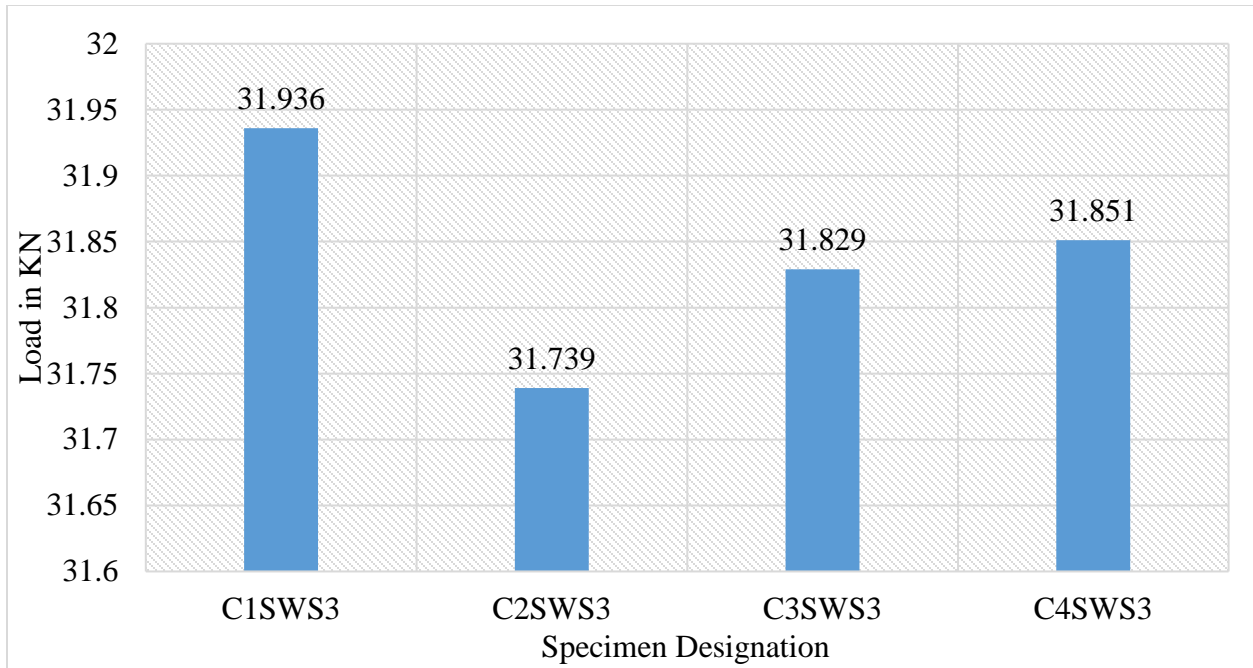


Figure 4.7 Comparisons of load carrying capacity of different connection type with the same aspect ratio of $T_s/T_w=1$.

4.3.1.7 Effects of Concrete Grade on Load Carrying Capacity

Figure 4.8 below describes the results of load carrying capacity for reinforced concrete shear wall-slab connection. The walls are the same with C1SWS1 and the only difference between these walls is the concrete compressive strength, which varies from 25 MPa, 30Mpa and 40MPa. It indicates that concrete compressive strength has obvious effect on the load carrying capacity of shear wall-slab connection. With the increase of concrete compressive strength, the load carrying capacity of shear wall-slab connection increases. The shear –slab connection with C-40Mpa concrete grade exhibited the load carrying capacity of 31.28 % greater than C-30Mpa and 4.24 % greater than C-25Mpa concrete grade.

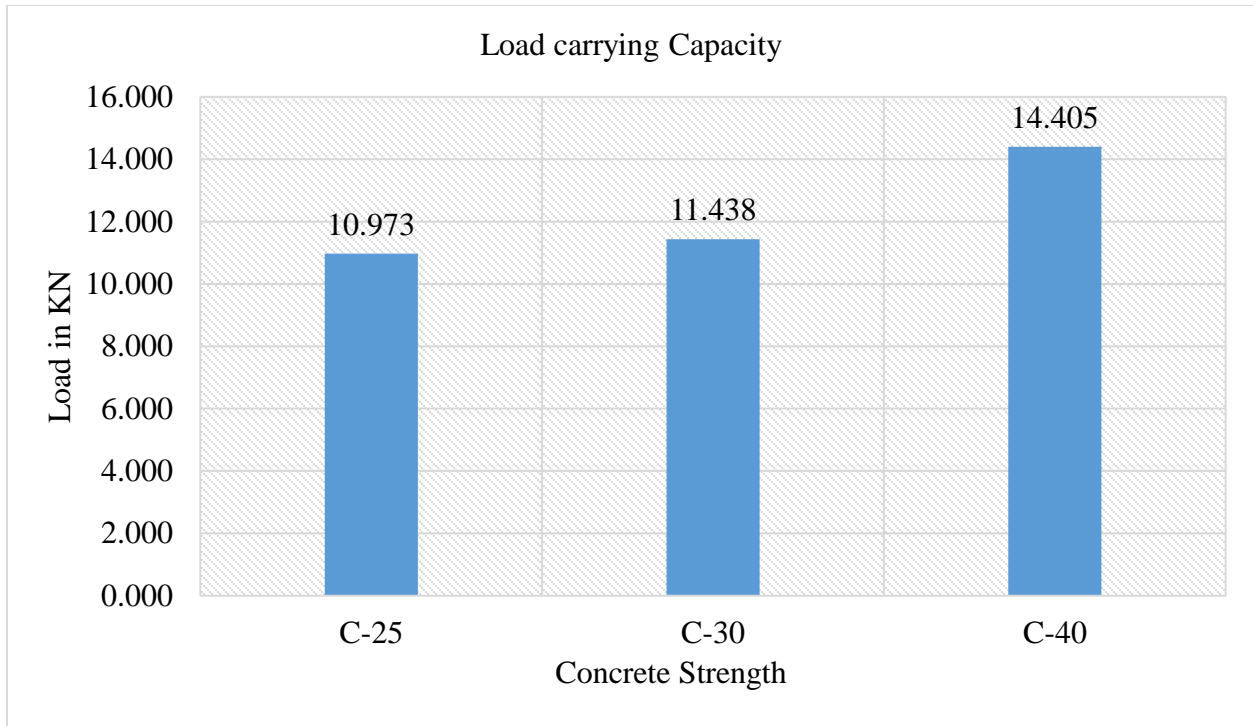


Figure 4.8 Concrete Strength versus Load carrying Capacity.

4.3.2 Energy Dissipation and Damping Ratio

The inelastic deformation of shear wall-slab connections helps to dissipate a sufficient amount of energy through hysteretic behavior and thereby reduce the energy transmission and ensure that a structure performs satisfactorily in the event of a strong earthquake. The cumulative energy dissipation and equivalent viscous damping ratio are important indicators and are calculated based on the hysteretic loops. The amount of dissipated energy at each cycle is calculated as the sum of the areas enclosed by the load –displacement hysteresis loops. The cumulative energy dissipation is expressed as the sum of the energy dissipation. The equivalent viscous damping ratio (EVD) or h_e computed as.

$$h_e = \frac{S_{AEBF}}{2\pi(S_{OAD} + S_{OBC})} \quad 4.1$$

Where S_{AEBF} is the area of the enclosed curve and is calculated by using origin lab software

S_{OAD} and S_{OBC} are the areas of OAD and OBC sections of the curve respectively as shown in the figure 4.9.

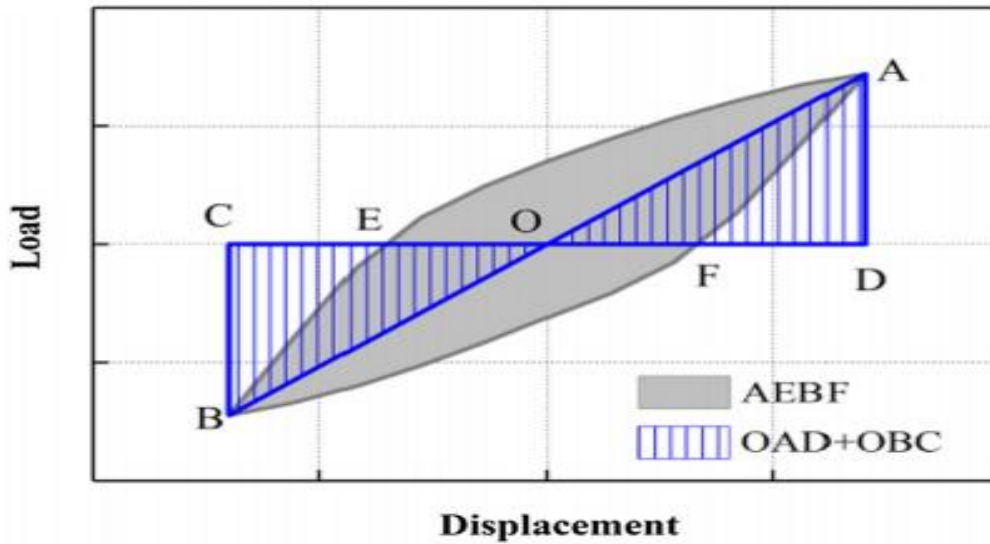


Figure 4.9 Definition of energy dissipation and Equivalent Viscous Damping ratio.

4.3.2.1 Energy Dissipation for U-Type Connection

Table 4.2 Cumulative energy dissipation and EVD of U-type Connection.

Specimen designation	Area of OAD	Area of OBC	$2*\pi *(S_{OAD} + S_{OBC})$ (KNmm)	Area of Loop (KNmm)	h_e
	Positive (KNmm)	Negative (KNmm)			
Ts/Tw=0.6	131.490	134.719	1671.793	1331.143	0.80
Ts/Tw=0.8	145.480	146.214	1831.839	1566.701	0.86
Ts/Tw=1	248.959	250.449	3136.285	3046.029	0.97

The comparison of energy dissipated during each cycle of loading, plotted against the corresponding number of cycle for the specimens, is shown in Figure 4.10. The 17.7 % increase was found in the cumulative energy dissipation capacity for the Ts/Tw=0.8 specimen, when compared to that of the Ts/Tw=0.6. The 128.83 % increase was found in the cumulative energy dissipation capacity for the Ts/Tw=1 specimen, when compared to that of the Ts/Tw=0.6. The increment of the energy dissipation is due to the increments of aspect ratio of Ts/Tw.

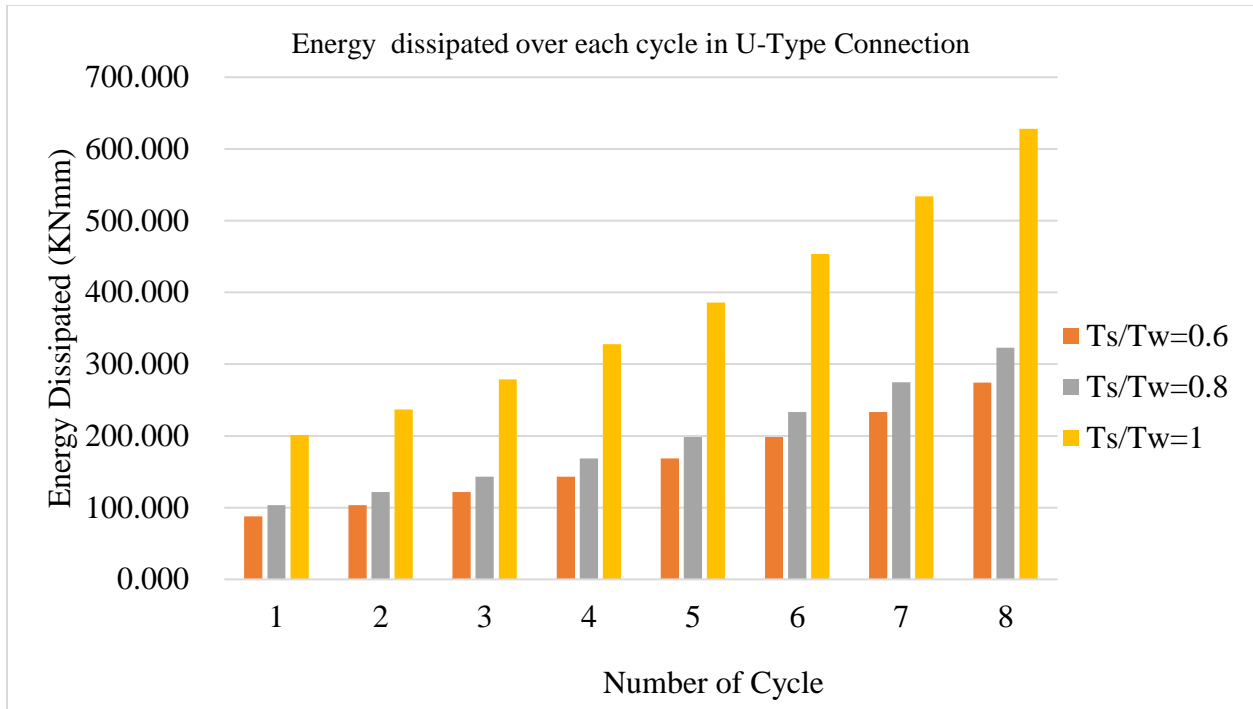


Figure 4.10 Comparison of Energy Dissipation Capacity of U-type connection with different aspect ratio of Ts/Tw.

4.3.2.2 Energy Dissipation for 90⁰-Type Connection

Table 4.3 Cumulative energy dissipation and EVD of 90⁰--type Connection.

Specimen designation	Area of OAD	Area of OBC	$2*\pi *(S_{OAD} + S_{OBC})$ (KNmm)	Area of Loop (KNmm)	h_e
	Positive (KNmm)	Negative (KNmm)			
Ts/Tw=0.6	132.079	134.503	1674.131	1339.000	0.80
Ts/Tw=0.8	145.847	146.623	1836.709	1548.0000	0.84
Ts/Tw=1	243.516	249.271	3094.702	2929.000	0.95

The comparison of energy dissipated during each cycle of loading, plotted against the corresponding number of cycle for the specimens, is shown in Figure 4.11. The 15.61% increase was found in the cumulative energy dissipation capacity for the Ts/Tw=0.8 specimen, when compared to that of the Ts/Tw=0.6. The 118.74% increase was found in the cumulative energy dissipation capacity for the Ts/Tw=1 specimen, when compared to that of the Ts/Tw=0.6. The increment of the energy dissipation is due to the increments of aspect ratio of Ts/Tw.

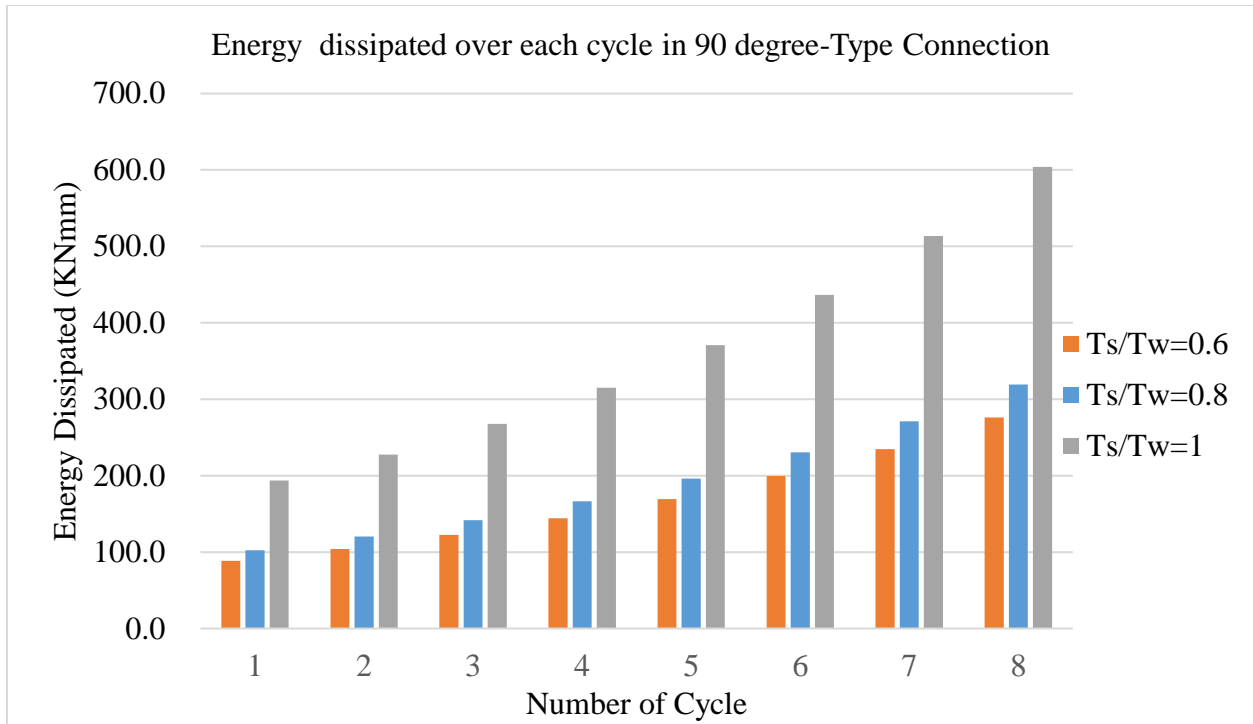


Figure 4.11 Comparison of Energy Dissipation Capacity of 90⁰-type connection with different aspect ratio of Ts/Tw.

4.3.2.3 Energy Dissipation for 135⁰-Type Connection

Table 4.4 Cumulative energy dissipation and EVD of 135⁰--type Connection.

Specimen designation	Area of OAD	Area of OBC	$2*\pi *(S_{OAD} + S_{OBC})$ (KNmm)	Area of Loop (KNmm)	h_e
	Positive (KNmm)	Negative (KNmm)			
Ts/Tw=0.6	131.492	133.862	1666.421	1316.800	0.79
Ts/Tw=0.8	145.811	146.669	1836.777	1533.541	0.83
Ts/Tw=1	247.403	249.383	3119.814	3050.471	0.98

The comparison of energy dissipated during each cycle of loading, plotted against the corresponding number of cycle for the specimens, is shown in Figure 4.12. The 16.46 % increase was found in the cumulative energy dissipation capacity for the Ts/Tw=0.8 specimen, when compared to that of the Ts/Tw=0.6. The 131.66 % increase was found in the

cumulative energy dissipation capacity for the $T_s/T_w=1$ specimen, when compared to that of the $T_s/T_w=0.6$. The increment of the energy dissipation is due the increments of aspect ratio of T_s/T_w .

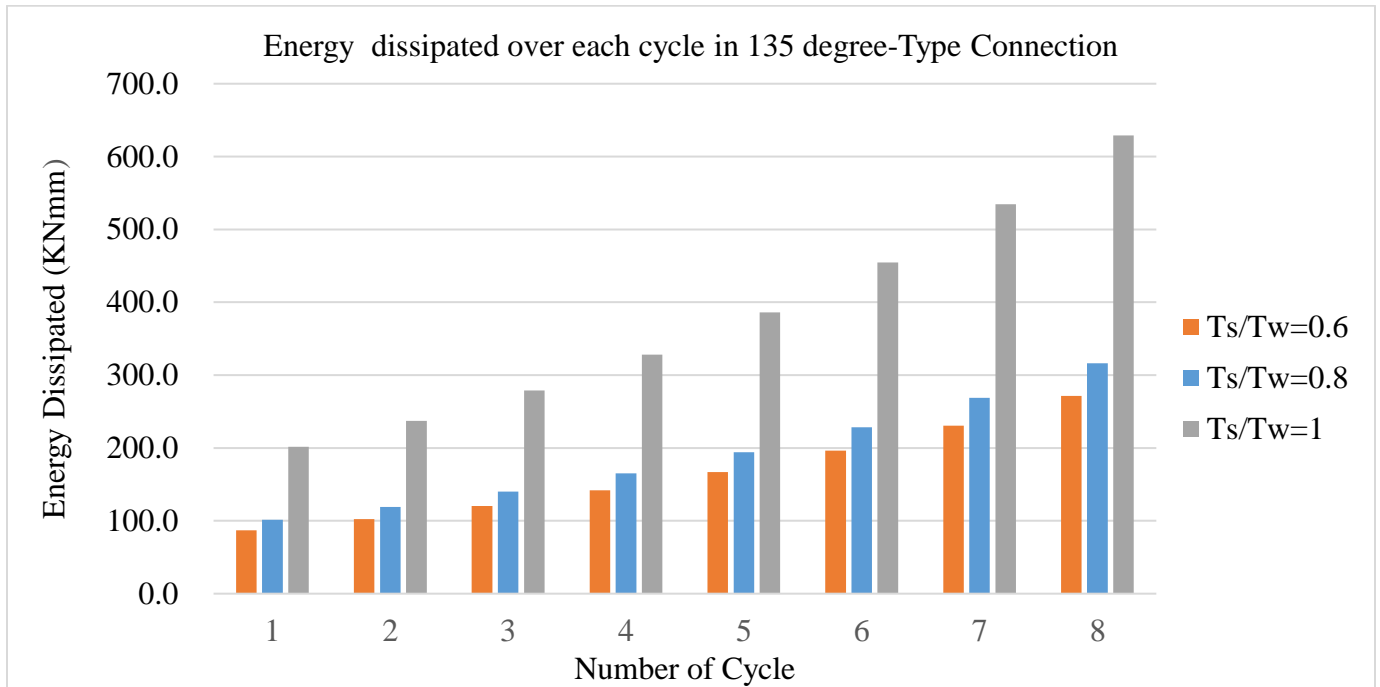


Figure 4.12 Comparison of Energy Dissipation Capacity of 135° -type connection with different aspect ratio of T_s/T_w .

4.3.2.4 Energy Dissipation for 150° -Type Connection

Table 4.5 Cumulative energy dissipation and EVD of 150° -type Connection.

Specimen designation	Area of OAD	Area of OBC	$2*\pi *(S_{OAD} + S_{OBC})$ (KNmm)	Area of Loop (KNmm)	h_e
	Positive (KNmm)	Negative (KNmm)			
Ts/Tw=0.6	132.178	133.955	1671.311	1310.346	0.78
Ts/Tw=0.8	145.926	146.450	1836.122	1501.657	0.82
Ts/Tw=1	247.403	251.583	3133.632	3072.68	0.98

The comparison of energy dissipated during each cycle of loading, plotted against the corresponding number of cycle for the specimens, is shown in Figure 4.13. The 14.6 % increase was found in the cumulative energy dissipation capacity for the $T_s/T_w=0.8$ specimen, when compared to that of the $T_s/T_w=0.6$. The 134.49 % increase was found in the cumulative energy

dissipation capacity for the $T_s/T_w=1$ specimen, when compared to that of the $T_s/T_w=0.6$. The increment of the energy dissipation is due the increments of aspect ratio of T_s/T_w .

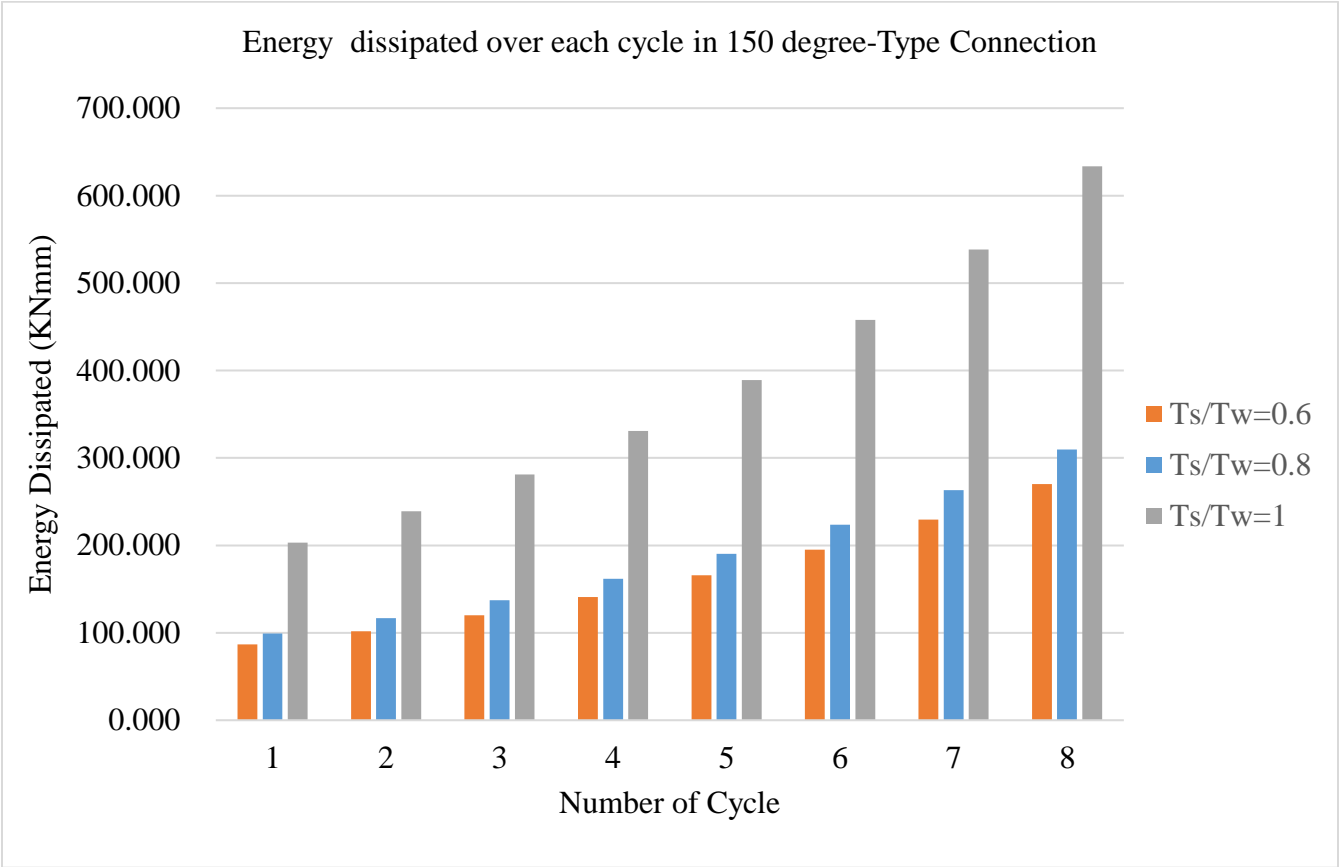


Figure 4.13 Comparison of Energy Dissipation Capacity of 150⁰-type connection with different aspect ratio of T_s/T_w .

4.3.2.5 Effect of Aspect Ratio of H/We on Energy Dissipation

The cumulative energy dissipation based on aspect ratio of H/We was shown in table 4.6 below it was concluded that as effective width of the slab increased from exterior shear wall the ability of the connection to absorb the cumulative energy was decreased.

The specimen with aspect ratio of H/We of 1.67 absorbs cumulative energy of 76.35% than aspect ratio of H/We of 1.46 and 106.70% than the aspect ratio of 1.30.

Table 4.6 Cumulative energy dissipation and EVD for aspect ratio of H/We.

Specimen designation	Area of OAD	Area of OBC	$2*\pi *(S_{OAD} + S_{OBC})$ (KNmm)	Area of Loop (KNmm)	h_e
	Positive (KNmm)	Negative (KNmm)			
H/We=1.67	131.490	134.719	1671.793	1331.143	0.80
H/We=1.46	88.066	85.184	1088.006	754.847	0.69
H/We=1.30	90.410	91.978	1145.396	643.984	0.56

4.3.2.6 Effects of Connection Type on Energy Dissipation

The cumulative energy absorbed due to the effect of connection type was shown in the table 4.7. The result shows that the specimen C4SWS3 shows better performance than the other connection. The C4SWS3 specimen exhibited the energy dissipation capacity that is by 0.89 % greater than C1SWS3, 4.9 % greater than C2SWS3 and 0.73 % greater than C3SWS3 specimen.

Table 4.7 Cumulative energy dissipation and EVD of Connection type.

Specimen designation	Area of OAD	Area of OBC	$2*\pi *(S_{OAD} + S_{OBC})$ (KNmm)	Area of Loop (KNmm)	h_e
	Positive (KNmm)	Negative (KNmm)			
C1SWS3	248.959	250.449	3136.285	3046.029	0.97
C2SWS3	243.516	249.271	3094.702	2929	0.95
C3SWS3	247.403	249.383	3119.814	3050.471	0.98
C4SWS3	247.403	251.583	3133.632	3072.68	0.98

4.3.2.7 Effects of Concrete Grade on Energy Dissipation

From the table shown below the cumulative energy of the model with concrete grade of C-40 dissipates more energy than the model with concrete grade of C-25 and C-30. The energy that was absorbed in the model with concrete grade of C-40 was 39.46% than the model with C-25 and

17.90% than the model with concrete grade of C-30. With respect to these values, it was concluded that the amount of energy absorbed was increased as concrete grade increased.

Table 4.8 Cumulative energy dissipation and EVD for grade of concrete.

Specimen designation	Area of OAD	Area of OBC	$2*\pi *(S_{OAD} + S_{OBC})$ (KNmm)	Area of Loop (KNmm)	h_e
	Positive (KNmm)	Negative (KNmm)			
C-25	125.93176	130.67538	1611.492839	1125.436	0.69
C-30	132.177591	133.9604275	1671.346756	1331.143	0.79
C-40	122.405338	145.569528	1682.882158	1569.476	0.93

4.3.3 Displacement Ductility Factor

Ductility is defined as the ability of a structure and its elements to resist huge inelastic deformation without any significant reduction in strength. Ductile structures are capable of dissipating hysterically large amounts of energy during inelastic cyclic deformations. A displacement ductility factor is defined as the ratio of ultimate displacement to displacement at yield; $\mu = \frac{\Delta_u}{\Delta_y}$ was used in this study to calculate the ductility of RC shear wall-slab slab connection. The load-displacement relation may not lead to a well-defined yield point due either to the nonlinear behavior of the materials or to the onset of yield at different load levels in different structural components. This leads to somewhat subjective determination of yielding deformation in reinforced concrete structures. Envelope curves were obtained by joining the peak points of all the cycles. Using these envelopes ductility factor for the specimens were obtained. For each model, the load–displacement envelope was used to define the yield and maximum displacements following the method used by [28].

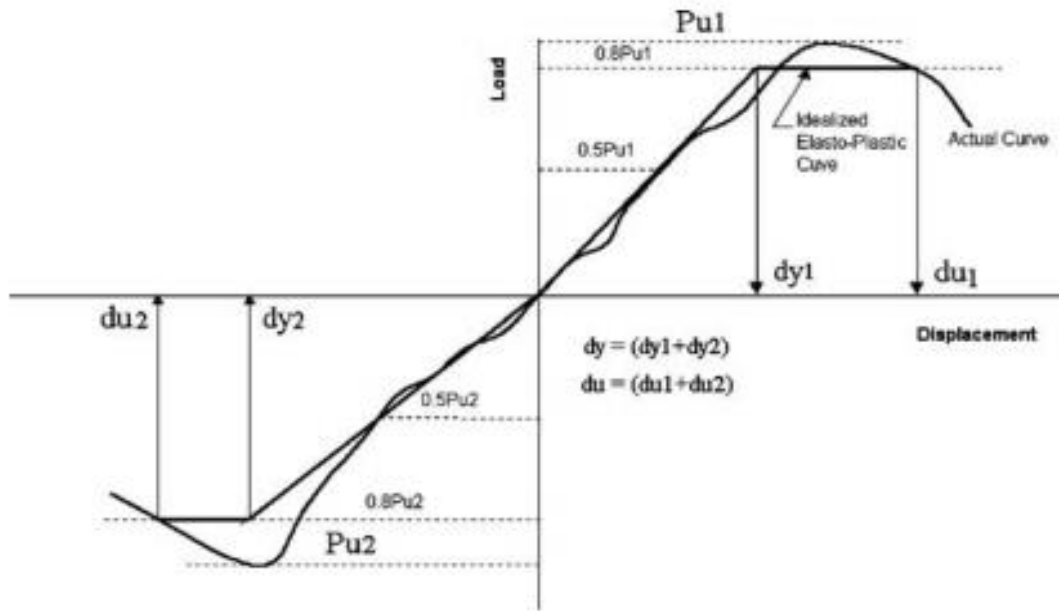


Figure 4.14 Method used to define the yield and ultimate displacements (Source:[28]).

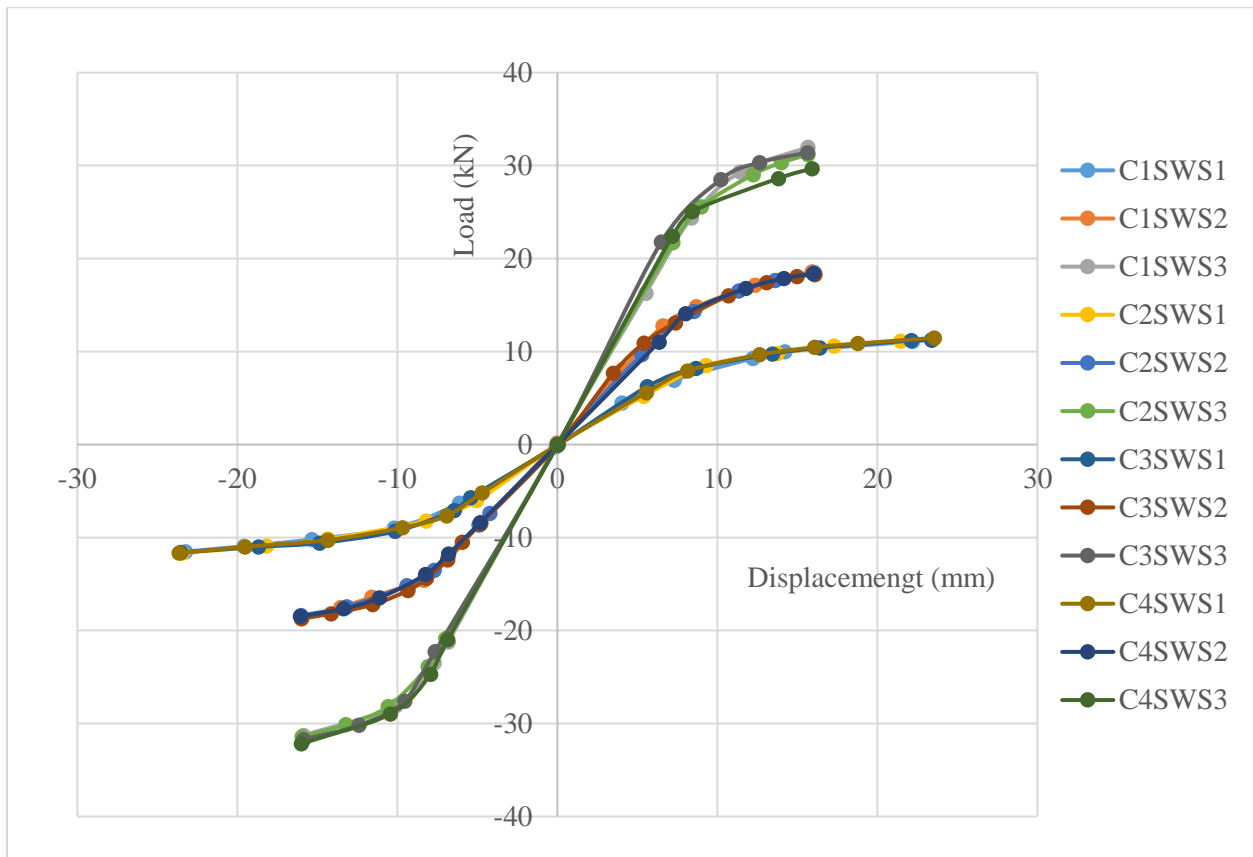


Figure 4.15 Comparison of load – displacement envelope curves of the specimen.

Table 4.9 Summary of displacement at yield and ultimate load for different specimen.

Specimen designation	Yield load (KN)	Displacement At yield load (mm) Δ_y	Ultimate load (KN)	Displacement At ultimate load (mm) Δ_u	Ductility factor $\mu = \frac{\Delta_u}{\Delta_y}$
C1SWS1	6.93	10.5	11.40	23.31	2.22
C1SWS2	12.77	6.60	18.64	15.95	2.42
C1SWS3	24.39	6.45	31.63	15.76	2.44
C2SWS1	8.50	9.92	11.51	23.47	2.36
C2SWS2	14.34	6.53	18.43	16.03	2.45
C2SWS3	21.72	6.37	31.40	15.96	2.51
C3SWS1	6.23	9.2	11.42	23.47	2.55
C3SWS2	10.93	5.56	18.51	16.06	2.89
C3SWS3	21.81	5.36	31.56	15.75	2.94
C4SWS1	7.93	11.87	11.56	23.59	1.98
C4SWS2	14.08	8.01	18.43	16.03	2.00
C4SWS3	22.40	7.18	30.93	15.96	2.22

From the analysis, it can be concluded that as aspect ratio of T_s/T_w increase for the same connection the ductility of the RC exterior shear wall-slab connection tends to increase. From table 4.9 it was concluded that the specimen C3SWS3 was more ductile than the other the connection type of this specimen was 135-degree connection with aspect ratio of $T_s/T_w=1$.

4.3.4 Stiffness Degradation

In the case of reinforced concrete shear wall-slab connection, stiffness of the joint gets reduced when the joint is subjected to cyclic/repeated/dynamic loading. This reduction in stiffness is due to the following reasons. During cyclic loading, the materials, viz. concrete and steel, are subjected to loading, unloading, and reloading processes. This will cause initiation of micro-cracks inside the joint and will sometimes lead to the fatigue limit of the materials. This, in turn, increases the deformations inside the joints, thus resulting in reduction in the stiffness. Hence, it is necessary to evaluate degradation of stiffness in the shear wall-slab joints subjected to cyclic or repeated

loading. In order to determine the degradation of stiffness, the following procedure was adopted. A line 0-1 joining the origin and the peak load of the first cycle, as shown in Figure 14.16, is drawn. The slope of this line is known as the secant stiffness [29]. Similarly, from the slope of the line joining the points 2 and 3 of the second cycle, secant stiffness of the second cycle is obtained. Similar procedure was adopted for all the other cycles.

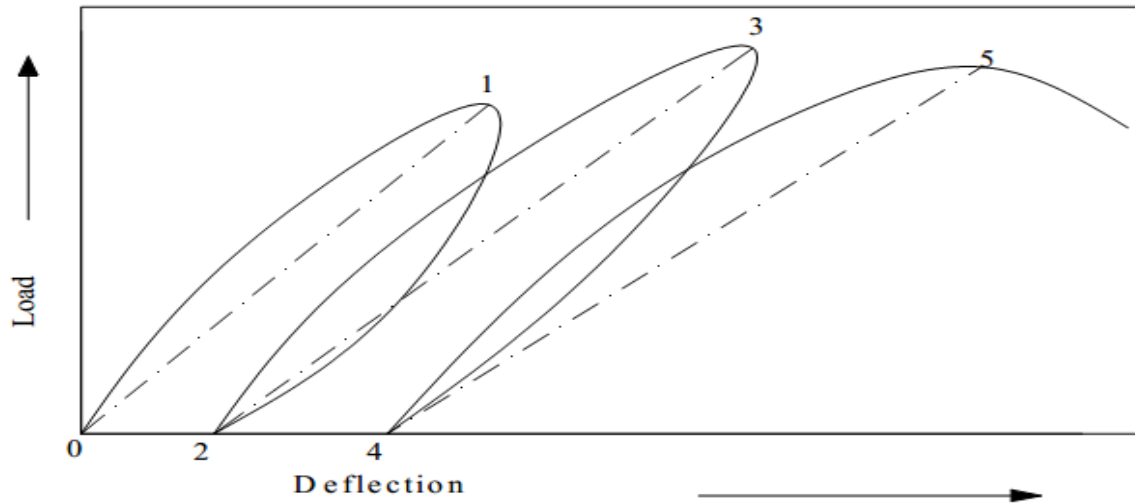


Figure 4.16 The procedure adopted for determining secant stiffness (Source: [30]).

The values of the secant stiffness obtained for each cycle are plotted for the specimens with the same aspect ratio of $T_s/T_w=0.6$ and different connection type are given on Figure 4.17. It may be noted from this figure that as the number of cycles increases, stiffness decreases.

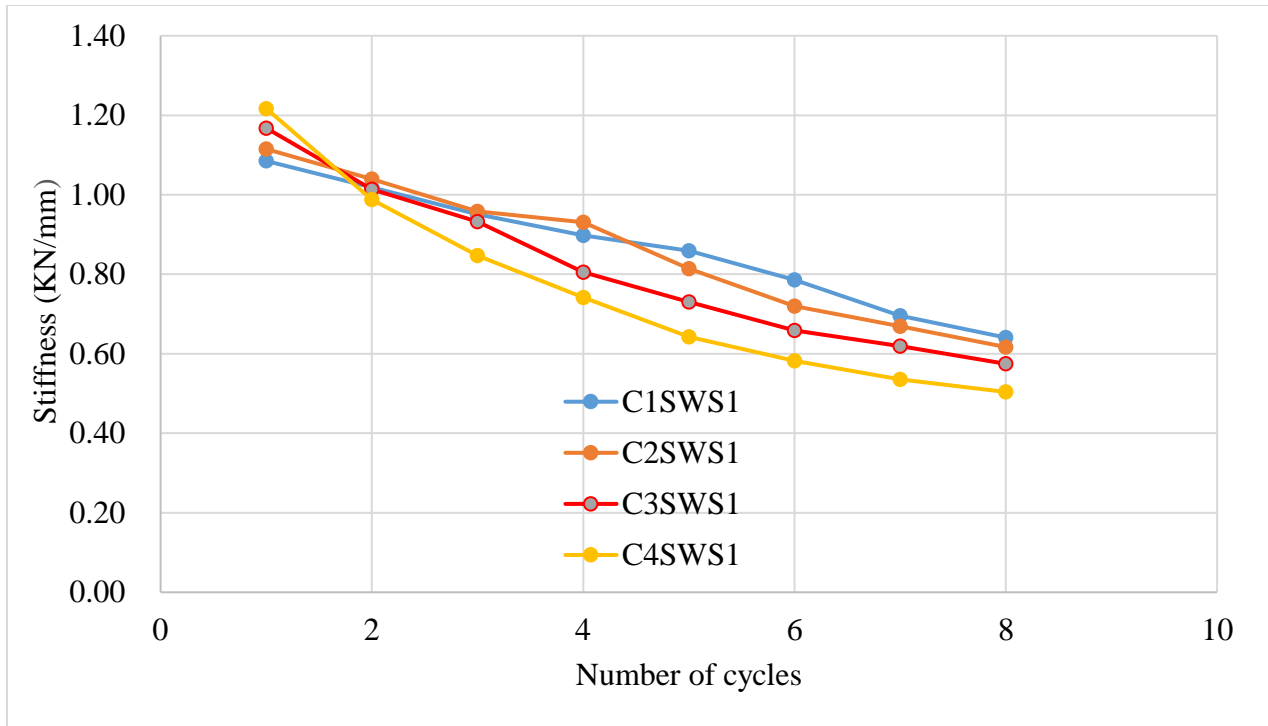


Figure 4.17 Relationship between stiffness and number of cycles for aspect ratio of $T_s/T_w=0.6$. The values of the secant stiffness obtained for each cycle are plotted for the specimens with the same aspect ratio of $T_s/T_w=0.8$ and different connection type are given on Figure 4.18. It may be noted from this figure that as the number of cycles increases, stiffness decreases.

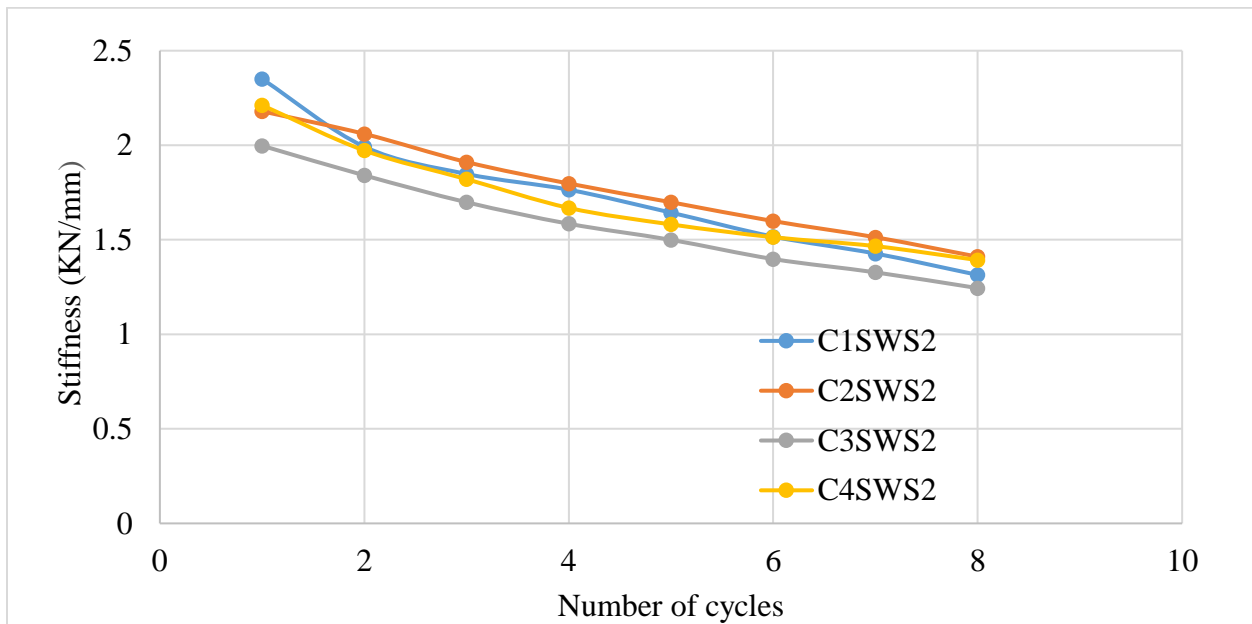


Figure 4.18 Relationship between stiffness and number of cycles for aspect ratio of $T_s/T_w=0.8$.

The values of the secant stiffness obtained for each cycle are plotted for the specimens with the same aspect ratio of $T_s/T_w=1$ and different connection type are given on Figure 4.19. It may be noted from this figure that as the number of cycles increases, stiffness decreases.

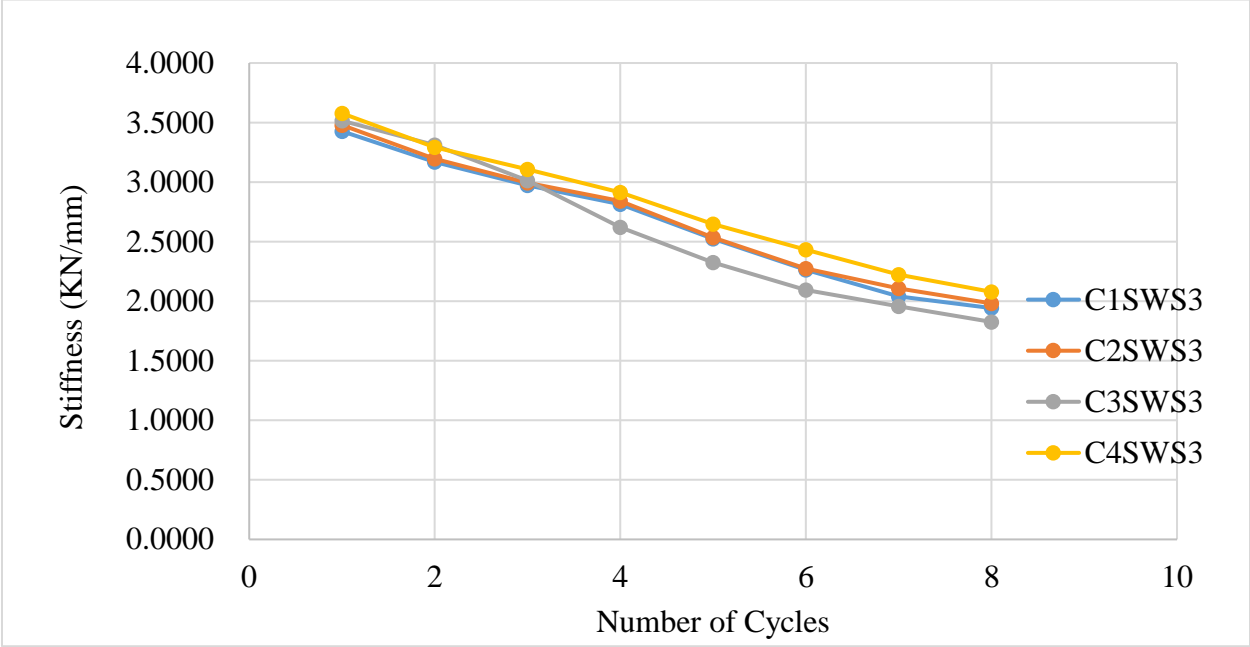


Figure 4.19 Relationship between stiffness and number of cycles for aspect ratio of $T_s/T_w=1$.

CHAPTER 5

CONCLUSION AND RECOMMENDATIONS

The main objective of this research is to study the load carrying capacity, energy dissipation, ductility and stiffness degradation behavior of reinforced concrete exterior shear wall - slab connection based on different thickness of slab to thickness of shear wall (t_s/t_w), height of shear wall to effective width of slab (w_e/H_w) ratio and connection types. This research included a nonlinear finite element analysis by ABAQUS Software package in order to predict the load carrying capacity and energy dissipation behavior reinforced concrete exterior shear wall-slab connection specimen presented in chapter three. In this chapter, conclusion based on analytical evidences as well as some recommendations for future extension of the work has been presented.

5.1 Conclusion

The main conclusions observed from each phase of investigation (finite element analysis) for exterior shear wall - slab connection based on different thickness of slab to thickness of shear wall (t_s/t_w), height of shear wall to effective width of slab (H_w/W_{es}) ratio and connection types is presented in this section which represents the summary and benefit of this research:

- Study on the effect of aspect ratio of T_s/T_w for U-type connection shows 0.8 (when the slab thickness 240mm and shear wall thickness 300mm) and 1 (when the slab thickness 300mm and shear wall thickness 300mm) aspect ratio have a larger load carrying capacity than the aspect ratio of 0.6 (when the slab thickness 180mm and shear wall thickness 300mm) by 61.7 % and 73.34 % respectively.
- Study on the effect of aspect ratio of T_s/T_w for 90° -type connection shows 0.8 (when the slab thickness 240mm and shear wall thickness 300mm) and 1 (when the slab thickness 300mm and shear wall thickness 300mm) aspect ratio have a larger load carrying capacity than the aspect ratio of 0.6 (when the slab thickness 180mm and shear wall thickness 300mm) by 61.49 % and 71.86 % respectively.
- Study on the effect of aspect ratio of T_s/T_w for 135° -type connection shows 0.8 (when the slab thickness 240mm and shear wall thickness 300mm) and 1 (when the slab thickness 300mm and shear wall thickness 300mm) aspect ratio have a larger load carrying capacity

than the aspect ratio of 0.6 (when the slab thickness 180mm and shear wall thickness 300mm) by 61.64 % and 72.35 % respectively.

- Study on the effect of aspect ratio of T_s/T_w for 150° -type connection shows 0.8 (when the slab thickness 240mm and shear wall thickness 300mm) and 1 (when the slab thickness 300mm and shear wall thickness 300mm) aspect ratio have a larger load carrying capacity than the aspect ratio of 0.6 (when the slab thickness 180mm and shear wall thickness 300mm) by 61.43 % and 72.49 % respectively.
- The load carrying capacity of RC exterior shear wall-slab connection mostly affected by ratio of T_s/T_w rather than connection type.
- In addition, aspect ratio of T_s/T_w , the aspect ratio of H/W_e also has effect on the cyclic load resistance capacity of shear wall-slab connection. As aspect ratio of H/W_e increase the lateral load carrying capacity decreases.
- The ductility of the RC exterior shear wall-slab connection increased as T_s/T_w increases and decreased as H/W_e decreased.
- The stiffness of RC exterior shear wall-slab connection decreased as the number of cycles decreased.

5.2 Recommendation for Future Studies

- ✚ Since the load, carrying capacity of exterior shear wall-slab connection is affected by different parameters; investigating the effect of each parameter individually on the shear strength of joint will be vital to give a reliable conclusion.
- ✚ Since this study covers the effect of thickness of slab to thickness of shear wall (t_s/t_w), height of shear wall to effective width of slab (H_w/W_{es}) ratio and connection types on load carrying capacity and hysteresis behavior of exterior shear wall-slab joint it's also important to examine its effect on other types of joint, like interior shear wall-slab connection.
- ✚ Further research regarding to load carrying capacity of exterior shear wall-slab connection needs to be conducted experimentally to identify the influence of those parameters considered in this study on the behavior of the connection.
- ✚ The designers should consider the seismic behavior of structure not only static analysis because the structures should be ductile especially under region of zone four.

References

- [1] G. S. Pillai, J. Krishnan Prabhakaran, and V. Rajkumar, "Parametric Study of Exterior Shear Wall–Floor Slab Connections," *J. Perform. Constr. Facil.*, vol. 29, no. 6, p. 04014156, 2013.
- [2] H. J. Lee and D. A. Kuchma, "Seismic Overstrength of Shear Walls in Parking Structures with Flexible Diaphragms Seismic Overstrength of Shear Walls in Parking," vol. 2469, no. May, 2007.
- [3] M. Y. Kaltakci, M. Ozturk, and M. H. Arslan, "An experimental investigation for external RC shear wall applications," pp. 1941–1950, 2010.
- [4] A. Gomez-bernal, "Interaction between shear walls and transfer-slabs , subjected to lateral and vertical loading Interaction between shear walls and transfer-slabs , subjected to lateral and vertical loading," no. November 2014, 2013.
- [5] A. A. N. Al-aghbari, S. H. Hamzah, N. H. A. Hamid, and N. A. Rahman, "Structural performance of two types of wall slab connection under out-of-plane lateral cyclic loading," *J. Eng. Sci. Technol.*, vol. 7, no. 2, pp. 177–194, 2012.
- [6] S. H. Luk and J. S. Kuang, "Seismic Behaviour of Rc Exterior Wide Beam-Column Joints," *15th World Conf. Earthq. Eng. Lisbon Port.*, 2012.
- [7] E. R. Kumar, E. Shagunveer, S. Sidhu, E. S. Sidhu, E. Harjot, and S. Gill, "Seismic Behavior Of Shear Wall Framed Buildings," vol. 2, no. 1, pp. 28–38, 2014.
- [8] M. Memon, "WALL -SLAB JUNCTION WITH SPECIAL SHEAR REINFORCEMENT WALL - SLAB JUNCTION WITH SPECIAL SHEAR," no. July, 2014.
- [9] Z. Sun, Y. Mao, J. Liu, Q. Zhao, and M. Chu, "Experimental Study on Assembled Monolithic Concrete Shear Walls Built with Precast Two-Way Hollow Slabs," no. 1, pp. 161–165, 2014.
- [10] A. A. Ansari, M. A. Bhutto, N. Bhatti, and R. A. Memon, "Strength of Wall-Slab Junction

- with New Form of Shear Reinforcement in a Laterally Loaded Tall Shear Wall Building,” vol. 9, pp. 193–206, 2015.
- [11] R. S. S. K. P. J. S. Greeshma, “Modelling and Assessment of Shear Wall – Flat Slab Joint Region in Tall Structures,” pp. 2201–2202, 2015.
- [12] S. Kaushik and K. Dasgupta, “Seismic Damage in Shear Wall-Slab Junction in RC Buildings,” *Procedia Eng.*, vol. 144, pp. 1332–1339, 2016.
- [13] R. Thanaykumar and T. H. S. Murthy, “BEHAVIOUR OF SHEAR WALL SLAB JUNCTION WITH SFRC SUBJECTED TO IN,” vol. 6, no. 6, pp. 98–110, 2016.
- [14] L. Wang, M. Chu, J. Liu, G. Wang, G. Qiu, and M. Liu, “Experimental Study on Shear Performance of Innovated Precast Shear Walls with Different Yield Strength Grades of Reinforcements,” pp. 946–954, 2017.
- [15] J. Lubliner, J. Oliver, S. Oller, and E. Onate, “a Plastic-Damage Model,” *Int. J. Solids Struct.*, vol. 25, no. 3, pp. 299–326, 1989.
- [16] J. Lee and G. L. Fenves, “Plastic-damage model for cyclic loading of concrete structures,” *J. Eng. Mech.*, vol. 124, no. 8, pp. 892–900, 1998.
- [17] J. G. Stoner, “Finite Element Modelling of GFRP Reinforced,” 2015.
- [18] A. A. User, “Abaqus 6.14,” vol. IV.
- [19] A. Hillerborg, M. Modéer, and P. E. Petersson, “Analysis of crack formation and crack growth in concrete by means of fracture mechanics and finite elements,” *Cem. Concr. Res.*, vol. 6, no. 6, pp. 773–781, 1976.
- [20] I. Edition, “Getting Started with Abaqus : Interactive Edition.”
- [21] R. Garcia, M. Guadagnini, K. Pilakoutas, and L. A. P. Poot, “Fibre-reinforced polymer strengthening of substandard lap-spliced reinforced concrete members: A comprehensive survey,” *Adv. Struct. Eng.*, vol. 20, no. 6, pp. 976–1001, 2017.

- [22] A. A. User, "Abaqus 6.14," vol. V.
- [23] B. S. En, "Eurocode 2 : Design of concrete structures —," vol. 3, 2004.
- [24] T. Wang and T. T. C. Hsu, "Nonlinear finite element analysis of concrete structures using new constitutive models," *Comput. Struct.*, vol. 79, no. 32, pp. 2781–2791, 2001.
- [25] R. Malm, "Predicting shear type crack initiation and growth in concrete with non-linear finite element method," no. 97, pp. xiv, 43, 2009.
- [26] I. Lapczyk and J. A. Hurtado, "Progressive damage modeling in fiber-reinforced materials," *Compos. Part A Appl. Sci. Manuf.*, vol. 38, no. 11, pp. 2333–2341, 2007.
- [27] S. R. Salim and K. P. Jaya, "EVALUATION OF REINFORCED CONCRETE WALL – FLAT SLAB CONNECTION WITH A NOVAL DUCTILE DETAILING," vol. 3236, no. Abstract ID, 2017.
- [28] M. J. Shannag, N. Abu-Dyya, and G. Abu-Farsakh, "Lateral load response of high performance fiber reinforced concrete beam-column joints," *Constr. Build. Mater.*, vol. 19, no. 7, pp. 500–508, 2005.
- [29] M. J. Shannag, N. Abu-dyya, and G. Abu-farsakh, "Lateral load response of high performance fiber reinforced concrete beam – column joints," vol. 19, pp. 500–508, 2005.
- [30] N. Ganesan, P. V. Indira, and R. Abraham, "Steel fibre reinforced high performance concrete beam-column joints subjected to cyclic loading," *ISET J. Earthq. Technol.*, vol. 44, no. 3–4, pp. 445–456, 2007.

Appendix A

Material properties

A. Concrete

Table A.1: Summary of concrete damage parameters

Concrete		Concrete Damage Parameter	
Grade	C30	Eccentricity (γ)	0.1
Density	2.40E-09	Dilation angle (β)	38
Modulus of elasticity	32836.6	k	0.667
Poisson's ratio	0.2	$\frac{\sigma_{bo}}{\sigma_{co}}$	1.16
		Viscosity parameter	0.0001

Table A.2 Compressive behavior of concrete damage plasticity for C-30

Compressive behavior		Compressive damage	
σ_c	e_{in}	d_c	e_{in}
15.2	0	0	0
21.45	9.14196E-05	2.96688E-05	1.9E-06
26.72	0.000180841	0.000507873	3.2E-05
31.01	0.000300453	0.00148381	9.1E-05
34.28	0.000450669	0.003002457	0.00018
36.54	0.000631913	0.005135187	0.0003
37.76	0.000844611	0.007972838	0.00045
38	0.00100463	0.011623379	0.00063
37.94	0.001089203	0.016208805	0.00084
37.06	0.001366134	0.019862497	0.001
35.10	0.001675857	0.021861358	0.00109
32.04	0.002018834	0.028719182	0.00137
27.88	0.002395537	0.036921546	0.00168
22.47	0.002815562	0.046603813	0.00202
		0.021861358	0.0024

		0.071195419	0.00282
--	--	-------------	---------

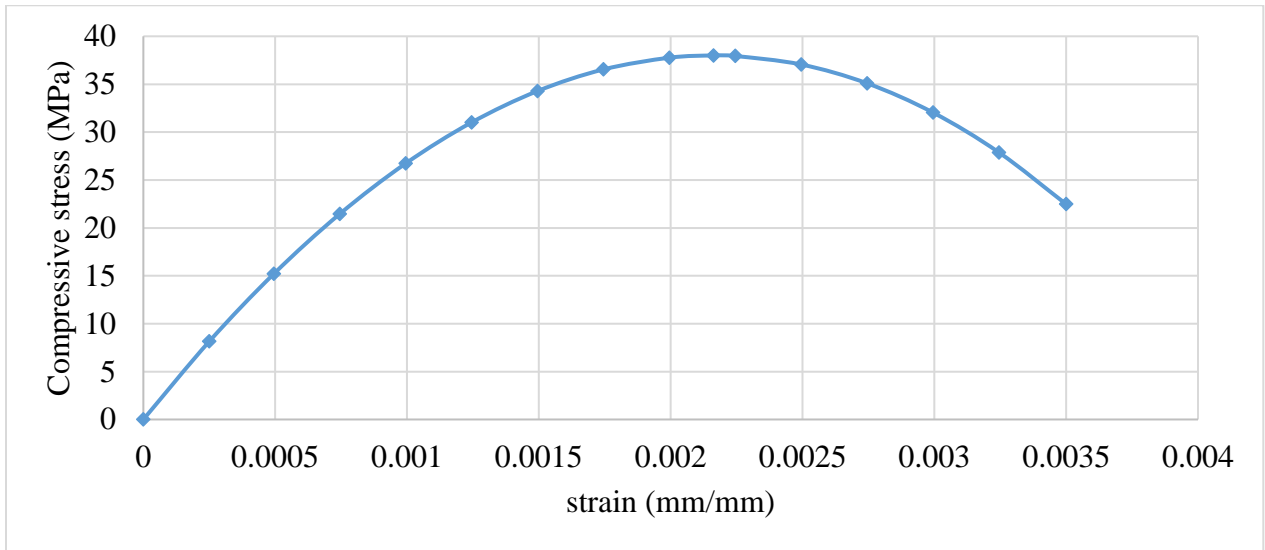


Figure A.1 Compressive stress versus inelastic strain

Table A.3 Tensile behavior of concrete damage plasticity for C-30

Tensile stress		Tension damage	
σ_t (Mpa)	ε_{cr} (mm/mm)	d_t	ε_{cr}
2.91192	0	0	0
2.20273	0.000432199	0.00576	1.1E-05
1.68238	0.001247676	0.21761	0.00043
1.30981	0.002458758	0.54285	0.00125
1.0473	0.004066566	0.8105	0.00246
0.86339	0.006072037	0.94429	0.00407
0.73349	0.0084759	0.9882	0.00607
0.63933	0.010896062		
0.56793	0.011278701		
0.51044	0.014480825		
0.46116	0.018082535		
0.41659	0.026485326		
0.37476	0.031286571		
0.33471	0.036487762		

0.2961	0.04208891
0.25892	0.048090016
0.22333	0.054491075
0.18955	0.061292079
0.15778	0.068493024
0.12818	0.076093905
0.10082	0.084094719
0.07574	0.092495465
0.05289	0.101296144
0.0322	0.11049676

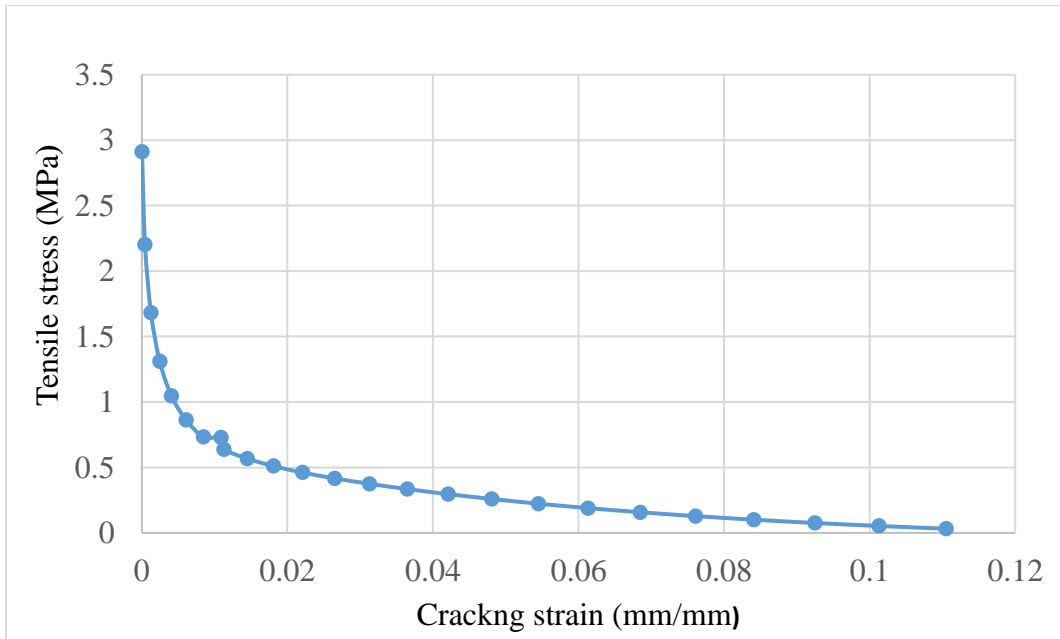


Figure A.2 Tensile stress versus cracking strain

Characteristic strength of concrete 25

Table A.4 Compressive behavior of concrete damage plasticity for C-25

Compressive behavior		Compressive damage	
σ_c	e_{in}	d_c	e_{in}
13.2	0	0	0
18.97	0.000100927	7.26968E-05	4.94744E-06
23.72	0.000200192	0.000508943	3.43856E-05
27.46	0.000331356	0.001518107	0.000100927
30.22	0.00049362	0.003082095	0.000200192
32.03	0.000686215	0.005253648	0.000331356
32.90	0.000908394	0.00810033	0.00049362
33	0.001020942	0.011700128	0.000686215
32.87	0.001159436	0.016137014	0.000908394
31.95	0.001438643	0.018495697	0.001020942
30.17	0.001745339	0.021496623	0.001159436
27.54	0.00207887	0.02786221	0.001438643
24.08	0.002438601	0.035310983	0.001745339
18.9536	0.002897952	0.043910921	0.00207887
		0.053718133	0.002438601
		0.066959359	0.002897952

Table A.5 Tensile behavior of concrete damage plasticity for C-25

Tensile stress		Tension damage	
σ_t (Mpa)	ϵ_{cr} (mm/mm)	d_t	ϵ_{cr}
2.578643728	0	0	0
2.000683435	0.000429504	0.005412079	1.14848E-05
1.563456851	0.001243135	0.197420124	0.000429504
1.239596346	0.002453232	0.503752441	0.001243135
1.003256263	0.0040606	0.774985224	0.002453232

0.832111308	0.006065936	0.925497852	0.0040606
0.707981947	0.008469806	0.981750506	0.006065936
0.702739695	0.010889969		
0.616715925	0.011272651		
0.547711009	0.014474802		
0.493305939	0.018076498		
0.448166112	0.022077906		
0.408728116	0.026479135		
0.372729832	0.031280258		
0.338831359	0.036481314		
0.306320665	0.042082328		
0.274892645	0.048083308		
0.244488679	0.054484256		
0.215184138	0.061285169		
0.187112695	0.068486045		
0.160418006	0.076086877		
0.13522516	0.084087662		
0.11162592	0.092488398		
0.08967321	0.101289082		

Characteristic strength of concrete 40

Table A.6 Compressive behavior of concrete damage plasticity for C-40

Compressive behavior		Compressive damage	
σ_c	e_{in}	d_c	e_{in}
19.20	0	0	0
28.92	9.97783E-05	6.92931E-05	2.45086E-06
34.78	0.000183142	0.000732662	2.56308E-05
39.68	0.000294064	0.002950373	9.97783E-05
43.53	0.000434735	0.00561316	0.000183142
46.25	0.000607583	0.009422869	0.000294064

47.74	0.000815311	0.014669727	0.000434735
48.00	0.000961406	0.021710946	0.000607583
47.89	0.00106093	0.030968617	0.000815311
46.60	0.001347808	0.037955335	0.000961406
43.71	0.001679728	0.042922747	0.00106093
39.09	0.002060946	0.05809837	0.001347808
32.56	0.002496274	0.077045863	0.001679728
30.06	0.002646393	0.100313819	0.002060946
		0.128414292	0.002496274
		0.138401432	0.002646393

Table A.7 Tensile behavior of concrete damage plasticity for C-40

Tensile stress		Tension damage	
σ_t (Mpa)	ε_{cr} (mm/mm)	d_t	ε_{cr}
3.527534999	0	0	0
2.552410205	0.000286538	0.00935815	9.70639E-06
1.875005329	0.000805177	0.264550227	0.000286538
1.418518719	0.001567738	0.616363283	0.000805177
1.115917256	0.002576065	0.86546632	0.001567738
0.91487749	0.003831596	0.96806545	0.002576065
0.777530331	0.005335376	0.99477789	0.003831596
0.771828683	0.006848033		
0.67811416	0.007088111		
0.600115672	0.009090257		
0.533625842	0.011342087		
0.473182675	0.01384375		
0.416144115	0.01659532		
0.361532658	0.019596822		
0.309258398	0.022848261		
0.259625557	0.026349626		

0.21304016	0.030100908
0.169853472	0.034102097
0.130292382	0.038353185
0.094442047	0.042854172
0.062257202	0.047605057
0.033586878	0.052605846
0.008203187	0.057856545

B. Steel Reinforcement

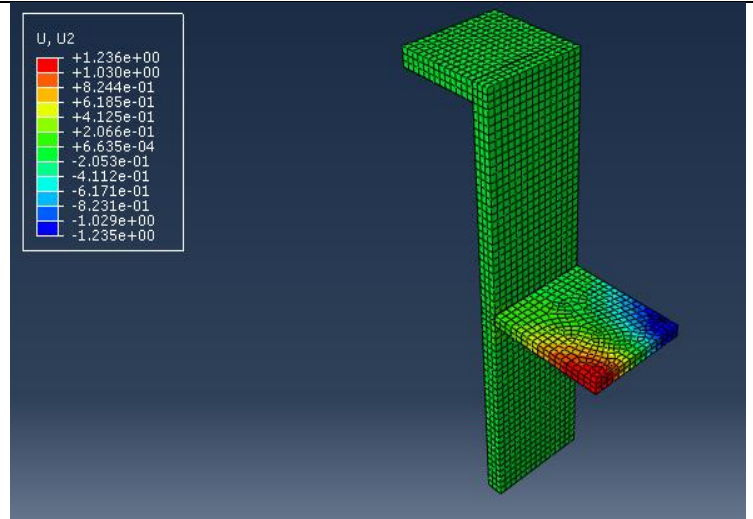
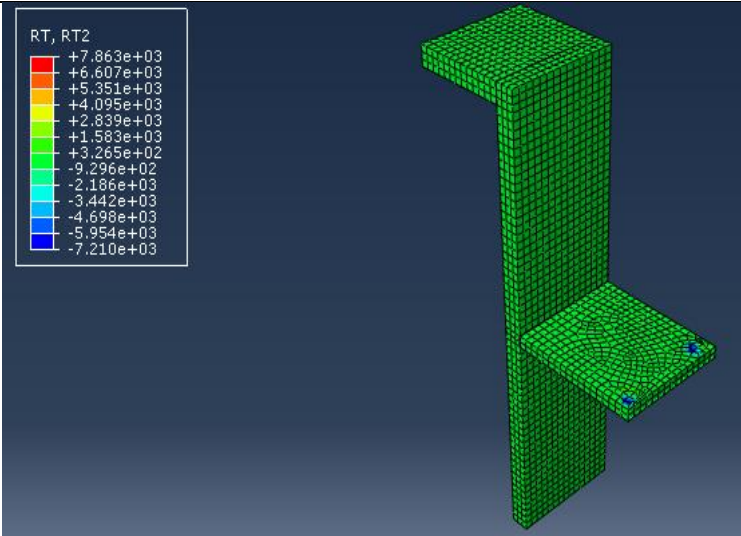
Table A.8 Steel properties

Steel properties	Diameter of bars		
	$\phi 6\text{mm}$	$\phi 12\text{mm}$	$\phi 18\text{mm}$
Elastic Modulus	200000 Mpa	200000 Mpa	200000 Mpa
Poisson's Ratio	0.3	0.3	0.3
Yield Strength	432	432	432

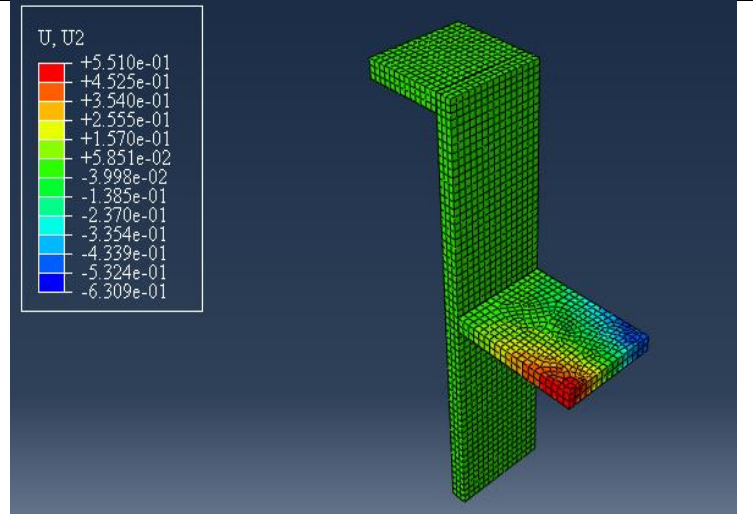
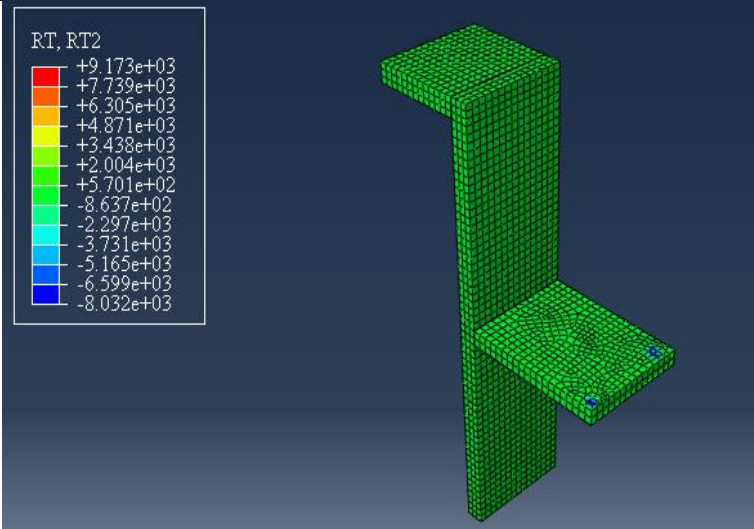
Appendix B

Table B.1 Samples of the Output from Software

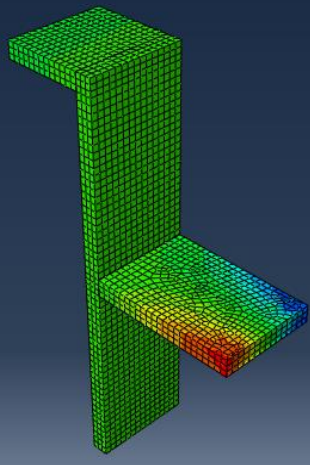
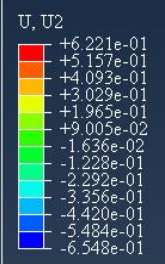
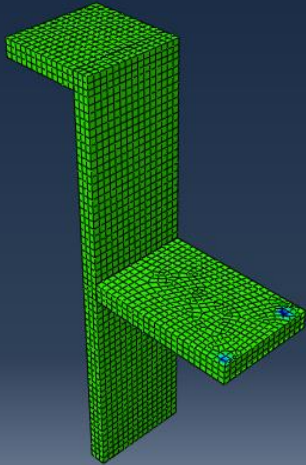
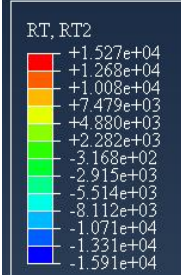
C1SWS1



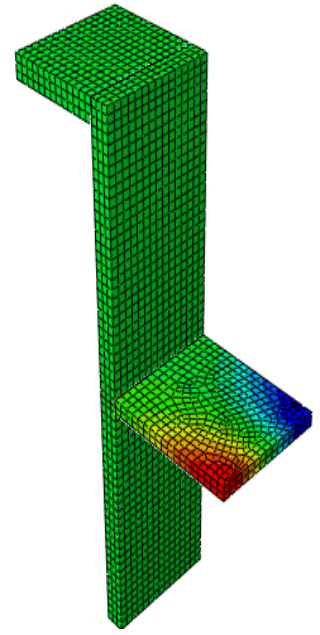
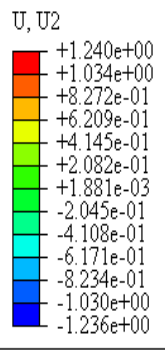
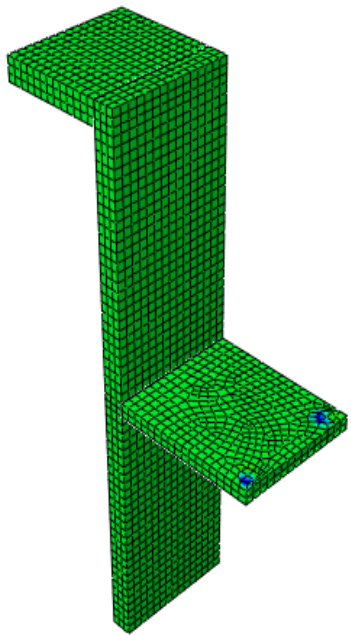
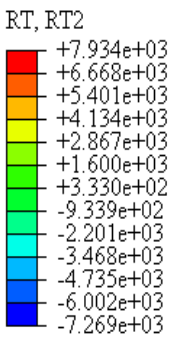
C1SWS2



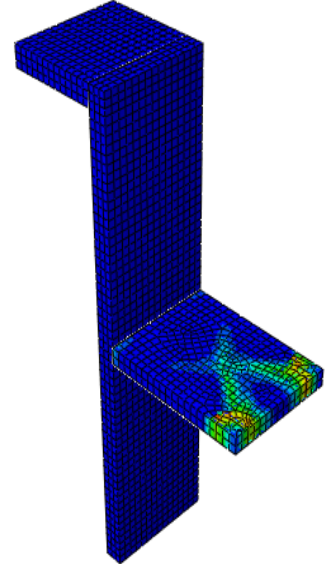
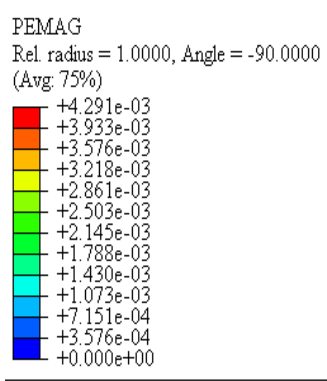
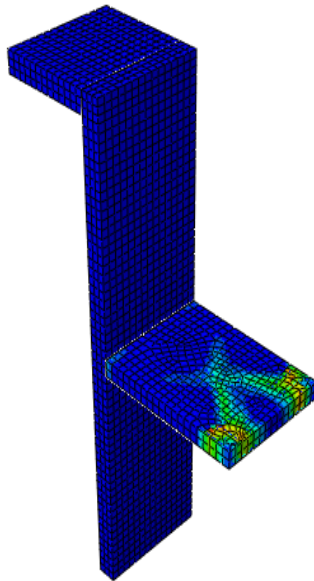
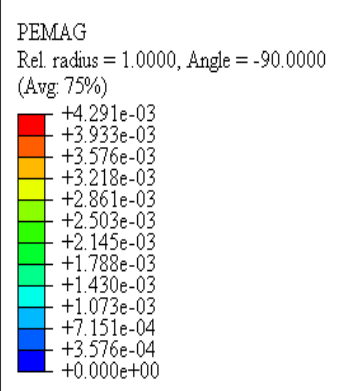
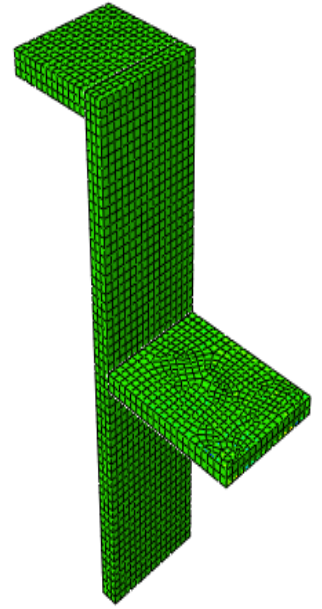
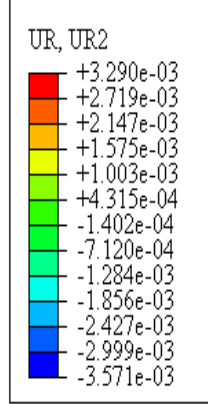
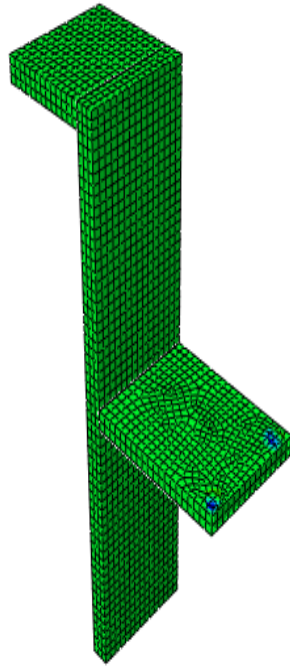
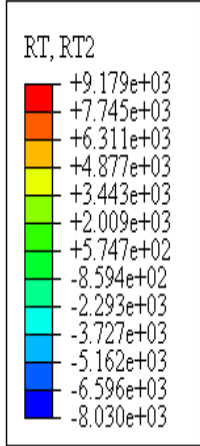
C1SWS3



C2SWS1

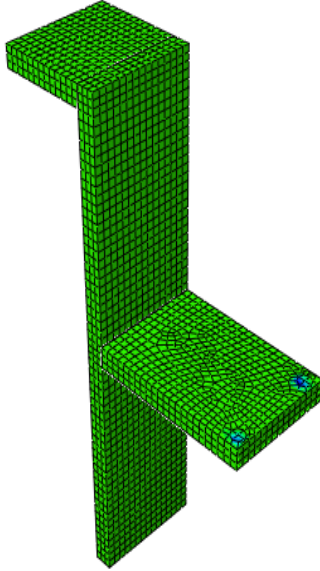
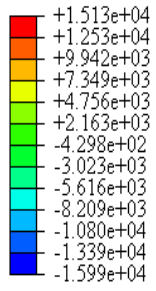


C2SWS2

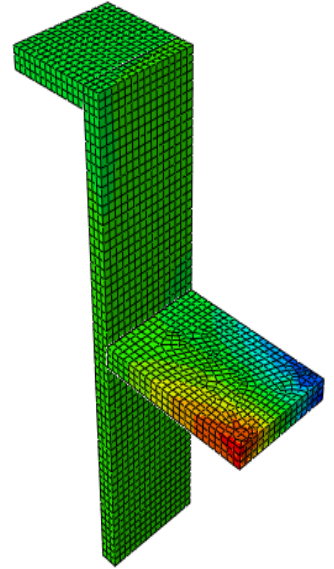
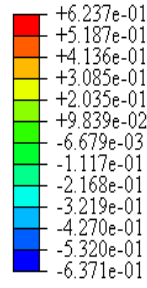


C2SWS3

RT, RT2

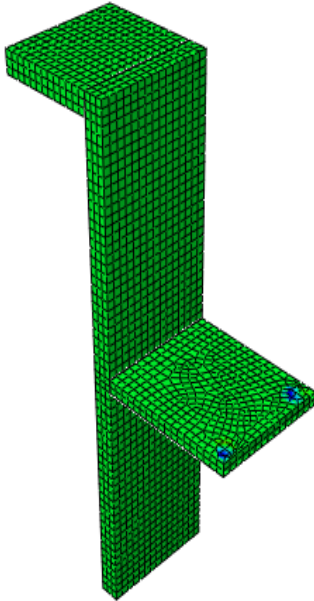
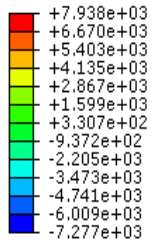


U, U2

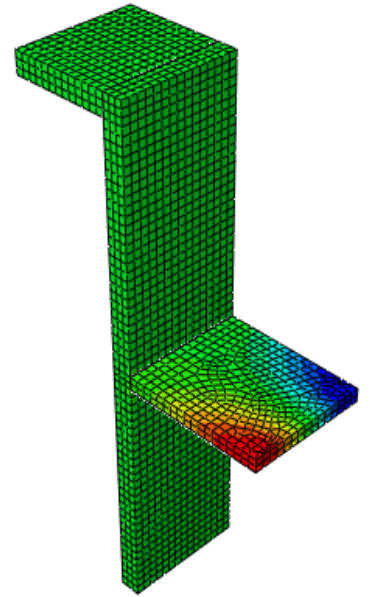
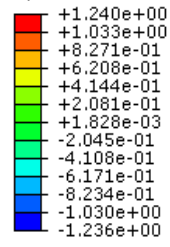


C3SWS1

RT, RT2



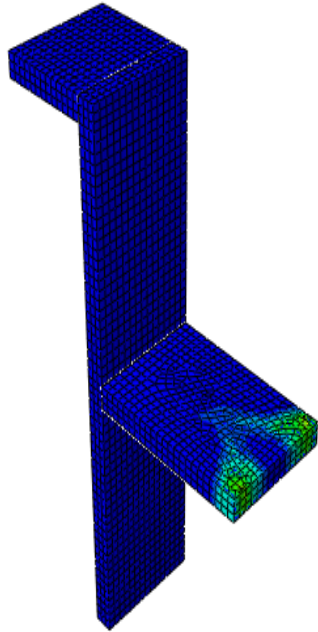
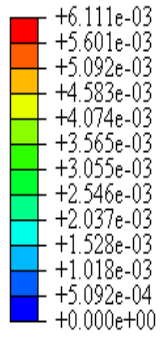
U, U2



PEMAG

Rel. radius = 1.0000, Angle = -90.0000

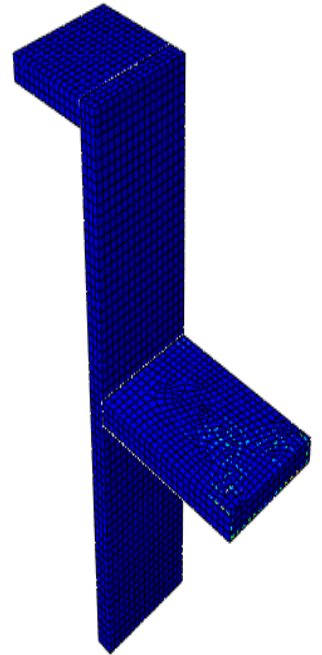
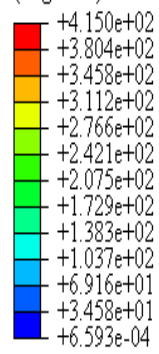
(Avg: 75%)



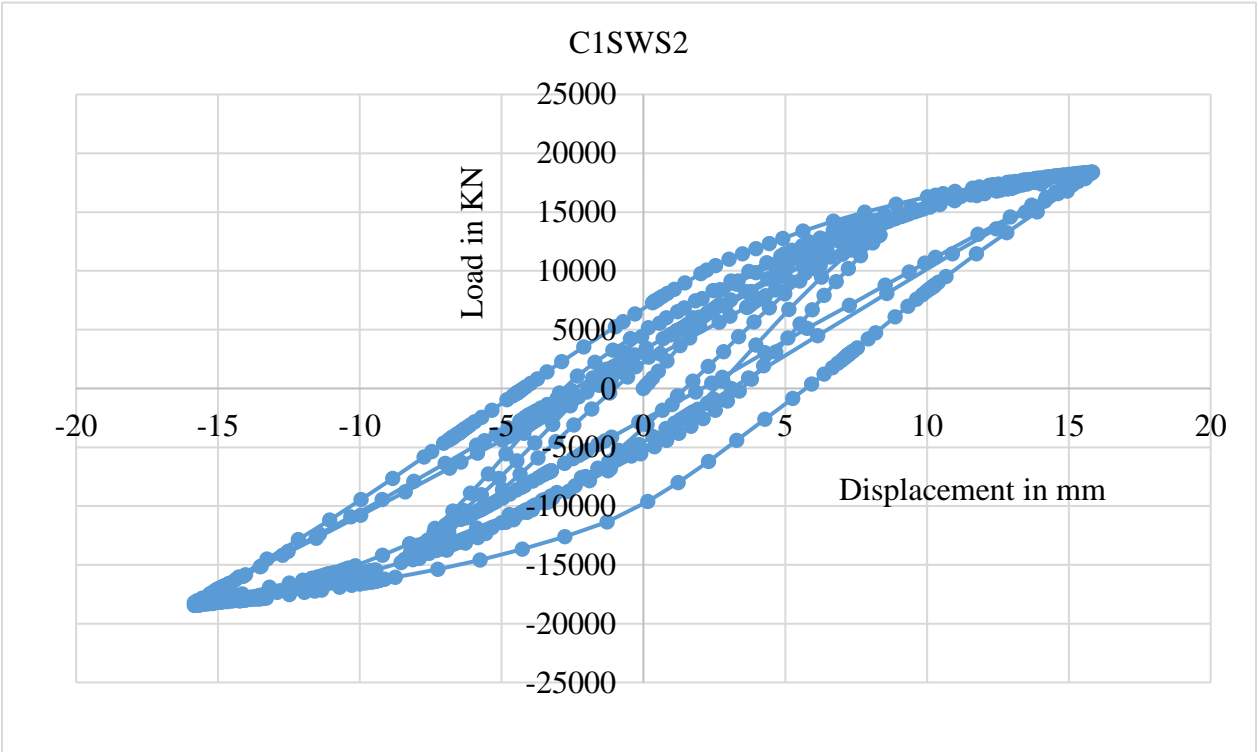
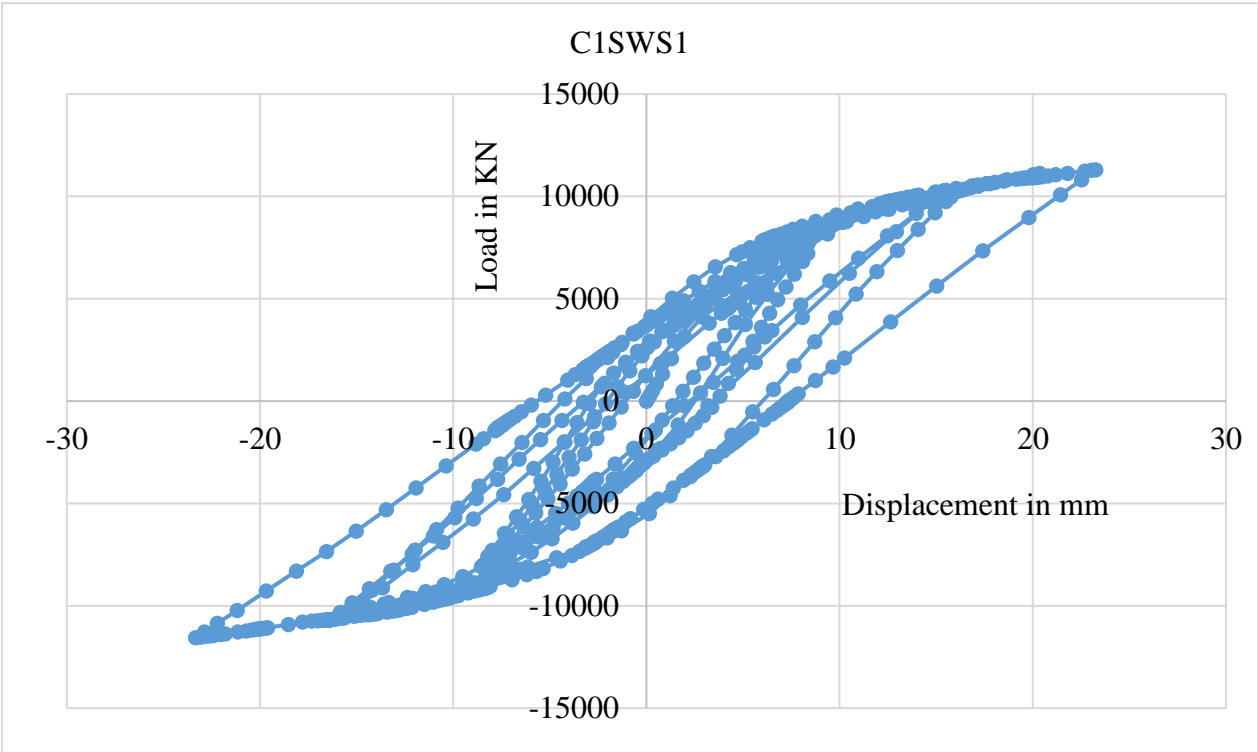
S, Mises

Rel. radius = 1.0000, Angle = -90.0000

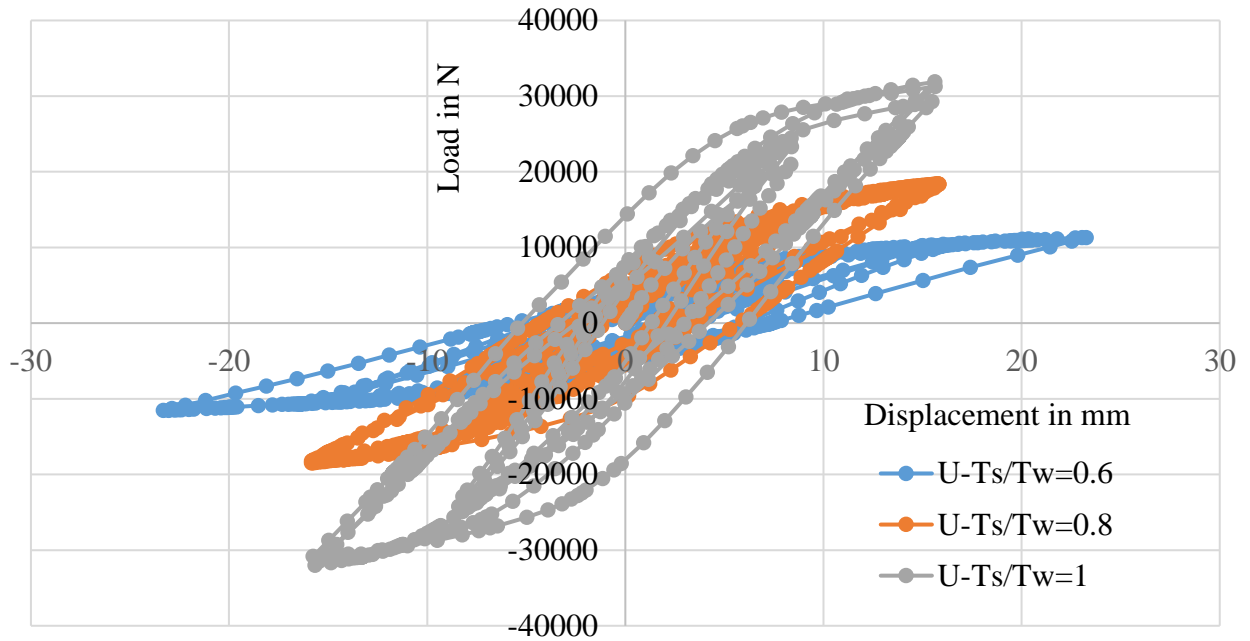
(Avg: 75%)



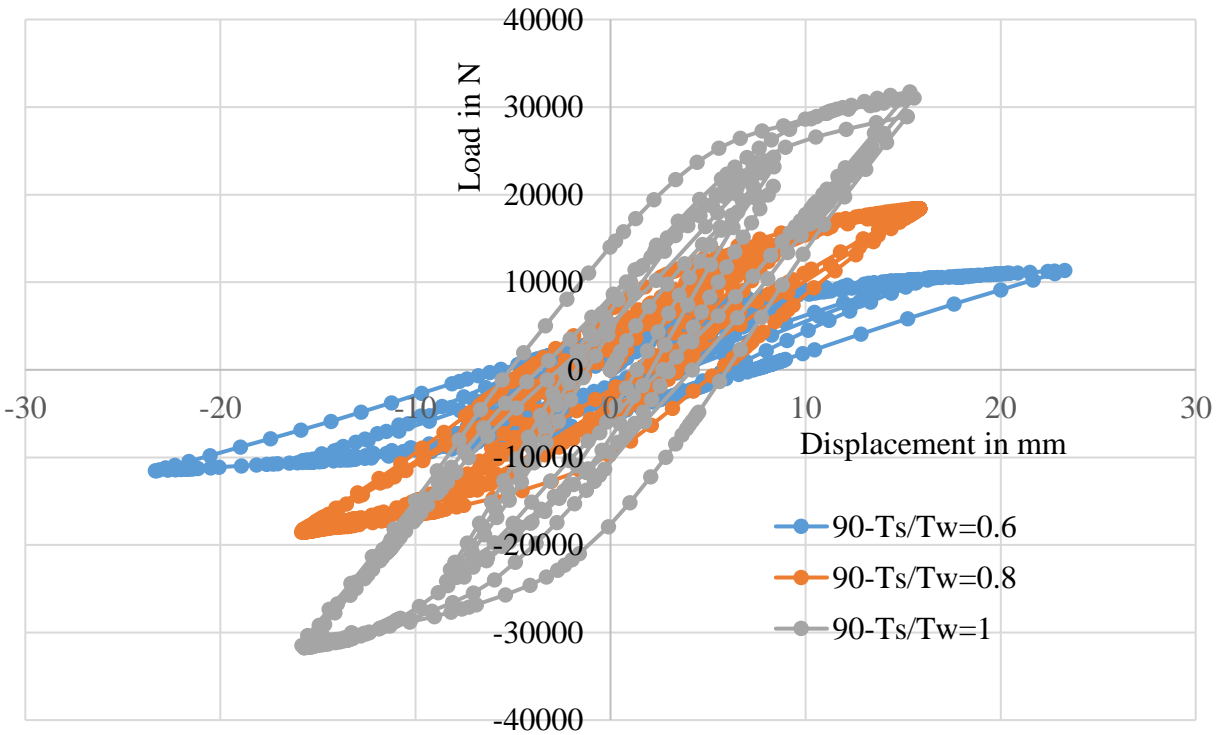
Some of the Hysteresis Behavior of RC Shear Wall-Slab Connection

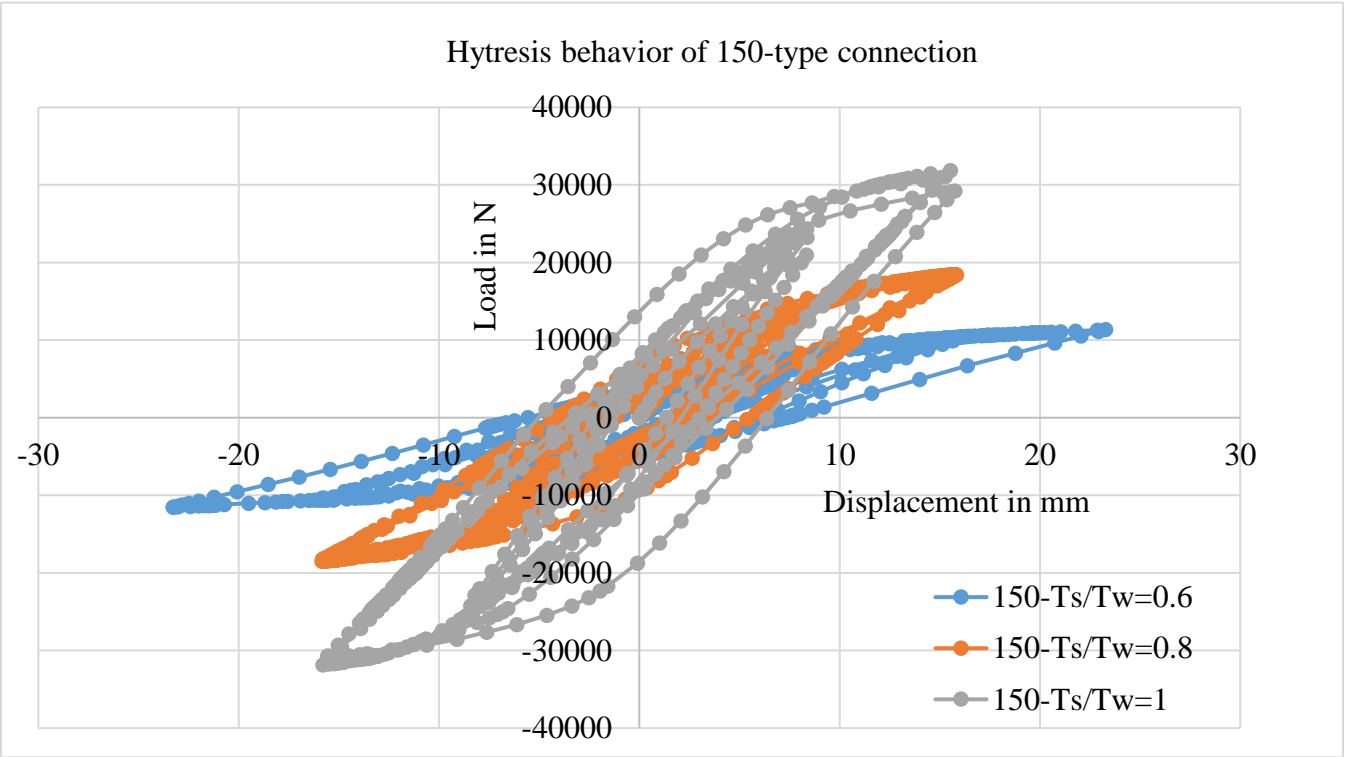
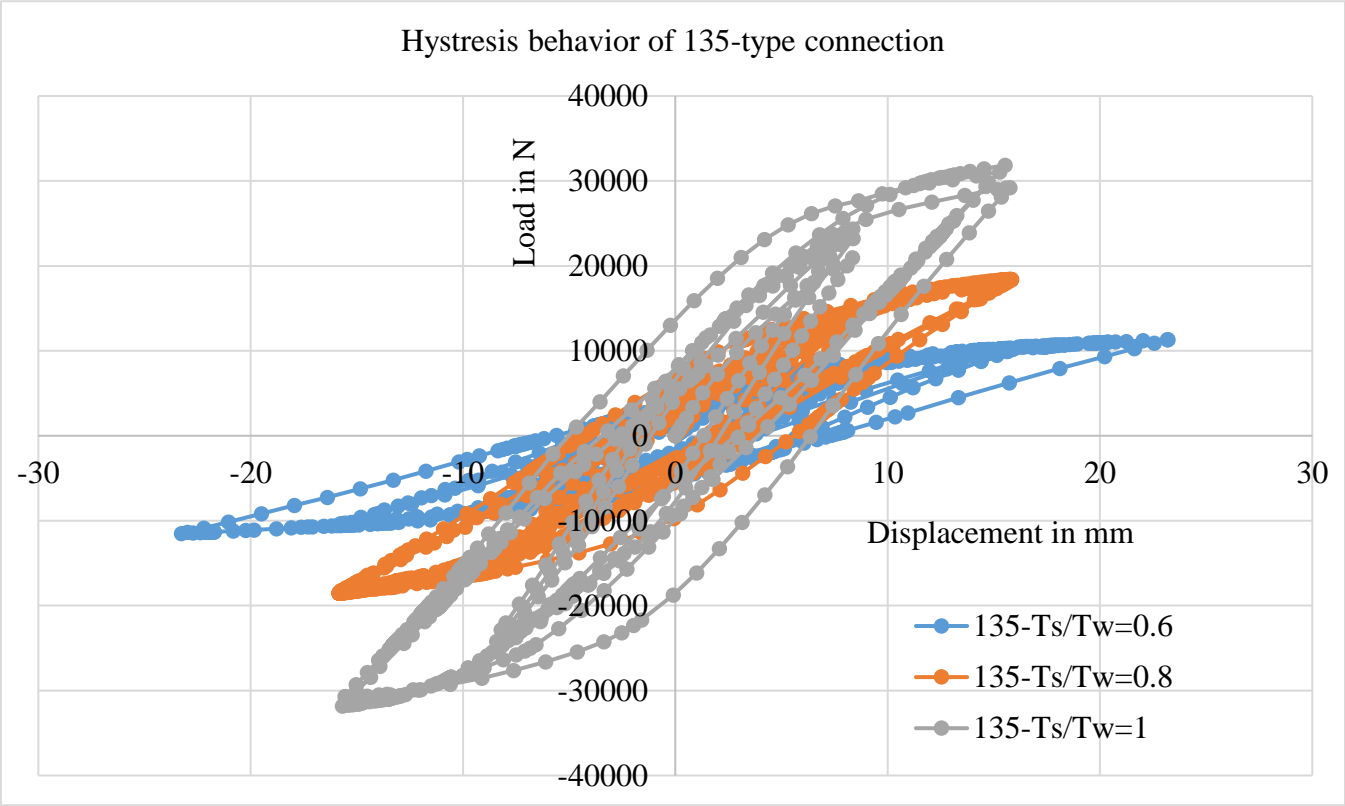


Hysteresis Curve of U-Connection type



Hysteresis behavior of 90-type connection





Appendix C

Origin Lab Software Used for Calculation of Energy Dissipation Under Hysteresis Curve

